The Abundance of PE 18:2 is Increased in Parkinson's Disease Patient Brain Tissue and DJ-1 Knockout Zebrafish Disease Models

by Sarah Torvholm Frøystad

Thesis submitted in partial fulfilment of the requirements for the degree of Master of Science

Faculty of Mathematics and Natural Sciences
Department of Biological Sciences
University of Bergen

June 2023

Acknowledgements

This project was carried out in Halskau research group at the Department of Biological Sciences, University of Bergen in the time period August 2022 – June 2023.

First, I would like to thank my supervisor Øyvind Halskau for the opportunity to work on such an interesting and educational project. I am truly grateful for your guidance and valuable feedback, and your expertise and enthusiasm in your field of research (especially NMR) does not go unnoticed. Thank you for your dedication and availability, despite your busy roles as both a researcher and family man.

Next, I want to extend my thanks to my co-supervisor, Diana, for your patience, problem-solving, positive attitude, and devotion to this project. This could not have been possible without you. Additionally, I want to acknowledge my second co-supervisor, Kari, for your consistent feedback, assistance, motivation, and genuine interest in this project. Furthermore, I would like to express my appreciation to Sissi, for your cheerful attitude, and for teaching me all you know about LC-MS (your alleged best friend/enemy, depending on the day). I also want to thank Martin Jakubec for taking the time out of your day to assist with LC-MS/MS analysis, and for helping me get an inch closer to one day being able to write MatLab scripts like you do. I must also extend my gratitude to Jarl Underhaug for your invaluable problem-solving expertise in the realm of NMR, and Espen Bariås for helping us make sense of our datasets. Special thanks are also due to the research group of Professor Charalampos Tzoulis at Neuro-SysMed Center, and Nansenfondet, for making this research possible.

I would also like to thank my fellow master students, especially my everyday lunch and lab buddies, Maria and Benjamin. Thank you, Maria, for your encouragement, lab-partnership, and shared laughs. And Benjamin, thank you for never failing to answer my questions about *Nematostella*. You both made the long lab days feel slightly shorter. An extended gratitude also goes out to the rest of the wonderful researchers in the NucReg group for the supportive and motivational environment.

Lastly, I would like to express my gratitude and appreciation to my family, sister, boyfriend, and friends for their unwavering encouragement and for always cheering me on throughout this journey.

Bergen, June 2023
Sarah Torvholm Frøystad

Table of Contents

Selected Abbreviations

PD – Parkinson's disease

SN – substantia nigra

KO – knockout

FA – fatty acid

C106 – Cysteine at position 106

ROS – reactive oxygen species

TBI – traumatic brain injury

UPLC – ultra-performance liquid chromatography

HRMS/MS – high-resolution tandem mass spectrometry

IE – iterative exclusion

ESI – electrospray ionisation

NMR – nuclear magnetic resonance

PC – phosphatidylcholine

PE – phosphatidylethanolamine

LA – linoleic acid

AA – arachidonic acid

PMI – post-mortem interval

pp – percentage points

Abstract

Parkinson's Disease (PD) is an age-related neurodegenerative disorder associated with both motor and non-motor symptoms. It is characterized by depletion of dopamine-producing neurons in the *substantia nigra* and the presence of aggregated protein-rich filaments within the brain, referred to as Lewy bodies. The brain, by dry weight, consists of about 50% lipids that can interact with proteins and other lipids. In environments characterized by elevated levels of oxidative stress and reactive oxygen species, such as in PD, lipids are readily oxidized, generating toxic oxidation products. Dysfunctional lipid metabolism in PD is implicated in inflammation, mitochondrial dysfunction, lipid peroxidation and oxidative stress, which are hallmarks of the disease. This thesis hypothesized a link between PD development and lipids through their metabolism and oxidation, and that this would be manifested in the brain tissue of affected individuals and PD zebrafish models. Protocols for lipid extraction and brain sampling were also evaluated.

PD-related phospholipid alterations were assessed in grey and white matter from the brains of a healthy individual and a sporadic PD patient, as well as from the brains of four months old wild-type (WT) and DJ-1 knockout (KO) zebrafish. The DJ-1 KO zebrafish line functioned as a PD model as it lacks the gene encoding the neuroprotective protein DJ-1, a mutation related to autosomal recessive PD. The lipids were extracted using a modified Bligh & Dyer extraction approach, and their phospholipid and fatty acid profiles were analysed using ^{31}P NMR and untargeted UPLC-HRMS/MS, respectively. Western blotting was also used to assess oxidative stress levels by examination of DJ-1 and oxidized DJ-1 expression levels, due to the role of DJ-1 as a cellular stress-sensor. Reduced levels of DJ-1 were detected, along with noteworthy increases in abundances of PC plasmalogens, sphingomyelin, PE 18:2 (linoleic acid), and PS 22:5 (DPA). Altogether, the findings suggest the presence of elevated oxidative stress levels and a potential counteracting defence mechanism to said oxidative stress, primarily due to the neuroprotective and anti-inflammatory properties exhibited by these compounds. Deviations in the phospholipid profile of the sporadic PD brain compared to those reported in the literature, combined with the observed up- and downregulations of phospholipids and fatty acids, highlights the dysregulated lipid metabolism typically reported in PD. However, larger sample sizes are needed to draw reliable conclusions. Future experiments could focus on developing methods for the detection of lyso-phospholipids and oxidized lipids, to provide insight into phospholipid degradation and related signalling pathways implicated in PD. In future experiments, it is recommended to use age-matched human samples, minimize variations in post-mortem interval times of the harvested tissue, and avoid freeze-thaw cycles and long-term storage of lipid samples to minimize their lipid degradation.

1 Introduction

As the proportion of elderly people in our population grows, so does the prevalence of age-related disorders. Dementia is a syndrome typically associated with age, and it causes a gradual deterioration in cognitive and emotional functioning [1]. On a global scale, the number of people who lived with dementia was estimated to have doubled in the timeframe from 1990 to 2016, going from 20.2 to 43.8 million cases [2, 3]. Neurodegenerative disorders like Alzheimer's Disease (AD), Parkinson's Disease (PD), amyotrophic lateral sclerosis, Huntington's disease and Prion diseases are all types of dementia [1]. PD is the second-most common neurodegenerative disease after AD, and it negatively affects not only the diseased individual, but also their families, communities, and health-care systems all over the world [4, 5]. As there is currently no available cure, more research is needed to reach a breakthrough in disease-prevention and treatment to lessen the burden of disease expected to be placed upon the present and future generations.

1.1 Parkinson's Disease

PD and its pathogenesis were initially described in medical terms by James Parkinson in 1817, where he classified the disease as a neurological syndrome named "Shaking palsy" [6, 7]. Today, we know PD as a progressive neurodegenerative illness with clinical motor-related symptoms including resting tremors, abnormal muscular stiffness or rigidity, postural instability [8], movement variability [9], and slowness of movement and thought, referred to as bradykinesia and bradyphrenia, respectively [10]. Furthermore, PD is known to cause non-motor psychological symptoms such as anxiety, depression, hallucinations, delusions, and cognitive decline as it progresses [1, 5, 11]. Symptoms of dysautonomia are also common, including hypertension, constipation, and sleep disturbances [11]. PD is without a doubt a burdensome condition.

1.1.1 Dopamine Depletion

PD has several notable features at the tissue, cellular and molecular levels. One of the characteristic neuropathological hallmarks of PD is the loss of dopaminergic neurons within the *substantia nigra* (SN), a large grey matter structure of the midbrain [5]. Dopamine (DA) is a neurotransmitter playing a key role in movement control [12]. The major relevance of DA in relation to PD became apparent when a discovery in 1960 showed significantly depleted levels of DA in the basal ganglia of individuals dying from PD [13]. Being a part of the basal ganglia circuitry, the SN has been a target of PD research due to its high concentration in DA-producing neurons. With the release of DA, neurons of the SN can communicate with the neurons of the basal ganglia – a biochemical

transaction responsible for fine-tuning the movements of an organism [14]. The SN therefore possesses a critical role in modulating motor movement [15]. Because of the degenerative nature of PD, the dopaminergic neurons of the SN are progressively lost (Figure 1.1.1). It is believed that the resulting hypofunctional DA states caused by neurodegeneration are a primary reason for the manifestation of the clinical motor symptoms seen in PD [5]. Why the dopaminergic neurons are selectively targeted for destruction in PD remains unknown.

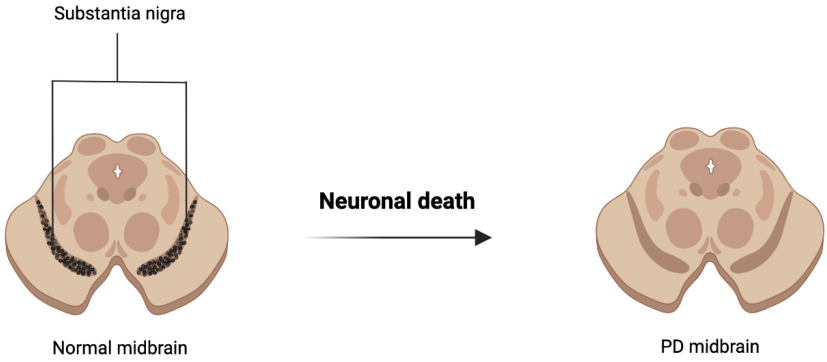

Figure 1.1.1. PD causes the progressive loss of dopaminergic neurons within the *substantia nigra*. As PD progresses, the DA-producing neurons within the SN are depleted. The SN got its nickname as the "black nucleus" (Latin: nigra, black) because the pigment neuromelanin accumulates during DA synthesis, creating a distinct contrasting colour compared to its surrounding brain tissue **[16]**. The illustration was made using BioRender.com.

1.1.2 The presence of Lewy Bodies

A second neuropathological characteristic of PD is the presence of Lewy bodies [5]. Lewy bodies are intracellular proteinaceous inclusions composed of ubiquitinated neurofilament proteins, and they can be found in a wide range of neurodegenerative diseases, including idiopathic PD and multiple system atrophy (MSA), as well as dementia in the form of diffuse Lewy-body disease (DLBD) [17]. They are found in a diffuse distribution within the brain, but mainly in the melanin-containing neurons within the SN. The main component of Lewy bodies has been found to be two mutated forms of the protein α-syn [18, 19]. Other components that are commonly found in Lewy bodies are ubiquitin, neurofilament proteins, 14-3-3 proteins, tau proteins, and lipids [20, 21]. Whether the plaques consisting of aggregated α-syn fibrils in the brains of PD patients play a causative role in disease development, rather than just being a disease-defining marker, is not yet fully understood.

1.2 The Etiology of PD

Decades of research have gone into understanding the complexity of PD, which has proven to be no easy task. PD is usually classified by whether the cause of disease is genetically inherited, referred to as familial, or a result of gene-environment interactions, referred to as idiopathic [22]. Up until the 1990s, the idea of PD being a hereditary disease was heavily rejected, but recent epidemiological studies have proposed that 10-15% of PD cases are a result of genetical predisposition [23]. What makes someone susceptible to developing PD is thought to be a complex interplay between genetic and exogenous factors, in combination with the molecular and cellular changes exacerbated by the ageing process [24].

1.2.1 Demographic Factors

When discussing the etiology of PD, the clear increase in prevalence with age does not go unnoticed. PD is an age-related disorder, and as cases in people under 50 years of age are rare, age is considered the largest risk factor for developing PD [24]. Idiopathic PD affects 1% of the population older than 60 years of age [25, 26], and this prevalence can rise to 3% in individuals 80 years of age and older [27]. Fortunately, even though we are all ageing, not all of us develop PD. Light has been shed on other demographic factors such as gender, ethnicity, and socioeconomic status. More men than women appear to develop PD, and it has been suggested that oestrogen could have a neuroprotective role in the ageing brain [28]. For ethnicity, older studies have shown a decreased risk of PD in Asians and Blacks compared to non-Hispanic Whites and Hispanic races [29]. Furthermore, areas with higher socioeconomic status have been associated with a lower incident rate of PD [30].

1.2.2 Environmental Risk Factors and Idiopathic PD

Several environmental factors have been suggested to play a part in the pathogenesis of idiopathic PD, including exposure to pesticides, heavy metals, solvents, drinking water from wells, traumatic brain lesions, inflammation, and bacterial and viral infections [22, 24, 31]. A lifestyle or an occupation involving regular exposure to various of these risk factors, like farming, rural living or working with heavy metals, welding and mining has therefore been associated with the development of PD [32]. An overview of these factors can be seen in Figure 1.2.2. Regardless, research done thus far on suggestive relationships between PD and specific environmental risk factors has showed inconsistent results. Several factors have also shown to have a preventative effect. Research into the effect of smoking, which is a well-known health hazard, interestingly suggested a neuroprotective effect in PD [33]. Caffeine has also been shown to have protective effects [34].

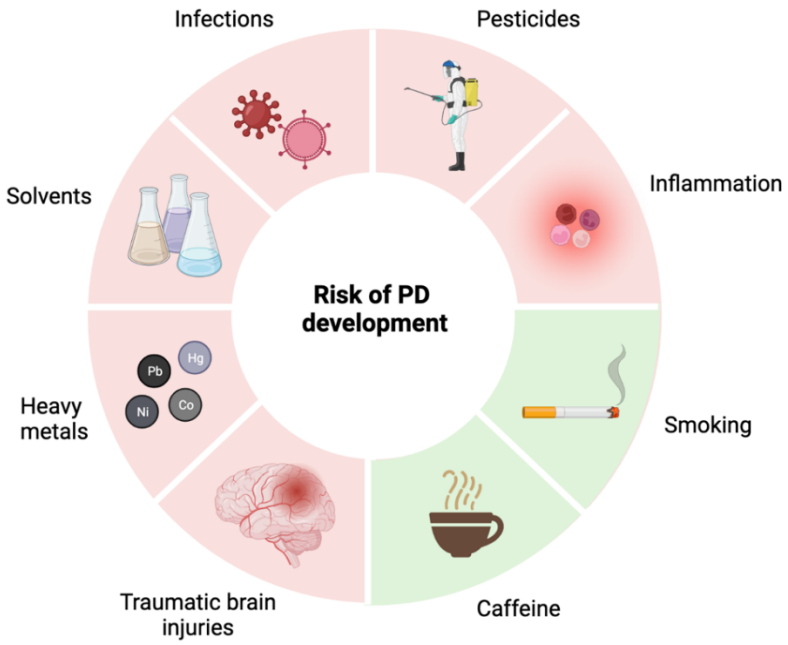

Figure 1.2.2 Environmental factors associated with risk of PD development. Several environmental risk factors are believed to be involved in development of sporadic PD, including exposure to heavy metals, pesticides, solvents, traumatic brain injuries, inflammation, viral and bacterial infections, and traumatic brain injuries. On the other hand, smoking and caffeine has showed neuroprotective effects [34]. The figure was made using BioRender.com.

Pesticides

Exposure to pesticides became of interest as a possible exogenous risk factor for PD in the 1980s when patients showed textbook PD symptoms after being exposed to MPTP, a biproduct of synthetic heroin [35, 36]. Astrocytes, specialized glial cells of the central nervous system, are responsible for converting MPTP to MPP^+ [37]. The structure of the metabolite MPP^+ has been shown to resemble pesticides like paraquat and rotenone, and it was found to selectively target and destruct dopaminergic neurons within the SN *pars compacta* [35]. Exposure to MPTP has been shown to induce Parkinsonism in not only humans, but also in nonhuman primates and mice [38].

1.2.3 Familial PD: The Genes at Play

Attention has in recent years been directed towards reviewing the complex role of genetic factors in PD development. Convincing gene-mapping research performed in the last decade has established the presence of monogenic mutations in both dominant and recessive inherited genes from more than 23 loci and 13 genes, and 90 different chromosomal loci have been shown to be related to PD [39-42]. Only a subgroup of all genes proposed to be PD-related have gained the status of *PARK* (Parkinson's disease) chromosomal regions. Mutations in for instance α-synuclein

(α-syn/*PARK1-4*) and LRRK2 (*PARK8*) are believed to be responsible for autosomal-dominant forms of PD, whilst the autosomal-recessive PD can be traced back to mutated Parkin (*PARK2*), PINK1 (*PARK6*), DJ-1 (*PARK7*) and ATP132A (*PARK9*) [40]. The implications of DJ-1 in relation to PD will be discussed in section 1.4.

1.3 Lipids and their role in PD

Despite decades of research, the origin of PD remains a mystery at the molecular level. In dry-weight, about 50% of the brain consists of lipids, but compared to adipose tissue, the brain is not simply a storage-location for fats [43]. Rather, the lipids found within the brain are mainly functional, where they regulate ion channels and receptors or serve as signalling molecules [44]. Disrupting or altering the intricate lipid homeostasis within the brain can therefore have serious consequences. Some of the genes and proteins implicated in PD, including α-syn and DJ-1, also interact with, or have downstream effects on lipids [45-47]. For this reason, shifting the focus towards the lipids could provide a better understanding of PD. In the following sections, the roles of lipids in PD pathology, as well as how they are believed to relate to various hallmarks of the disease are discussed, including lipids in cell signalling, inflammation, lipid peroxidation, and mitochondrial dysfunction.

1.3.1 Lipids are Structural and Functional Macromolecules

In molecular biology we categorize fatty, oily, and wax-like compounds as lipids. They make up one of the four major building blocks of biological materials, alongside carbohydrates, proteins, and nucleic acids [48]. Lipids can be categorized into different classes based on their chemical structure, but because of the great variation between one lipid and another, their classification is quite complex and multiple classification systems exist. An example is the Lipid Metabolites and Pathways Strategy (LIPID MAPS) classification system, where lipids are grouped into one of eight categories; fatty acyls, glycerolipids, (glycero)phospholipids, sphingolipids, sterols, prenol lipids, saccharolipids, and polyketides [49]. The LIPID MAPS classification system will be used in this thesis.

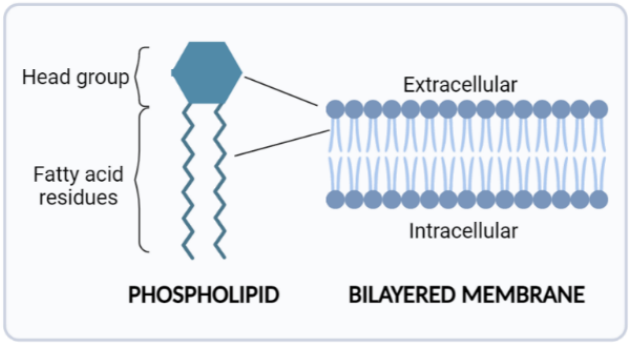

Figure 1.3.1a Phospholipids make up cell membranes. The typical structure of a lipid consists of a polar headgroup attached to two hydrophobic fatty acid residues. Made with BioRender.com.

Apart from sterols, lipids structurally consist of various combinations of hydrophobic side chains attached to different polar head groups – making lipids a truly diverse group of macromolecules [48]. Because lipids have both hydrophilic polar head groups, as well as hydrophobic nonpolar ends, they are considered amphipathic molecules. Their amphipathic nature is what makes them the structural building block of cell membranes because they can function as hydrophobic barriers between the cytoplasmic interior and the extracellular environment, in this way playing a crucial role to the life of the cell. Likewise, for the eukaryotic organelles, such as the mitochondria, endoplasmic reticulum and the Golgi complex, their membranes define their boundaries and produce a compartmentalized environment. Phospholipids, together with cholesterol, are the main components of biological membranes [48], and their structure can be seen in Figure 1.3.1a.

Differences in the physical properties of cholesterol and sphingomyelin, compared to the surrounding phospholipids, can lead to the formation of distinct microdomains of the cellular bilayer with a different lipid phase than the rest, known as lipid rafts [50]. The combination of these lipids produces a physicochemical environment that is both highly saturated and viscous – a platform where both protein-lipid and protein-protein interactions can take place. Studies on lipid rafts in relation to PD became of great interest when it was discovered that gene products associated with neurodegeneration, including DJ-1, α-syn, LRRK2, parkin, and PINK1, specifically associate with them [51, 52]. Cholesterol of lipid rafts has also been suggested to play a role in α-syn aggregation as it interacts with α-syn through two distinct cholesterol-binding domains [53]. Lipid rafts showcase the diversity of lipids; while providing structure and fluidity, they also act as platforms for signalling transduction [54].

Lipids in Cell Signalling

Although scientists in the field of cell biology long credited proteins for being the main macromolecules involved in leading and organizing signalling cascades, research has shown that lipids play a particularly important role in both intracellular- and transcellular signalling [44]. In recent years, there has also been growing evidence linking lipids to PD. In particular, PD has been found to alter signalling pathways and thereby dysregulate lipid metabolism [55]. Whilst being a

major source of energy and providing cells with structural integrity, organization, and fluidity in the form of protective cell membranes, lipids are working closely and directly with proteins to regulate transcription factors, gene expression, inflammation, and signal transduction through interactions with ion channels and receptors [43, 44, 56]. Lipid head groups can also undergo modifications that are essential to their functional abilities. A well-known example are the phosphoinositides, a family of phospholipids (PL) located in cell membranes, where the headgroups are phosphorylated at specific positions, giving rise to different regulatory roles [57]. An overview of various functional lipids and their role in intracellular signal transduction are shown in Figure 1.3.1b.

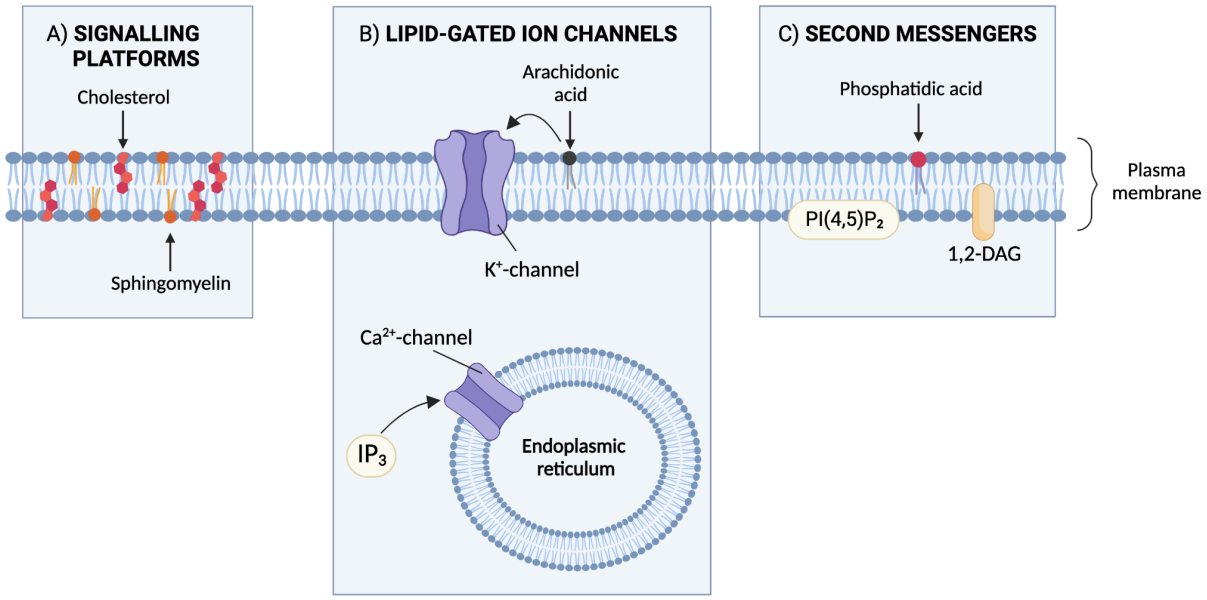

Figure 1.3.1b The many roles of lipids in cell signalling. Lipids have various functional roles in cell signalling. **A)** Sphingomyelin and cholesterol play structural roles as they are important for assembly of lateral membrane domains, lipid rafts, involved in membrane trafficking and cell signalling [58]. **B)** Various ion channels are regulated by lipids, such as K^+ channels regulated by exogenous unsaturated FAs like arachidonic acid [59], or inositol triphosphate-gated (IP_3) Ca^{2+} channels in the endoplasmic reticulum [60]. C) Other lipids function as messengers. The cleavage of the second messenger membrane-lipid $PI(4,5)P_2$ produces another second messenger molecule, namely 1,2-diacylglycerol (1,2-DAG), which itself can be phosphorylated to form phosphatidic acid, yet another intracellular messenger [61]. The illustration was created using BioRender.com.

1.3.2 Lipid Peroxidation and Reactive Oxygen Species (ROS)

Biochemistry of ROS

A "free radical" is a term used to refer to chemical species that have one or more unpaired electrons [62]. The ground state of oxygen (O_2) is an example of a free radical, and oxygen can readily react to form partially reduced species. These reduced oxygen-species are generally both highly reactive and short-lived, and they are referred to as ROS [63]. ROS, like the hydroxyl radical ($HO^{\bullet}$) and hydroperoxyl radical ($HO^{\bullet}_2$), can directly affect lipids. Once formed, the hydroxyl radicals ($HO^{\bullet}$) unspecifically attack nearby biomolecules such as lipids, and they are therefore involved in cellular disorders, including neurodegenerative disorders like AD and PD [64]. Similarly, the hydroperoxyl radicals ($HO^{\bullet}_2$) can become protonated and form hydrogen peroxide (H_2O_2), which subsequently can, through Fenton or Haber-Weiss reactions, react with redox-active metals to generate even more hydroxyl radicals ($HO^{\bullet}$). An overview of the Fenton and Haber-Weiss reactions can be seen in Figure 1.3.2.

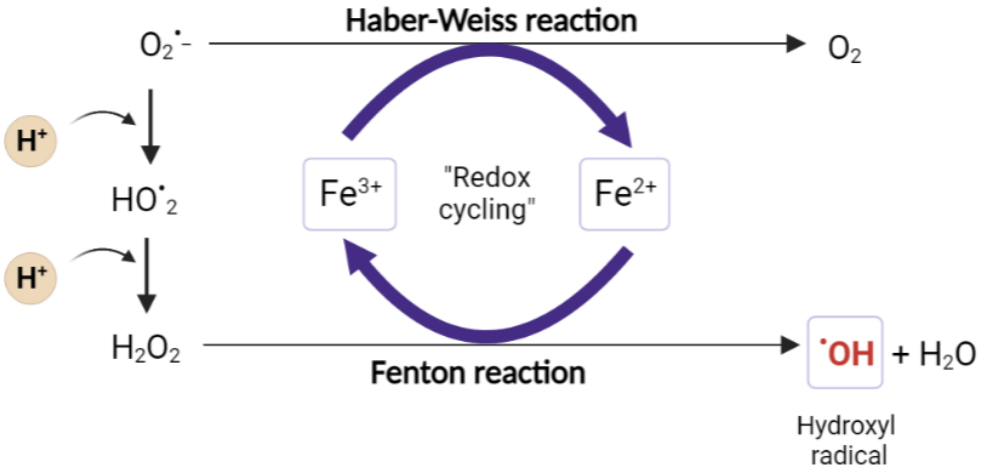

Figure 1.3.2 Fenton and Haber-Weiss reactions form ROS through the process of redox cycling. An example of the Fenton reaction is when reduced free iron (Fe^{2+}) reacts with hydrogen peroxide (H_2O_2) to generate the hydroxyl radical ($HO^{\bullet}$), and water as a biproduct **[65]**. Reduced free iron (Fe^{2+}) is available because of Haber-Weiss reactions, where transition metals like iron or copper go through a process called "redox cycling", and ferric (Fe^{3+}) is reduced to (Fe^{2+}) after gaining an electron from a superoxide radical ($O_2^{\bullet-}$), forming oxygen (O_2). In this way, Fenton reactions are complemented by Haber-Weiss reactions to form a continuous process of redox cycling, allowing the generation of $HO^{\bullet}$. Protonated hydroperoxyl radicals ($HO^{\bullet}_2$) forms hydrogen peroxide (H_2O_2), which again can react with reduced Fe^{2+}. The figure was made at BioRender.com, inspired by a figure by Ayala *et al.* [65].

Lipid Peroxidation

Lipid peroxidation is the process where oxidants in the form of ROS such as the hydroxyl radical ($HO^{\bullet}$) attack the carbon-carbon double bonds found in lipids to form lipid radicals ($L^{\bullet}$) [65]. The victims of $HO^{\bullet}$ and ROS attacks are typically polyunsaturated FAs [66]. The lipid radical ($L^{\bullet}$) can team up with oxygen to form lipid peroxy radicals ($LOO^{\bullet}$), which can steal a hydrogen from another lipid molecule - thereby generating a new lipid radical and lipid hydroperoxide (LOOH). Targets especially prone to undergo damaging lipid peroxidative modifications are glycolipids, phospholipids and cholesterol.

Lipid peroxidation is known to generate a wide array of oxidation products, with lipid hydroperoxides (LOOH) being the main ones. 4-hydroxy-2-nonenal (HNE) is a toxic biproduct of lipid peroxidation of cellular membrane lipids, and it has shown its implications of PD pathogenesis [67, 68]. HNE is also considered a marker for oxidative stress, as well as a stimulating factor in inflammation [69]. Furthermore, research has shown that HNE can interact with soluble α-syn, promoting toxic oligomer aggregation [45].

1.3.3 Inflammation and Oxidative Stress in PD

Lipids are involved in regulating inflammation, where they provide anti-inflammatory effects, or induce immune responses [70]. The mechanism of inflammation is highly regulated, aiming to protect the host from agents causing damage, and promote tissue repair of existing damage. Secreted factors from damaged neurons or certain protein aggregates can lead to a persistent type of neuroinflammation. In relation to PD, chronic neuroinflammation has been suggested as a factor for progression of the disease [38]. What exactly triggers the neuroinflammation in PD remains unclear, but the continuous loss of neuronal cells has been tied to inflammation [71]. In particular, it has been proposed that dying neurons can trigger persistent, chronic activation of microglia, leading to elevated levels of oxidative stress, which in turn contributes to both neuronal and lipid degradation [72, 73]. Under conditions of uncontrolled oxidative stress, lipids are primary targets of ROS attacks.

The Role of Proinflammatory M1 Microglia Chronic in Neuroinflammation

Microglia are macrophages that make up the frontline defence of the innate immune system. In the case of inflammatory challenges, the microglia will become functionally customized towards the proinflammatory M1 or anti-inflammatory M2 phenotypes [74]. Microglia-mediated neuroinflammation, specifically a state of chronic neuroinflammation, is considered a prominent

feature in the progressive neuronal degeneration seen in neurodegenerative disorders, including PD. Microglia activation, and transformation into M1 microglia, is initiated by damage-associated molecular patterns (DAMPs), which are secreted by damaged or dying neurons (Figure 1.3.3) [72]. Moreover, as a stress-response, damaged and dying neurons can release more DAMPs, resulting in generation of oxidative stress and ROS – sustaining chronic neuroinflammation [72]. Under high levels of oxidative stress, the probability of ROS reacting with lipids are greatly increased. A combination of DNA oxidation and lipid peroxidation has the possibility of inducing apoptosis because of the damage caused to both the DNA and plasma membrane. In this way, the elevated levels of ROS seen in relation to inflammation can induce lipid peroxidation, thereby intensifying neurodegeneration [73].

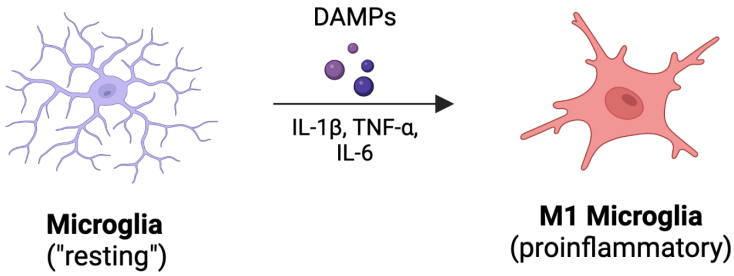

Figure 1.3.3 DAMPs stimulate formation of M1 microglia. Damage-associated molecular patterns (DAMPs) can be secreted from damaged neurons, stimulating surveying ("resting") microglia to become proinflammatory microglia. The M1 phenotype has been associated with increased expression of mediators that are considered proinflammatory, such as the cytokines interleukin (IL) 1β, IL-6 and tumour necrosis factor (TNF) alpha [75]. These proinflammatory mediators then reinforce the existing local inflammatory response. The figure was made using BioRender.com.

Another example of M1 microglia activation is related to exposure to MPTP, a precursor to the neurotoxic MPP^+. Exposure to MPTP and its metabolite MPP^+ was mentioned previously in section 1.2.2 as a potential PD-associated environmental risk factor. MPP^+ is believed to inhibit mitochondrial complex 1 of the electron transport chain, resulting in depletion of ATP and an increase in oxidative stress, causing cell death of the dopaminergic neurons of SN and the activation of proinflammatory M1 microglia [38].

Traumatic Brain Injury

In section 1.2.2, various environmental risk factors associated with PD-development were mentioned, including traumatic brain injury (TBI). Elevated levels of ROS can be detected following a TBI [73]. A study on TBI showed that military veterans with a history of mild TBI have

a 56% higher risk of PD, and the risk increases with injury severity [67, 76]. Lines of research studying the connection between TBI and PD are pointing towards an upregulation of inflammation, dysregulation in metabolic pathways and protein accumulation, believed to either initiate or accelerate PD following a TBI.

In the matter of minutes following a TBI, an inflammatory response is elicited. The neurovascular damage creates a situation where the energy homeostasis of the brain is disrupted, production of reactive oxygen species (ROS) is initiated, and inflammation is induced [77]. The sudden increase in ROS following a TBI is characterized by a pronounced damage-response from microglia as they migrate to the site of injury to prevent cell death [73]. If this situation is prolonged, a neuroinflammatory signalling cascade is activated – believed to induce nucleation of PD. The initial impact and damage caused by TBI causes an intracellular overload of calcium, leading to a loss of mitochondrial function, initiation of catabolic processes and overproduction of neuronal ROS [67, 78]. Such a high level of neuronal ROS causes a lot of stress on these cells, which is where lipid peroxidation comes into play [73].

1.3.4 Mitochondrial Dysfunction and Cell Death

Mitochondrial dysfunction can be considered another hallmark of PD, and the dysfunctional states are related to oxidative stress caused by ROS and aberrant Ca^{2+} signalling [5]. One of the organelles particularly responsible for endogenous ROS production is the mitochondria, alongside the plasma membrane, endoplasmic reticulum, and peroxisomes [63]. ROS production in mitochondria is especially active in processes leading up to apoptosis, and mitochondrial dysfunction in PD is therefore associated with neuronal cell death. Being the site of ATP, NADH and $FADH_2$ production through fatty acid (FA) oxidation, the citric acid cycle and oxidative phosphorylation, the mitochondria play a vital role in keeping a cell alive. Low levels of mitochondrial Ca^{2+} are necessary for optimal ATP production, but under oxidative stress conditions where the cell is experiencing Ca^{2+} overload, a rise in intramitochondrial Ca^{2+} functions as a death signal [60, 63]. In other words, abnormal Ca^{2+}-signalling and increased oxidative stress levels go hand-in-hand on the road to cell death [60].

Cardiolipin, an acidic lipid found in the inner mitochondrial membrane, functions as a signalling platform as it can serve as a binding site [79, 80]. Experimental studies have indicated that the PD-relevant α-syn is a lipid-binding protein as it associates with bilayered membranes, specifically with phospholipids with negatively charged, acidic headgroups, such as cardiolipin [81, 82]. An

interaction between cardiolipin and A53T α-syn has been found to induce aberrant Ca^{2+}-signalling, leading to an increase in oxidative stress as mitochondrial ROS production is altered, and subsequently Ca^{2+}-dependent cell death [46, 83, 84]. The following rise in oxidative stress levels and lipid peroxidation has shown to impact both complex I and ATP-synthase of complex V, two structures found in the inner mitochondrial membrane as parts of the mitochondrial electron transport chain. ATP-synthase, as its name suggests, is a structure involved in energy production through ATP-formation [43]. Both complex I and ATP-synthase are impaired as a response to oxidative damage [85], in this way interrupting mitochondrial function and thereby ATP production. The drop in energy (ATP) production due to this impairment magnifies the generation of mitochondrial ROS, subsequently promoting the mitochondrial permeability transition pore (mPTP) to open, which causes the mitochondria to become permeabilized and swell, finally resulting in cell death [85]. In this way, oxidative stress and subsequent lipid peroxidation is involved in inducing cell death as ATP-production is impaired.

1.3.5 Changes in Brain Lipid Profiles and its Relevance for PD

In order to grasp the nature of PD, it is necessary to consider that it is an age-related disorder. One hypothesis is that PD occurs mostly in the elderly because of accumulated life-long oxidative damage and inflammatory responses [86]. Yet, age-related disorders are still considered distinct pathologies, and not an inevitable outcome of ageing. As PD is more prevalent in the later stages of life, it is assumed that there are distinct changes that happen to the brain to initiate disease development. Recently, there has been a focus on changes in lipid profiles as a possible underlying risk-factor for developing PD. Several studies have characterized the diverse lipid profile of the human brain [87]. The main phospholipids present in the human brain are phosphatidylcholine (PC), phosphatidylethanolamine (PE), phosphatidylserine (PS) and phosphatidylinositols (PI), whilst cholesterol is the main sterol [43]. Phospholipids make up about 4.5 – 5.4% of the wet weight of the brain, with PE being the main phospholipid (35.6%), and PS making up about 16.6% of the total phospholipid content [87].

Studies done on patients with AD have suggested differences in the fatty acid (FA) composition of the grey and white matter of the brain when compared to control subjects [88]. For instance, the amount of adrenic acid, a long polyunsaturated FA, was 3-4 times higher in grey matter compared to three brain regions of white matter in the control group. Metabolomic studies have also shown changes in the lipid profile of sebum (oily secretions from sebaceous glands in the skin) in PD, suggesting how certain metabolites can predict the PD phenotype [89]. The sebum analyses showed

an altered lipid metabolism where certain lipid pathways, specifically related to sphingolipid and arachidonic acid metabolism, as well as FA biosynthesis, were affected.

Beyond changes in lipid profiles, the aforementioned research has implicated the role of lipids in inflammation, lipid peroxidation and oxidative stress, and mitochondrial dysfunction – hallmarks of PD [5]. Furthermore, it has showed how proinflammatory M1 microglia activation, ROS production, oxidative stress, abnormal calcium signalling, impairment of ATP production and mitochondrial dysfunction can result in neuronal cell death. Taking this into consideration, the role of lipids in PD is a matter that can be justified to further explore.

1.4 DJ-1 Knockout Zebrafish as a Model Organism for PD

For this thesis, it was of interest to find a suitable model organism for PD research. A limiting factor in human-based neuroscience research pursuing molecular disease mechanisms, including PD research, is that the experiments on the brain must usually be performed on live patients. Only having access to post-mortem human brain material therefore produces several challenges, including ethical dilemmas, the effect of post-mortem interval (PMI), tissue degradation in the time elapsed between death and tissue freezing or fixation [90], and the lack of *in vivo* studies, which a suitable animal model could overcome.

1.4.1 Zebrafish are Viable Models for Biomedical Research

Zebrafish (*Danio rerio*) check all the boxes for being great models in biomedical research – they are both cheap and easy to sustain, are easily manipulated using genetic methods, breed rapidly and in large amounts, and their embryos are transparent, allowing detailed observations of the developmental process [91]. Living for approximately three years on average, zebrafish have shown to have a gradual senescence that is similar to humans – suggesting a role for zebrafish as an animal model for studies of the ageing process [92]. Additionally, the nervous system of the zebrafish is well-characterized, and studies have shown close similarities in neurofunction, behaviour, oxidative stress responses, and even similar age-related degenerative changes when compared to humans [92, 93]. As a result, it has become an emerging model for human diseases in neuroscience, making it suitable for neurodegenerative research and thereby a viable PD animal model.

To perform studies on the lipid profile of the zebrafish brain for PD research, it is critical that they metabolise fat in a comparable manner to humans. Genetic studies have shown that zebrafish express the lipoprotein gene MTP, the fatty acid transport protein *slc27a* and acyl-CoA synthetase

– proteins needed for lipid metabolism and transportation [94]. Furthermore, proteins needed for cholesterol transport and lipoprotein assembly, as well as enzymes necessary for synthesis of important lipid-signalling molecules like prostaglandins and thromboxanes, have all been shown to be expressed in zebrafish [95-97].

1.4.2 Knocking Out the Neuroprotector DJ-1

DJ-1 is a multifunctional protein involved in regulation of antioxidant gene expression, signal transduction, immune cell modulation, oxidative stress responses, and inflammation, with functionality both as a chaperone and enzyme [47]. Its key role in the involvement of inflammation and oxidative stress has indicated a role for DJ-1 in development of a variety of diseases, including cancer, type 2 diabetes, and neurodegenerative disorders, such as PD. DJ-1 has been associated with a rare form of autosomal recessive PD as it has shown to be mutated in 1-2% of early-onset (onset of disease before 50 years of age) PD cases [40, 98]. Notably, oxidated forms of DJ-1 can also be found in individuals with idiopathic PD, making it a protein of interest when studying both familial and sporadic PD [99]. To better the understanding of PD, genetic modifications to induce overexpression of autosomal dominant genes such as *SNCA* (α-syn) and *LRRK2*, or conversely knockout/knockdown of autosomal recessive genes like *DJ-1* and *Parkin* has been performed in various animal models [100]. For this thesis, a previously established Zebrafish line where DJ-1 had been knocked out was the chosen animal model [101]. A recent study published on the same zebrafish line showed how loss of DJ-1 expression resulted in progressive motoric and non-motor symptoms that are associated with PD [102].

DJ-1 as an Oxidative Stress Sensor

In relation to PD, the main importance of DJ-1 is its function as a sensor for oxidative stress [99]. Amongst the 189 amino acids (20 kDa) of DJ-1, a conserved cysteine residue at position 106 (C106) has been emphasized as the primary location for oxidative protein modification, with cysteines at positions 46 and 53 being other stress-sensitive residues [103, 104]. C106 of DJ-1 has shown to be unusually reactive and therefore sensitive to oxidation by ROS. This could be explained by the nucleophilic thiol group of cysteines residues, which makes them more prone to oxidation in comparison to other amino acids [105]. Oxidation of C106 has shown to be necessary for DJ-1 to gain its neuroprotective properties, allowing DJ-1 to not only function as a sensor of the cellular redox homeostasis, but also enabling its participation in cytoprotective signalling pathways [106, 107]. As one of its known roles is neuroprotection, loss of DJ-1 has therefore been shown to correlate with the death of dopaminergic neurons [107]. Depending on the level of oxidative stress,

DJ-1 C106 will take on different forms as shown in Figure 1.4.2. In conditions of mild oxidative stress, C106 of DJ-1 is oxidized to a sulfinic acid form, C106-SO_2H. However, DJ-1 is inactivated in the presence of high oxidative stress levels, as it is oxidized to a sulfonic acid form, C106-SO_3H [103]. In this regard, the oxidation status of DJ-1 can function as a biomarker for oxidative stress levels [108].

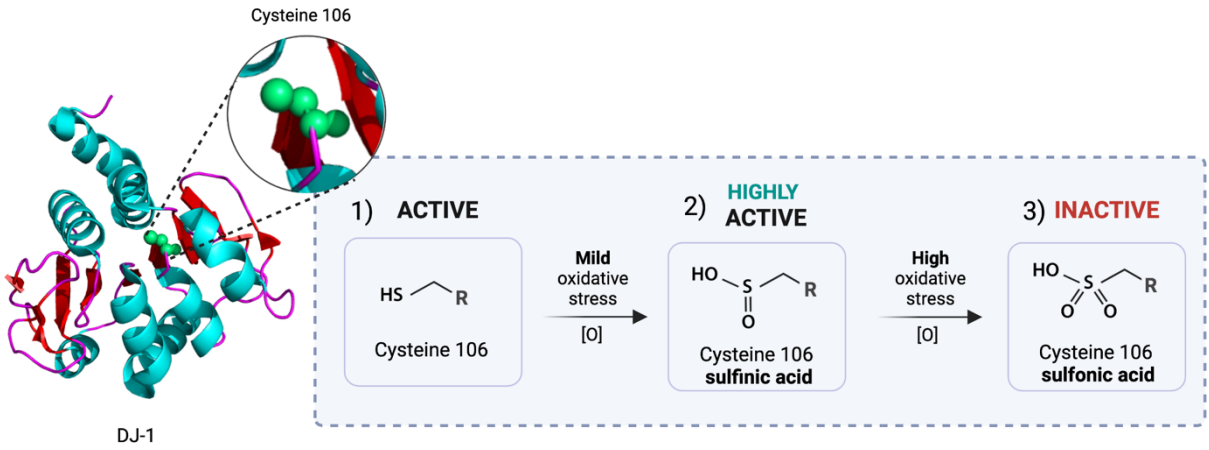

Figure 1.4.2 High oxidative stress conditions lead to overoxidation of cysteine 106 of DJ-1, rendering it inactive. Amongst all the amino acids found in DJ-1, C106 (in green) is especially sensitive to oxidation. **1)** When C106 (show in green in the structure) of DJ-1 is in its reduced state, C106-SH, DJ-1 functions as a neuroprotectant. **2)** In the presence of moderate oxidative stress levels, the reduced form can be oxidized to C106-SO_2H, a stable and highly active sulfinic acid form**. 3)** However, shall the oxidative stress levels rise even higher, the sulfinic form of C106 can be oxidized further to C106-SO_3H, a sulfonic acid form [106]. This over-oxidized state of the C106 sulfonic acid form has shown to render DJ-1 unstable and inactive, causing a loss of its function [107]. The Figure was made at BioRender.com, with inspiration from an article by Repici *et al.* [99]. The structure of DJ-1 was displayed using Molview and obtained from the RCSB Protein Data Bank (PDB).

1.5 Methodology for Brain Lipid Profiling and Identification

1.5.1 Lipid Isolation by Solvent Extraction

The goal of any lipid analysis is to extract sufficient amounts of a lipid subclass from the source material, whilst avoiding bias within this subclass. Aside from their impractical adhesive texture and insoluble nature, working with lipids also has its challenges as they are readily degraded by exposure to oxygen, light, heat, free radicals and lipases [109]. Different types of lipid extraction exist, including saponification and supercritical CO_2 extraction, or mechanical methods such as ultrasonication and high-pressure homogenization [110, 111]. Still, the traditional organic solvent extraction is commonly used as the affordable equipment and necessary solvents are accessible in most laboratories.

The Choice of Solvent System

Biphasic solvent mixtures containing both an organic and aqueous non-organic solvent such as methanol are frequently used because their immiscibility leads to the formation of two separate phases. This allows most lipids, if not all, to migrate into the organic phase, in that way separating them from the polar proteins and sugars that are retained in the non-organic phase [112]. Because lipids are chemically diverse macromolecules and differ in their physiochemical properties, the extraction solvent is chosen to cater to the lipid class of interest. In the case of this thesis, the lipid subclass of interest was the phospholipids. Negatively charged phospholipids are water-soluble and can be retained in the aqueous phase of simple biphasic solvent systems, so multi-step extraction approaches and varying amounts of polar solvents, such as methanol, are adjusted to avoid discriminatory effects towards acidic phospholipids. For phospholipids like PC and PE, their lipid head is zwitterionic and they can therefore be extracted using dichloromethane only. However, for anionic lipids such as PS or phosphatidylglycerol (PG), the addition of methanol in necessary to allows a small amount of water into the organic phase in the form of a "water shell" surrounding the anionic headgroups [113].

The most well-known lipid extraction approaches include the Folch method, and a slightly modified Folch method, developed by the Bligh & Dyer [114, 115]. The Folch and Bligh & Dyer approaches are considered "gold standards" for lipid extraction, and while they both use the same ternary solvent mixture consisting of chloroform, methanol, and water, they vary in solvent/solvent and solvent/tissue ratios [116]. While the initial solvent/tissue ratio in the Folch extraction method is 20:1, the ratio (3+1):1 is used in the Bligh & Dyer approach, a modification allowing for the use of less solvent [117].

Replacing Chloroform with Dichloromethane

Even though these methods are efficient and reliable, working with large amounts of chloroform, a highly toxic and carcinogenic solvent, has its disadvantages for both the environment and human health [118]. Dichloromethane (DCM), an organic solvent with molecular similarities to chloroform, has been suggested as a safer alternative, not only for safety reasons, but as a greener alternative for larger scale projects (Figure 1.5.1) [116]. When comparing total lipid extraction with DCM and methanol, compared to extraction with chloroform and methanol, negligible differences are observed [119]. Little to no variation in extracted lipid classes has been reported when comparing the two solvent systems, and a DCM-based extraction has showed a >99% extraction yield from lipid fractions [120, 121].

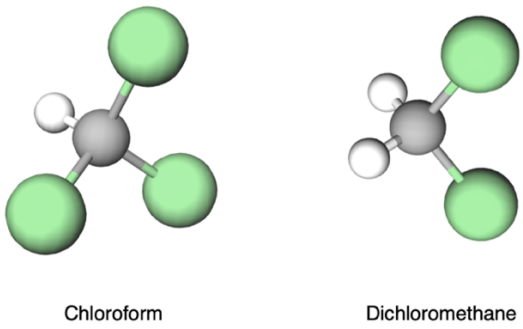

Figure 1.5.1 Chloroform and dichloromethane are similar molecules in composition and structure. While chloroform contains three chlorine atoms (green), dichloromethane (DCM) has two. With respect to HSE-concerns, DCM has been suggested as a better alternative to chloroform in lipid extraction procedures [116]. Carbons are shown in grey, and hydrogens in white. The Figure was made using Molview.

1.5.2 Mass Spectrometry

Lipid profiling of a lipid fraction can be performed using various analytical chemistry techniques, such as mass spectrometry (MS). Recent advances in MS technology have enabled more comprehensive lipid profiling of biological samples. Gas chromatography (GC) is traditionally used for FA analysis, functioning as a reliable tool for quantitative analysis of samples containing complex FA mixtures [122]. However, the development of electrospray ionization (ESI) has significantly expanded the range of lipids that can be analysed by MS. Coupling ESI-MS with ultra-performance liquid chromatography (UPLC) has become a popular approach in lipidomic studies because of its selectivity and good separation of various types of lipids [122, 123]. Moreover, MS/MS analysis, where ions are fragmented into their fragment ions, provide the detailed structural information needed for characterization of novel lipids [124].

The Mass Spectrometer

Mass spectrometers are generally composed of an ionization source (such as ESI), mass analysers (such as orbitrap) and a detector. In the ionisation source, the analyte molecules are converted to their ionised state, and under vacuum conditions the ions and potentially fragmented ions are detected based on their mass to charge ratio (m/z) [125]. Various types of mass spectrometers exist, with different technology for both the ionisation process and ion analysis. ESI is among the most commonly used ionisation sources, where samples in liquid form are pumped through a metal capillary to convert the solvent droplets into a fine mist. At the metal capillary tip, charged droplets undergo successive size losses as the solvent evaporates, converting them to gas-phase ions. Heat, coupled with an inert gas like nitrogen, is typically used to aid solvent evaporation [126]. Depending

on their physiochemical properties, analytes are ionized in positive (protonation) or in negative (deprotonation) mode. Ionised analytes travel under vacuum in a series of lenses and quadrupoles to reach the Orbitrap mass analyser [127].

Mass Spectrometry and Liquid Chromatography – a "Dream Team"

A challenge with MS is that molecules are competing for ionisation, resulting in an ion-suppression effect. Combining MS with HPLC allows the molecules to reach the MS at different times based on their affinity to a stationary (chromatographic columns) or mobile phase (gradient of solvents) [125]. This affinity depends on the physiochemical properties of the molecules, including their polarity, and analytes will therefore be retained for different durations in the column – giving rise to the term "retention time". Separating the lipids using HPLC prior to MS can therefore reduce the ion-suppression effect because the number of competing analytes competing for ionisation as they enter the MS is drastically reduced [123]. In terms of LC, high-performance liquid chromatography (HPLC) has become a popular approach in lipidomics because of its selectivity, high efficiency, lipid separation, and the isolated system it provides to lipids, protecting them from oxidation [122, 123].

Tandem Mass Spectrometry

In tandem MS (MS/MS), three mass spectrometers are coupled in series [128]. In the first, MS1, the initial "parent" lipid ions are selected for fragmentation. In the second, MS2, the ionized parent ions from MS1 are fragmented by collision induced dissociation, where an inert gas, such as nitrogen, "forces" ions to become fragmented through gas collisions, thereby producing lipid "daughter" ion fragments [125]. In the third, MS3, the daughter fragment ions are selected. The mass detector detects the signal per time of the ion current, which is generated from the incident ions, and converts it into a frequency-based plot – a mass spectrum. MS/MS allows greater specificity compared to single-stage MS1 because the resulting MS2 spectra can function as "analyte fingerprints", allowing their identification [128].

A challenge with tandem HPLC-MS/MS when analysing complex biological samples, is the discriminatory process placed upon unidentified compounds, typically isomeric lipids [129]. High resolution MS (HRMS) is required to determine the exact mass of the lipids, thereby discriminating lipid species with the same nominal mass but different molecular formula (isobaric compounds), in order to identify them. Another challenge with MS/MS is that in a single injection, numerous ions with differing m/z ratios will be eluted at the same time, but not all of them can be selected for fragmentation. Data-dependent topN (ddMS^2-topN) can provide a solution, a "top-down" approach

where the ions with the highest intensity (most abundant) are selected for fragmentation [130]. ddMS^2-topN analysis can also be performed multiple times on the same sample, where precursor ions selected in the previous run are excluded in each sequential analysis, an approach referred to as iterative exclusion (IE) [130]. In this way, the MS/MS instrument is not overloaded with fragments as certain fragments are excluded per run, drastically improving the total lipid coverage of the sample.

Untargeted Lipidomics

An untargeted approach where all ions are selected for analysis makes it possible to analyse hundreds to thousands of individual lipids simultaneously. Large amounts of raw data makes the lipid identification challenging, so the process is typically simplified with the use of scripts where m/z values and fragmentation patterns from HRMS, and retention times from HPLC, provide a unique fingerprint that can be matched to predicted and reported data from large lipid databases. In this way, lipids can be identified. The lipid identification process is operated in reverse; starting with comparison of predicted fragmentation of lipid species in lipid libraries and experimental MS2 spectra. When a hit is identified and score, its parent ion can be found in the MS1 data, and its identified m/z ratio can thereafter be matched to its retention time from the HPLC run.

HPLC-HRMS/MS can also be "semi-quantitative". For instance, in MS lipid studies on phospholipids, the presence of specific lipid moieties with the same phospholipid head group can be quantified. While the quantity of detected lipid moieties found in different subclasses of phospholipids, for instance PC 18:0 and PS 18:0, cannot be compared against each other, lipid moieties found within the same subclass of phospholipids, such as PC 18:1 and PC 18:0, can be quantified and compared – thereby the name "semi-quantification". This limitation has to do with how LC-MS separates lipids, which is by their m/z ratio. Different head groups of PLs will ionize differently based on their ionization efficiency; the ratio of the number of ions formed to the number of electrons/photons used during the ionization process [131]. Total quantification across different phospholipid head groups is therefore not possible [132].

1.5.3 Nuclear Magnetic Resonance

Nuclear magnetic resonance (NMR) spectroscopy is a powerful analytical technique which manipulates the magnetic properties of atomic nuclei [133]. Nuclear energy levels have "spin states" that point in pre-defined directions, according to the laws of quantum mechanics. The nuclear spin states can be manipulated when an external magnetic field is applied, by excitation of

the spin states using radiofrequency waves with a user-defined frequency that make the nuclei of interest oscillate [133]. After excitation of the nuclear spins, the spins return to a state of thermodynamical equilibrium in a process called relaxation, releasing a nuclei-specific amount of electromagnetic radiation energy. The released radiation energy can be registered, and the nuclei can in this way be identified [134]. NMR spectroscopy can be used to study and quantify a variety of atoms present in biological molecules, such as ^{1}H, ^{13}C, ^{19}F and ^{31}P, and it is also a well-established technique for studying lipids, both structurally and quantitatively [122, 135]. This separates NMR from MR, because NMR allows for total quantification of sample contents. By combining MS and NMR, samples can be analysed both qualitatively and quantitatively.

^{31}P NMR in Phospholipid Studies

NMR can be used in quantitative lipid studies, such as quantifying the total phospholipid content in a sample, by means of phosphorus NMR [136]. Phosphorus-31 (^{31}P) is a naturally occurring NMR active isotope that gives rise to the polarity of head groups of phospholipids [137, 138]. ^{31}P NMR therefore works well for phospholipid quantification because it produces a separate signal for every phospholipid subclass [136]. ^{1}H and ^{13}C can also provide useful data about phospholipids in a sample, but they are less practical for analysis of complex lipid mixtures due to the high number of generated signals – creating very complex NMR spectra.

A significant drawback when working with NMR is the low sensitivity of the technique. Compared to MS, a highly sensitive technique where the sample material can be in concentrations of nM, NMR has a limit of detection in the μM range [139]. When applied as a quantitative tool, NMR can detect either the absolute or relative amounts of individual molecules present in a sample. Before initiating data acquisition, certain settings related to the magnet and spectrometer must be taken into consideration. First, high signal-to-noise levels are the goal of a successful NMR analysis, as the low sensitivity of the technique can produce more spectral noise than other spectroscopic techniques. A common solution is to increase the number of scans and average together the individual spectra [133]. Second, complete proton decoupling during data acquisition is necessary to simplify complex NMR spectra as the number of split peaks, a result of spin-spin coupling, are reduced [140]. Third, complete relaxation of the nuclei involved between each sample scan is required to make sure the nuclei are relaxed before the next pulse of radiofrequency waves are initiated. Finally, in order to quantify the acquired signals, they must be converted to area by means of integration or deconvolution, with the latter method being the preferred approach in crowded spectra [141].

2 Aims

We hypothesise that development of PD is linked to lipids through their metabolism and oxidation, and that this will manifest itself in the brain tissue of diseased individuals or PD zebrafish models. With this in mind, and with access to brain tissue of both zebrafish and human origin, it was of interest to look for PD-related alterations in the phospholipid and fatty acid composition in both types of brain tissue.

Goals:

1. Establish routines for the sampling, and subsequent phospholipid extraction from brain tissue of human and zebrafish origin.
2. Perform Western blot analysis to examine DJ-1 and oxDJ-1 expression levels and acquire ^{31}P NMR and UPLC-HRMS/MS data of control and PD-relevant human and zebrafish brain tissue.
3. Critically assess key differences, as well as extraction and analytical protocol.

3 Materials

3.1 Instruments and Equipment

Table 3.1.1 Instruments and Equipment.

Name	Implementation	Supplier
Amersham™ Protran® 0.45 NC	Western blotting	GE Healthcare
AVANCE NEO600	NMR	Bruker BioSpin
ChemiDoc XRS+ System	Western blot imaging	Bio-Rad
Dionex™ UltiMate 3000 system	UPLC	Thermo Fisher
Epoch Microplate Spectrophotometer	Absorbance readings	BioTek Instruments
FastPrep-24™	Tissue homogenization	MP Biomedicals
Fresco™ 21 Microcentrifuge	Centrifugation	Thermo Scientific
Mini-PROTEAN® 3 Electrophoresis Cell	SDS-PAGE, Western blotting	Bio-Rad
PowerPac™ 200 Power Supply	SDS-PAGE	Bio-Rad
Q Exactive™ Mass Spectrometer	HRMS/MS	Thermo Scientific
Reacti-Vap III	Degassing	Thermo Scientific
Rotavapor R-100	Solvent evaporation	Buchi
Separatory funnel Squibb 50 ml	Lipid extraction	Witeg
Transsonic T460	Sonication	Elma
Vibra Cell	Sonication	Sonics
Whatman™ 3 MM paper	Western blotting	GE Healthcare

3.2 Reagents and Chemicals

Table 3.2.1 Reagents and chemicals used for experiments.

Name	Supplier	Cat. #
10x Tris/Glycine Buffer	Bio-Rad	1610771
10x Tris/Glycine/SDS Buffer	Bio-Rad	1610772
Acrylamide/Bis-acrylamide - 30% solution	Sigma-Aldrich	A3699
Ammonium persulfate (APS)	Sigma Aldrich	248614
Bovine Serum Albumin (BSA)	Sigma	A8806
Bromophenol blue	Sigma	B-5525
CHAPS	Merck	C3023
cOmplete™ Protease Inhibitor Cocktail	Roche Diagnostics	11836153001
d-Chloroform	Sigma-Aldrich	151823
D609	Tocris Bioscience	1437

Dichloromethane (DCM)	Thermo Fisher	75-09-2
Dimethyl sulfoxide (DMSO)	Sigma	D8418
Dipotassium hydrogen phosphate	Sigma-Aldrich	P8281
Dithiothreitol (DTT)	Sigma	D9163
Dried Skimmed Milk Powder	Marvel	-
Ethanol	VWR Chemicals	64-17-5
Ethylendiaminetetraacetic acid (EDTA)	Merck	-
FIPI	Tocris Bioscience	3600
Glycerol	Sigma	G5516
Glycine	Sigma	50046
Guanidium chloride	Alfa Aesar	A13543
Isopropanol	VWR Chemicals	67-63-0
Methanol (hypergrade for LC-MS)	Sigma	1.06035.2500
N, N-Dimethylformamide-d_7 (DMF-d)	Sigma-Aldrich	189979
N, N, N', N'-Tetramethylethylenediamine (TEMED)	Thermo Scientific	17919
Nitrogen	Nippon Gases	7727-37-9
Pierce™ BCA Protein Assay Reagent A	Thermo Scientific	23228
Pierce™ BCA Protein Assay Reagent B	Thermo Scientific	23224
Polysorbate 20 (Tween-20)	-	-
Potassium dihydrogen phosphate	Merck	1.04873.1000
Precision Plus Protein Dual Color Standards	Bio-Rad	1610374
Sodium chloride	VWR Chemicals	27810.295
Sodium dodecyl sulfate (SDS)	Sigma-Aldrich	L5750
Sodium fluoride	Merck	S7920
Sodium orthovanadate	Merck	S6508
SuperSignal™ West Pico PLUS Chemiluminescent Substrate	Thermo Scientific	34580
Triethylamine (TEA)	Sigma-Aldrich	471283
Triethylamine hydrochloride (TEAC)	Sigma Aldrich	90350
Tris-HCl buffer, pH 6.8	Bio-Rad	161-0799
Tris-HCl buffer, pH 8.8	Bio-Rad	1610798
U 73122	Tocris Bioscience	1268

3.3 Buffers and Solutions

Table 3.3.1 All prepared buffers and solutions.

Homogenization buffer

- 10 mM K_2HPO_4
- 10 mM KH_2PO_4
- 1 mM EDTA
- 0.6% (w/v) CHAPS
- 50 mM Sodium fluoride
- 1 mM Sodium orthovanadate
- 1x Protease inhibitor cocktail

CUBO solvent

- 800 mM Guanidium chloride (dissolved in d_7-DMF)
- 75% (v/v) Dimethylformamide (d_7-DMF)
- 25% (v/v) Triethylamine (TEA)

15% Resolving gel

- 15% (v/v) Acrylamide/Bis-acrylamide (37.5:1)
- 380 mM (v/v) Tris-HCl, pH 8.8
- 0.1% (w/v) SDS
- 0.1% (w/v) APS
- 0.04% (v/v) TEMED

4% Stacking gel

- 4% (v/v) Acrylamide/Bis-acrylamide (37.5:1)
- 125 mM Tris-HCl, pH 6.8
- 0.1% (w/v) SDS
- 0.1% (w/v) APS
- 0.1% TEMED

5x SDS sample buffer

- 65 mM Tris-HCl, pH 6.8
- 5% (v/v) SDS
- 20% (vs/v) Glycerol
- 0.2% (w/v) Bromophenol blue
- 250 mM Dithiothreitol (DTT)

Running buffer (SDS-PAGE)

- 25 mM Tris, pH 8.3
- 192 mM Glycine
- 0.1% (w/v) SDS

Transfer buffer (Western blotting)

- 25 mM Tris, pH 8.3
- 192 mM Glycine
- 20% (v/v) Methanol

1x TBS-T

- 1.5 M NaCl
- 100 mM Tris-HCl, pH 8.0
- 0.05% (v/v) Tween-20

Mobile phase A (LC-MS/MS)

- 40% (v/v) Acetonitrile
- 60% (v/v) Water
- 10 mM Ammonium acetate

Mobile phase B (LC-MS/MS)

- 10% (v/v) Acetonitrile
- 90% (v/v) Isopropanol
- 10 mM Ammonium acetate

3.4 Antibodies

Table 3.4.1 Primary and secondary antibodies used for Western blotting.

	Antibody	Type	Supplier	Cat. #
Primary	anti-*PARK7*/DJ-1	Mouse, monoclonal	abcam	ab11251
	anti-*PARK7*/DJ-1	Rabbit, polyclonal	Novus Biologicals	NB300-270
	anti-oxDJ-1 (C106)	Human, monoclonal	Bio-Rad	HCA024
	anti-β-actin	Mouse, monoclonal	Santa Cruz	sc69879
Secondary (all HRP)	anti-penta Histidine	Mouse, monoclonal	Bio-Rad	MCA5995P
	anti-mouse	Goat, polyclonal	Thermo Scientific	G21040
	anti-rabbit	Goat, polyclonal	Thermo Scientific	G-21234

3.5 Zebrafish lines

Table 3.5.1 The zebrafish lines used in experiments.

Name	Background line	Genotype
Tübingen AB	-	Wild type
Uib2000 (Edson *et al.* [142])	Tübingen AB	*PARK7*-/-

3.6 Human Brain Matter

Table 3.6.1 The white and grey human brain tissue used in experiments. PMI; post-mortem interval – time elapsed after the death of an individual.

Disease status	Brain region	PMI	Sex
Healthy*	Brodmann area 9	14h	F
Idiopathic PD	Brodmann area 9	48h	M

* No clinical diagnosis of neurological disease nor pathological evidence of α-synucleinopathy.

3.7 Software

Table 3.7.1 Computer software used for analysis and post-processing of results.

Name	Use
BioRender.com	Illustrations

Bruker TopSpin™ 4.2.0	NMR data analysis & processing
Gen5	Microplate absorption readings
ImageJ	Image processing
ImageLab	Western blot visualization
LipMat script (Jakubec *et al.* [135])	HRLC-MS/MS data processing
MestreNova	NMR spectra figures
Microsoft Office Excel	Data Analysis

4 Methods

The goal of this thesis was to study the total lipid composition in brain tissue, aiming to identify differences in PD and non-PD brains. The methods used spanned zebrafish maintenance, preparation of tissues for lipid extraction, lipid extraction using a modified Bligh & Dyer approach, Western blotting, as well as qualitative and quantitative techniques using ^{31}P NMR and UPLC-HRMS/MS. A project outline can be seen below, in Figure 4.1.

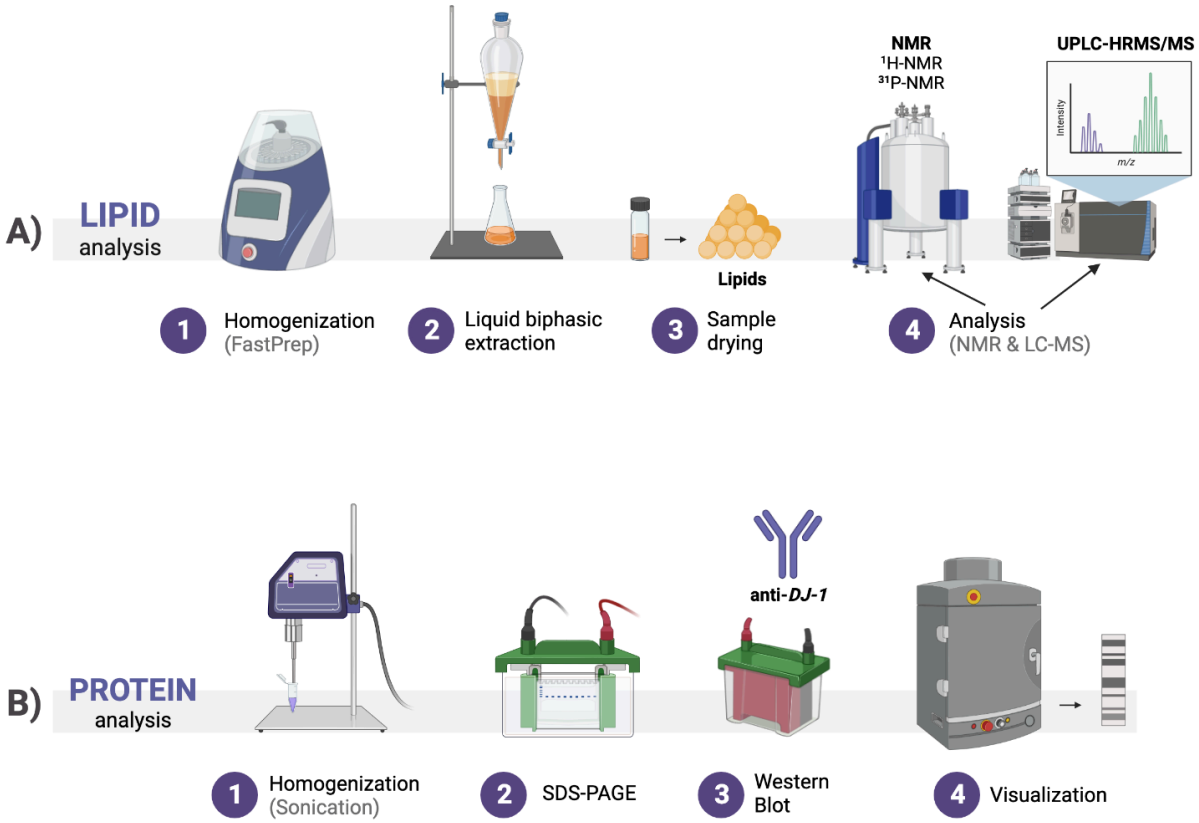

Figure 4.1 **Project outline for this thesis. A)** Brain tissues from human and zebrafish were homogenized, and their lipids were isolated with a biphasic extraction system using dichloromethane, methanol and water, a modified Bligh & Dyer method [115]. The extracted lipid solvent layer was dried under nitrogen gas, and the dried lipids were then separated into samples for UPLC-HRMS/MS, ^{1}H and ^{31}P NMR analysis. **B)** Protein analysis was performed on homogenized brain tissue of human and zebrafish origin by separating the protein bands by SDS-PAGE and subsequently electroblotting them onto a membrane for Western Blot analysis. Lastly, bands stained with antibodies to DJ-1 and DJ-1 oxidized at C106 were visualized. The illustration was made using BioRender.com.

4.1 Zebrafish Brain Tissue

4.1.1 Animal Maintenance

The choice of Zebrafish as a model system has been discussed in section 1.4. Animals used in this study were housed in the Zebrafish Facility located in the Department of Biological Sciences at the University of Bergen. This facility is run in accordance with the European Convention for the Protection of Vertebrate Animals used for Experimental and other Scientific Purposes. Zebrafish were fed twice daily and maintained in recirculating aquarium systems with a water temperature of 26-28°C, with a 14-h day/10-h night light cycle.

4.1.2 DJ-1 KO Zebrafish Line

The Zebrafish lines used for the experiments were a Tübingen AB (TAB) wild type (WT) line, in addition to a previously established TAB-based line where the *PARK7*/DJ-1 gene had been knocked out [142]. In this modified line, CRISPR-Cas9 was used to target exon 1 of the *PARK7* gene to produce the transgenic DJ-1 knockout (KO). Establishment of the DJ-1 KO line and euthanization of adult zebrafish were approved by the Norwegian National Animal Research Authority at Mattilsynet (FOTS ID8039 & ID14039).

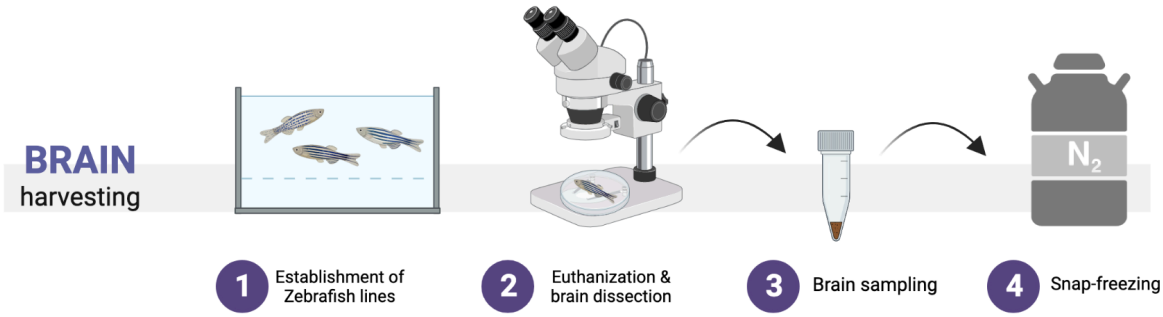

Figure 4.1.2 **Zebrafish brain harvesting.** WT and DJ-1 KO Zebrafish lines were established, and their brains were harvested four months later. The brains were snap-frozen in liquid nitrogen immediately upon harvesting.

4.1.3 Zebrafish Brain Harvesting

Age-matched (four months old) male and female WT and DJ-1 K/O zebrafish were euthanized in a <4°C ice-water slurry. Their brains were immediately dissected out, snap-frozen in liquid nitrogen and stored at -80°C until further use (Figure 4.1).

4.2 Human Brain Tissue

Human brain tissue from both grey and white matter were used in this study (Table 3.6.1). Grey and white matter make up the central nervous system of the brain and they both have different functional roles (Figure 4.2). Grey matter are areas highly concentrated in neuronal cell bodies, making up the outermost layer of the brain [143]. On the other hand, white matter is made up of axons that connect and organize the neuronal networks [143, 144]. As the *substantia nigra* is a large grey matter structure and its neurons are lost as PD progresses – this directly affects the balance of grey matter [5]. The shift in the grey matter balance disrupts the communication within the neural networks of the brain and for this reason, PD can be referred to as a grey matter disease [143].

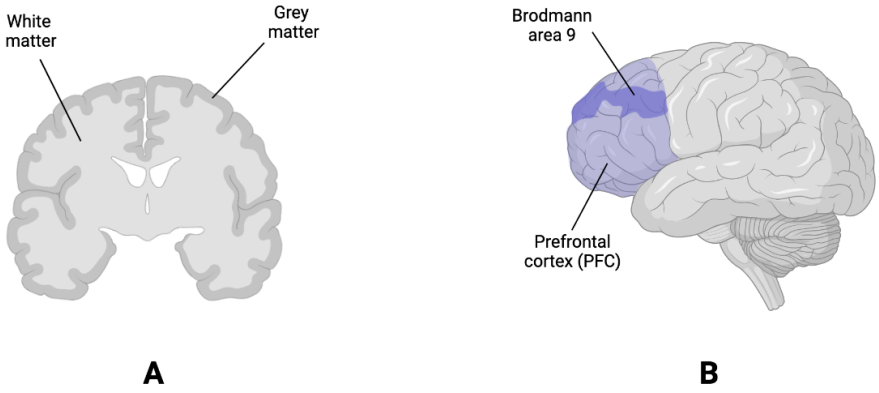

Figure 4.2 **The human brain. A)** The brain is made up of both grey and white matter, and the outermost grey matter layer of the brain is known as the cerebral cortex [145]. **B)** With such a complex cytoarchitecture, the cerebral cortex is divided into 52 numbered Brodmann areas based on their cellular organization [146]. Brodmann area 9 is found in the dorsolateral prefrontal cortex (DL-PFC) and this region plays a significant role in cognitive functioning, organization, working memory and problem solving [146]. The figure was made at BioRender.com.

4.2.1 Human Brain Tissue Sampling

Grey and white human brain tissue samples were provided by the research group of Professor Charalampos Tzoulis at Neuro-SysMed Center, Haukeland Hospital, Bergen. It comprised fresh-frozen brain tissue samples from a male idiopathic PD patient and a neurologically healthy female control (i.e., no clinical diagnosis of neurological disease nor pathological evidence of α-synucleinopathy). Samples were collected at autopsy, snap-frozen in liquid nitrogen and stored at -80°C. The brain sampling for the PD individual and control were both from the dorsolateral prefrontal cortex (Brodmann area 9, Figure 4.2)), and they took place 14 and 48 hrs post-mortem interval time (PMI), respectively (Table 3.6.1).

4.3 Western Blot Analysis

4.3.1 Protein Extraction from Zebrafish and Human Brain Tissue

A homogenization buffer was used to prepare protein extracts from both the zebrafish and human brain tissues. The homogenization buffer contains the detergent CHAPS, which disrupts membranes and thereby solubilizes the membrane proteins. Additionally, the buffer keeps the proteins intact and protected from degradation with the addition of the phosphatase inhibitors EDTA, sodium fluoride (NaF) and sodium orthovanadate (Na_3VO_4) [147, 148]. Additionally, the buffer is supplemented with lipase inhibitors [200 µM FIPI, 1 mM U73122, 1.5 mM D609, 10% (v/v) DMSO].

The protein extracts were prepared using five zebrafish brains or 30-40 mg of grey and white human brain matter. Samples were combined with 150-200 µl of homogenization buffer mixed with a protease inhibitor cocktail. The samples were homogenized by sonication (Vibra Cell) for 30 sec with 5 sec on and 5 sec off at an amplitude of 50%. If debris was still present, an extra sonication step was added to disrupt as much of the tissue as possible. Once homogenized, the samples were incubated on ice for 15 min before they were spun down (Fresco™ 21 Microcentrifuge) at 13 000 rpm for 15 min at 4°C.

4.3.2 Determination of Protein Concentration by BCA Assay

The protein concentration in the supernatant was determined with a standard BCA protein assay, using the Thermo Scientific™ Pierce™ BCA Protein Assay Kit [149]. Triplicate samples were pipetted into a 96-well microplate with 2 µL brain tissue supernatant and 200 µL Pierce™ BCA Working Reagent. Triplicates of bovine serum albumin (BSA) standards with concentrations of 0, 0.25, 0.5, 1.0, 1.5, 2.5 and 5 mg/mL BSA were prepared in the same manner. The 96-well plate was incubated for 20 min at 37°C whilst shaking at 150 rpm. Absorption measurements were then obtained at 562 nm using the Epoch Microplate Spectrophotometer and the data analysis software Gen5. Absorption values were plotted against the known standard BSA concentrations, and this linear function was used to determine the protein concentration in the brain tissue samples.

4.3.3 Sodium Dodecyl Sulphate Polyacrylamide Gel Electrophoresis (SDS-PAGE)

Samples for SDS-PAGE were prepared with 20 µg protein in SDS sample loading buffer. The mixture was thereafter boiled for 5 min at 95°C to denature the proteins. Protein separation of the

samples was performed by SDS-PAGE with a 15% polyacrylamide/bisacrylamide (37.5:1) gel. The gel was run in running buffer for 30 min at 80 V, followed by an hour at 120 V.

4.3.4 Western Blot Analysis

The proteins were electroblotted onto a nitrocellulose blotting membrane (Amersham™ Protran™) in transfer buffer for 1 hr at 120V (4°C). Next, the membrane was blocked in 5% skimmed milk (<1% fat) in TBS-T overnight at 4°C. The blot was incubated for 1 hr at RT with primary antibodies diluted in TBS-T to *PARK7*/DJ-1 (NB300-270 (1:3000) for zebrafish samples, ab11251 (1:500) for human samples), DJ-1 oxidized at C106 (oxDJ-1, 1:100), and β-actin (1:10,000). Following washing in TBS-T for 3x20 min, the membrane was incubated with corresponding HRP-conjugated secondary antibodies anti-penta Histidine (1:1000), anti-mouse (1:5000) and anti-rabbit (1:10,000) for 1 hr at RT. After washing for 2x20 min in TBS-T, protein band visualization was achieved using the SuperSignal™ West Pico PLUS Chemiluminescent Substrate Kit, and subsequently pictures were obtained using the Bio-Rad ChemiDoc XRS+ imaging system and the ImageLab software. Relative quantification of blotted bands was achieved using the software ImageJ (Fiji) by normalizing the strength of the protein bands to β-actin.

4.4 Lipid Extraction

4.4.1 Lipid Isolation by Biphasic Solution Extraction

With access to brain material from both zebrafish and post-mortem human samples, the lipid extraction method had to prove functional for both, especially with respect to the relatively low mass of zebrafish brains. Pilot lipid extraction experiments were carried out with different amounts of zebrafish brains to determine the mass needed to obtain a decent NMR spectrum, and ultimately 60 mg of brain tissue provided sufficient results. Lipids were extracted using a multi-step extraction approach, a modified version of the Bligh & Dyer method where instead of the traditional chloroform-based extraction procedure, chloroform was replaced with dichloromethane (DCM) [115, 150]. Compared to chloroform, DCM minimizes the chemical degradation of lipid species [112]. Furthermore, triethylammonium chloride ions (TEAC) were added as a means of aiding the acidic phospholipids present in the upper inorganic phase to migrate into the lower organic phase [114]. The triethylammonium cation is lipophilic and association with an anionic lipid therefore increases its solubility in the organic phase [115, 150, 151].

First, brain samples were thawed on ice before being resuspended in a cooled (4°C) organic extraction mixture (3:1 (v/v) DCM/methanol, 0.5 mg/mL TEAC). Brains were crushed with FastPrep-24™ for 1-2 x 20s at 6.0 m/s, using four zirconium oxide ceramic beads (1.4 mm, VWR®) designated for soft tissue. Thereafter, the volume was increased to 5 mL using the same organic extraction mixture. Next, the sample was vortexed till homogenized and transferred to a glass separatory funnel. The concentration of methanol was raised to 62.5% with the addition of 5 mL methanol. A biphasic solution was achieved by adding 5 mL MilliQ-water (3:1 non-organic/organic), gently mixing the solvents together and incubating the solution for 1-2 min. One phase was re-formed by gently mixing in 5 mL DCM, and this solution was then incubated for 20 min at RT. Thereafter, another 5 mL of DCM was added (55% (v/v) total DCM), and two phases were formed. The lower organic layer containing the lipids was collected in an Erlenmeyer flask. This process of "washing" with DCM and collecting the lower layer was repeated 5x to increase the yield of the lipid extraction process. The extracted lipid fractions were made uniform with a few drops of isopropanol.

4.4.2 Drying and Sampling for NMR and UPLC-HRMS/MS Analysis

The Rotavapor R-100 was used to gently evaporate the organic DCM layer and isolate the lipids. The organic layer was moved to an evaporating flask which was placed in a water bath at 40°C. After initiating the drying process at 500 mBar, the pressure was gradually lowered to avoid abrupt boiling by keeping the solvent right below its boiling point. By steadily lowering the pressure, the boiling point for the solvent was also decreasing, causing the solvent to boil and slowly evaporate. Once reaching 40 mBar, the pressure was kept constant for 1 hr till completely dry. The lipids were resuspended in a few mL of DCM and LC-MS grade methanol (3:1, v/v). To dissolve as much of the lipids as possible, the flask was swirled multiple times and placed on ice for 15 min at 4°C whilst shaking (100 rpm). The solution was then split into three glass Reacti-Vials; 100 µl for LC-MS, 250 µl for ^{1}H-NMR and the rest (the majority, approx. 1.2 mL) for the least sensitive ^{31}P-NMR sample. All the samples were then degassed under nitrogen gas (Reacti-Vap III) for 1.5 hrs till completely dry. For the ^{31}P-NMR sample, only 450 µl was dried at a time to avoid the lipids drying too high up on the walls of the glass vial. This allowed for use of less solvent for the upcoming resuspension. The dried lipids were stored at -80°C till further use.

4.5 ^{1}H- and ^{31}P-NMR

4.5.1 Preparation of ^{1}H and ^{31}P NMR samples

Two types of NMR, ^{1}H and ^{31}P, were used in this project. Dried lipids for ^{1}H and ^{31}P NMR analysis were resuspended in 450 µl d-Chloroform and CUBO solvent, respectively. Once dissolved, the d-Chloroform sample was vortexed and directly transferred to an NMR glass tube. The CUBO sample was vortexed before being spun down (Fresco™ 21 Microcentrifuge) for 2 min at 14,800 rpm (4°C) to remove any salts or brain tissue debris. Subsequently, the supernatant was transferred to an NMR glass tube. Both the d-Chloroform and CUBO samples were thereafter immediately placed in the NMR machine (Bruker BioSpin NEO 600). In total, ten individual samples were analysed by NMR, four human and six zebrafish brain samples. For each sample, one ^{1}H and one ^{31}P spectrum were acquired.

4.5.2 Solution-Phase ^{1}H and ^{31}P NMR

Data acquisition for ^{1}H and ^{31}P NMR was achieved using a Bruker BioSpin NEO600 spectrometer equipped with a QCI-P CryoProbe operating at 298 K. ^{31}P spectra were acquired with inverse-gated decoupling of ^{1}H with a transmitter frequency of 242.91 MHz, apart from the second nuclei (^{1}H) acquisition which was irradiated and decoupled at 600.07 MHz. A presentation of the most important NMR parameters used for data acquisition are listed in Table 4.5. The ^{1}H spectra were all acquired at 600.07 MHz.

Table 4.5 NMR parameters used for ^{1}H and ^{31}P NMR.

Parameter	^{1}H NMR	^{31}P NMR	Description
Pulse program	noesy1d	zgig	Depends on the nuclei of interest (^{1}H or ^{31}P), and desired properties of data generated.
Number of scans	16	4096	^{31}P is less sensitive and more scans are needed.
Spectral width (ppm)	19.8388	7.9167	Frequency range where signals can be observed. Depends on the type of nuclei.
Recovery delay (sec)	10	6	Pulse delay between each scan; set high to allow full relaxation.

Acquisition time (sec)	2.7525120	0.5324800	Time needed after pulse for signal-detection. Too high results in too much spectral noise.
Size of FID (Hz)	65536	2048	Total size of processed data, determined by acquisition time.
Pre-scan delay (µsec)	40	18	Time delay before data points are sampled.

4.5.3 ^{31}P NMR Spectral Analysis

For this study, NMR was used mostly as a quantitative, but also qualitative tool. Spectral peaks would indicate the presence of certain phospholipids and sterols, and by comparing the area under each peak to each other, the relative quantity of specific lipids in the sample could be determined. With the release of TopSpin 4.2.0 (Bruker), a novel machine learning based deconvolution algorithm developed to work on one-dimensional ^{1}H spectra was introduced with the command "mldcon" [141]. Topspin 4.2.0 was therefore chosen to process and deconvolute the ^{1}H and ^{31}P NMR data.

First, the ^{31}P spectra were calibrated by setting the most abundant peak in the sample, phosphatidylcholine (PC), to 0 ppm. The spectra were then deconvoluted using the command "mldcon". The results were mathematically reconstructed spectra, where each peak, either manually picked or identified by the algorithm, was expressed as pseudo-Voigt functions, i.e., linear combinations of Gaussian- and Lorentzian curves. In addition, the algorithm provided a list containing the ppm-values of the peaks and their areas. Subsequently, this list was opened in Microsoft Excel for further processing where the amount of each lipid was relatively quantified. Assigning the peaks to specific phospholipids and sterols was done using previously published work [135, 152]. As the deconvolution algorithm is suited for proton spectra, the ^{31}P spectra were handled differently. An overview of the deconvolution process, including the visual "mldcon" command output and the additional processing for the ^{31}P spectra is shown in Figure 4.5.

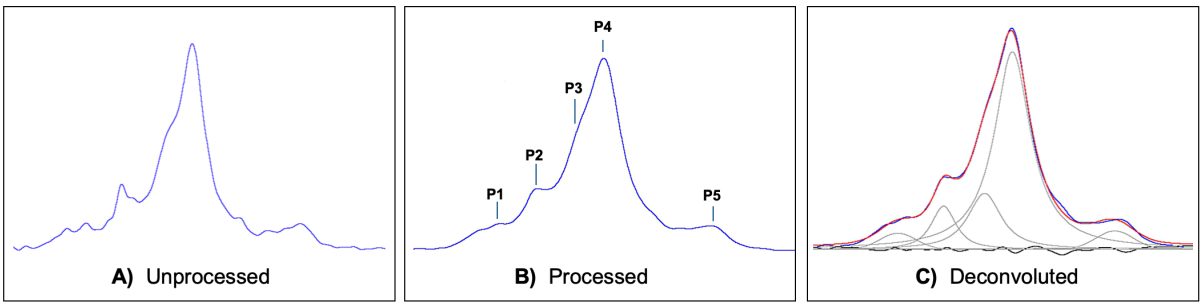

Figure 4.5.3 Example of ^{31}P machine learning deconvolution (mldcon) in Bruker TopSpin 4.2.0. A) The deconvolution algorithm was developed for ^{1}H spectra, so the ^{31}P spectrum was processed to make it easier for the algorithm to handle. Exponential line broadening to reduce the signal-to-noise ratio was executed using the command "efp" with the line broadening (lb) parameter set to 3.0 Hz. The command "abs" was then run to correct the baseline. **B)** Once the spectrum was processed, a peak list was created by manually selecting relevant peaks for optimal accuracy. Finally, "mldcon -f -pp" was run. Parameters "-f -pp" were used to force ("-f") the ^{1}H deconvolution command ("mldcon") to run on a ^{31}P spectrum, using the peaks from the established peak list ("-pp"). **C)** Results were presented in a deconvolution visualization window, displaying the original input spectrum (blue), areas of the single peaks (grey), their sum (red), and the residuals (differences between the initial and reconstructed spectrum, in black). The mldcon command was developed by Schmid *et al*. [141], and released along with Bruker TopSpin 4.2.0.

4.6 UPLC-HRMS/MS

4.6.1 Preparation of UPLC-HRMS/MS samples

To study the global lipid profile in human and zebrafish brain samples, a combination of ultra-performance liquid chromatography (UPLC) and high-resolution mass spectrometry (HRMS/MS) was used. Accurate mass UPLC-HRMS/MS analysis was performed using a Dionex UltiMate 3000 liquid chromatography system (UPLC) coupled with a QExactive mass spectrometer (HRMS/MS) from Thermo Fisher. An electrospray ionization source (H-ESI) was used to ionize the molecules and evaporate the solvents. Dried brain lipid samples from both human and zebrafish origin were reconstituted in 150 µL of a methanol:ethanol (1:1, v/v) solution. The samples were then vortexed for 20 sec and subsequently sonicated in an ultrasonic water bath (Transsonic T460) for 5 min. Thereafter, the samples were centrifuged (Fresco™ 21 Microcentrifuge) at 12 000 *x g* for 10 min (RT) to precipitate out any salts or brain tissue debris left over from lipid extraction. The supernatant (130 µL) was collected and directly injected on the UPLC-HRMS/MS.

4.6.2 Ultra Performance Liquid Chromatography (UPLC)

Analytes were separated on an Aquity UPLC HSS C18 (2.1 x 100 mm, 1.8 µm, Waters, USA) column, using an Aquity UPLC HSS C18 (2.1 x 5 mm, 1.8 µm, Waters, USA) as guard column.

Column temperature was set to 55°C with a flow rate of 0.3 mL/min. The injection volume was 5 µL and the total runtime was 20 min. Mobile phase A consisted of acetonitrile:water (40:60, v/v) and mobile phase B of acetonitrile:isopropanol (10:90, v/v), both buffered with 10 mM ammonium acetate. Separation of individual lipids based on their physical-chemical properties was achieved using a multistep gradient of A and B. Mobile phase B composition was 40-70% over 3 min, 70-80% over 9 min, 80-100 for the next 3 min, increasing to 100% over 2 min, followed by 3 min of column equilibration at 100-40%.

4.6.3 High Resolution Mass Spectrometry (HRMS/MS)

Ions were monitored in both positive and negative Full MS/data-dependent Top 5 (ddMS^2-top5) mode to automatically switch between one full scan MS and MS/MS acquisition. The full MS scan range was 300-2000 *m/z* with a resolution of 140,000 at *m/z* = 200. The initial peaks obtained in the M1 spectrum were fragmented using a normalized collision energy of 24 to create a second MS2 detector spectrum. Using an isolation window of 0.4 *m/z* with a resolution of 17,500 and the dynamic exclusion parameter set to "auto", the MS2 spectrum was collected. Other MS parameters were automatic gain control (AGC) target of 2E5, maximum injection time 200 seconds, sheath gas flow rate 50 (arbitrary units), aux gas flow rate 13 (arbitrary units), sweep gas flow rate 3 (arbitrary units), spray voltage 2.5 kV, capillary temperature 263°C, and S-lens RF level 90.

4.6.4 Data-Processing by Iterative Exclusion

ddMS^2-top5 analysis was repeated three times on the same sample, excluding previously selected precursor ions in each sequential analysis. In the first injection, the five ions with the highest intensity were selected for fragmentation. Using an IE script in RStudio (software) [135], an exclusion list (IE1) was created and applied for the second injection. During the second injection, all ions listed (IE1) were excluded from the analysis. The process was repeated, and a second exclusion list (IE2) was created for the third injection. In this way in each sequential injection, unique precursor ions were fragmented and all ions above a certain intensity were selected [130]. Six zebrafish and four human brain samples were analysed for each mode (positive or negative), resulting in a total of 60 UPLC-HRMS/MS runs.

4.6.5 Lipid Identification by LipMat Scripts

With the method described above applied to brain samples of human (two grey matter samples, two white matter samples) and zebrafish origin (three controls, three DJ-1 knockouts), a large amount

of data was generated. To identify the m/z rations and assign them to specific lipids, a combination of published work and one of the most widely used lipid-specific databases, Lipid MAPS, were used, [153]. Lipid MAPS hosts several databases in which lipid structures are listed according to their nomenclature and classification. The identification process was done automatically on all obtained MS data, using the LipMat script developed by Jakubec *et al*. [135]. Each identification is accompanied by a quality factor, guiding the inclusion or exclusion of a given signal for further analysis and interpretation. The retention times obtained from the LC are also considered and compared to MS elution peaks in order to determine the presence of lipid species.

The output of these scripts are lipid fragmentation figures with identified lipid species, a table of the identified lipid species and their respective scores, and semi-quantitative identification of the relative abundance of fatty acid moieties attached to each broad lipid class excluding sterols (i.e., sphingomyelins, phospholipids, diacylglycerols, triglycerols, monoglycerols). For this thesis, only lipids identified in negative mode (phospholipids) were analysed. Furthermore, in order to perform semi-quantitative analysis, only lipids fragments from an unfiltered list, IE0, was used because it was not affected by iterative exclusions, and IE0 therefore contained all of the most abundant lipid species. To account for the lack of data filtering, the figures of identified lipid species were manually assessed, and lipid figures with less than three identified fragments and/or lacking identification of fatty acyl fragments were excluded from the semi-quantitative analysis.

5 Results

5.1 Protein analysis of Human and Zebrafish Brain Samples

The hypothesis of this thesis is that the development of PD is linked to lipids through their metabolism and oxidation, and that this will manifest itself in the brains of diseased individuals or PD zebrafish models. For this reason, it was of interest to look for PD-related alterations in the FA and phospholipid profile of PD-diseased relative to healthy brain tissue. Brain tissue originating from both human and zebrafish were used for this purpose. For the human brain samples, grey and white matter samples were extracted from Brodmann area 9 of the DL-PFC, from both a healthy control and a PD brain (Table 3.6.1). The zebrafish brains were harvested from four months old zebrafish, from both a wild type (WT) line and a genetically modified DJ-1 knockout (KO) zebrafish line, functioning as a PD model.

5.1.1 Western Blot Analysis of DJ-1 KO Zebrafish Brain Tissue

Loss of function of DJ-1 due to its mutation and hyper-oxidation is associated with familiar and sporadic PD, respectively [99]. More detailed information on this topic can be found in section 1.4.2. Because the DJ-1 KO zebrafish line was to be used as a PD-model, protein analysis was performed to confirm the absence of DJ-1 expression in the KO zebrafish line. Protein lysates were prepared using brains from WT and DJ-1 KO zebrafish, and Western blotting was performed using an antibody to DJ-1 (refer to section 4.3 for experimental details). The Western blotting confirmed the presence of DJ-1 in the WT zebrafish, and its absence in the DJ-1 KO line (Figure 5.1.1).

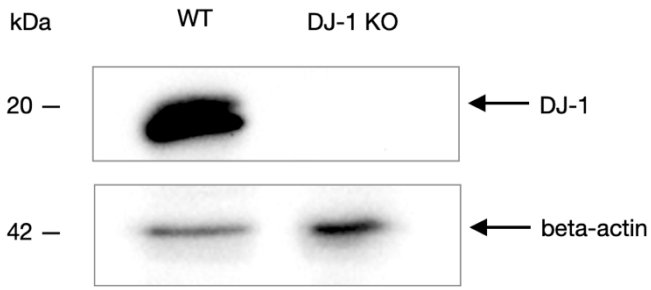

Figure 5.1.1 Western blot analysis of protein lysates of brain tissue from WT and DJ-1 KO zebrafish. Protein lysates were prepared using five brains of WT or DJ-1 KO zebrafish per sample, and subsequent SDS-PAGE and Western blot analysis were performed. The membrane was incubated with an antibody to DJ-1 or β-actin, followed by the appropriate secondary antibodies. β-actin was used as a loading control.

5.1.2 Western Blot Analysis of Healthy and PD Human Brain Tissue

With access to post-mortem human DL-PFC brain tissue from both a female control and a male PD individual (Table 3.6.1), a Western blot analysis was performed in the same manner as for the zebrafish brains, using both an antibody to DJ-1, and an additional antibody recognizing an oxidized form of C106 of DJ-1 (oxDJ-1). Among all the residues of DJ-1, C106 is assumed to be the residue most sensitive to oxidation, and quantifying the amount of oxDJ-1 can thereby function as a sensor for oxidative stress, as described in section 1.4.2 [107]. Both white and grey matter of the control (n = 1) and PD (n = 1) human brain samples were analysed and amounts of DJ-1 and oxDJ-1 were quantified by normalising their relative band intensities to the intensity of their respective β-actin (control) bands (Figure 5.1.2).

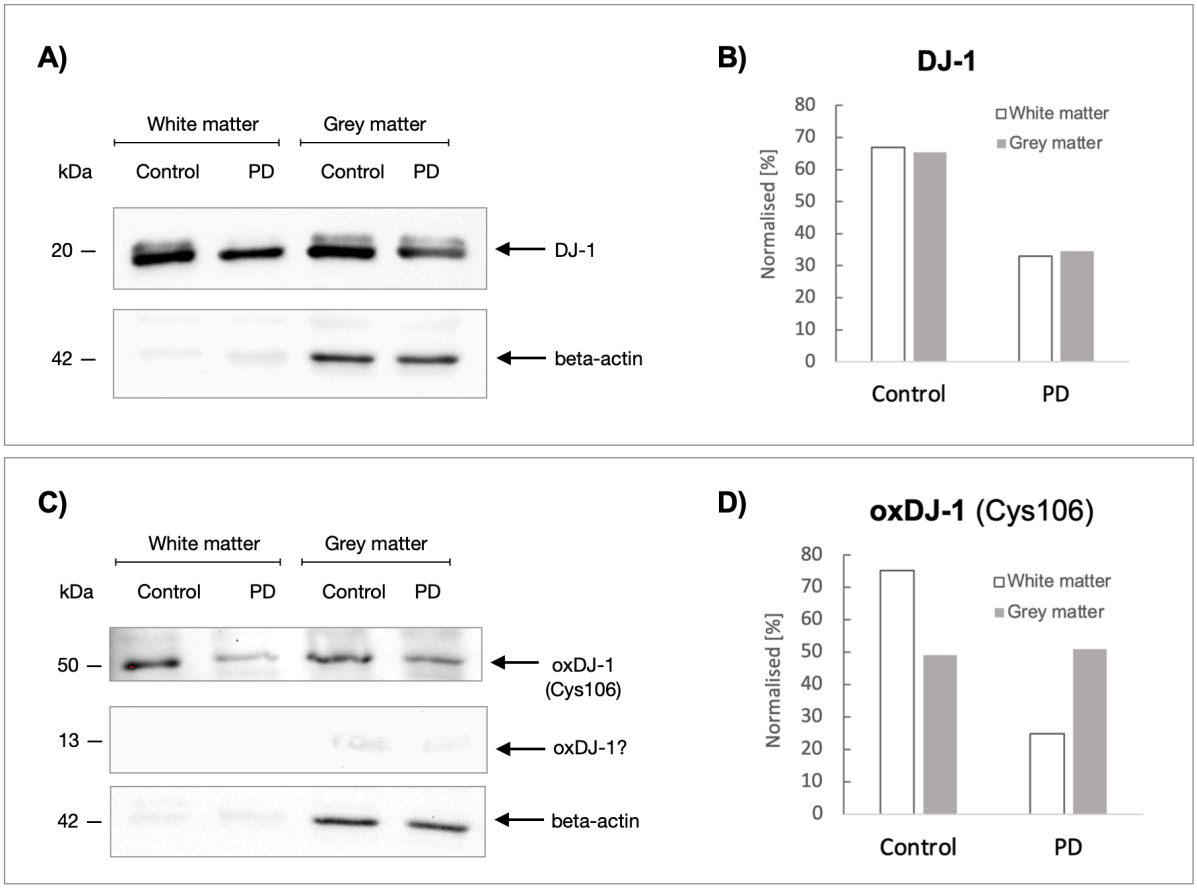

Figure 5.1.2 Quantification of DJ-1 and oxDJ-1 in grey and white matter of control and PD human brains. Protein lysate samples from white and grey matter of a healthy individual and an individual with PD were analysed by Western blotting before subsequently probing with antibodies towards **(A)** DJ-1 and **(C)** oxidized C106 of DJ-1 (oxDJ-1). β-actin was used as a loading control. Relative band densities are presented as **(B)** DJ-1 and **(D)** oxDJ-1 normalized to β-actin, according to their respective β-actin-levels. Considering the bands present at 13 kDa in **C)**, their weak presence proved challenging to quantify and they were therefore not included in the bar plot **(D)**. ImageJ was used for band quantification.

A notable reduction could be seen in DJ-1 levels in both white (-33.9 percentage points (pp)) and grey (-30.9 pp) matter of the PD brain compared to the control brain. The bands of DJ-1 had the expected size of 20 kDa, appearing as two overlapping bands [104]. For oxDJ-1, Western blot analysis suggested a notable reduction of 50.3 pp in the white matter of the PD individual when compared to the control brain. On the other hand, the levels of oxDJ-1 in the grey brain matter remained unchanged with a slight increase of 1.7 pp in the PD brain compared to the control (Figure 5.1.2). Furthermore, the bands of oxDJ-1 appeared at slightly above 50 kDa, suggesting potential SDS-resistant DJ-1 dimerization [154]. Notably, bands barely noticeable to the naked eye appeared at 13 kDa, suggesting the presence of what could be cleaved or partially fragmented DJ-1 [155].

5.2 Phospholipid Identification and Total Quantification by ^{1}H and ^{31}P NMR

The lipid analysis in this thesis had sub goals; 1) to assess the approach of using a modified Bligh & Dyer lipid extraction procedure to obtain an accurate phospholipid profile of brain matter samples of human and zebrafish origin, and 2) to study the differences observed between healthy and PD brain tissue in hopes of better understanding the role of lipids in PD pathogenesis.

The lipids were initially extracted using a modified Bligh & Dyer lipid extraction where chloroform was replaced by DCM [115]. The lipid solvent layer was evaporated using nitrogen gas, and the lipids were subsequently resuspended in CUBO solvent for ^{31}P NMR analysis (refer to methods section 4.5 for experimental details). The CUBO (Culeddo-Bosco) solvent was used due to its stability and monophasic behaviour, combined with its excellent ability to disperse the resonances of the ^{31}P signals [156]. The extracted lipids were analysed by ^{1}H and ^{31}P NMR spectroscopy, where ^{31}P NMR was used to identify and quantify the phospholipid profile found in the human and zebrafish brain samples. ^{1}H NMR spectra are very quick (minutes) to accumulate, due to the inherent sensitivity of hydrogens, but produces crowded spectra. They nonetheless served a purpose in assessing the general sample quality in this thesis (Figure 9.2 displays an example of a ^{1}H spectrum). ^{31}P and ^{1}H NMR spectra were all acquired using a Bruker BioSpin AVANCE NEO600 spectrometer, fitted with a cryogenically cooled probe that ensured enhanced sensitivity and therefore reasonable experimental times (less than 8 hrs per ^{31}P lipid sample). To relate NMR ^{31}P lipid signals to lipid abundances, a neural network-based deconvolution tool implemented in Bruker TopSpin 4.2.0 was used [141], allowing total phospholipid identification and quantification of the brain lipid samples.

5.2.1 Determination of Necessary Brain Mass for NMR analysis

Compared to the human brain, the zebrafish brains are much smaller, and it was therefore necessary to determine how many brains were required for the lipid extraction to obtain sufficient signal-to-noise ratios for NMR analysis, considering the sensitivity of the method. Weighing the WT and DJ-1 KO zebrafish brains showed a notable difference in mass, where the weight of DJ-1 KO zebrafish brains was reduced by 33%, with an average weight of 2.70 mg (n = 41), compared to the average weight of the brains of WT zebrafish, 4.03 mg (n = 51).

With access to limited amounts of adolescent/adult (four months old) zebrafish, producing datasets that could be used to perform statistical tests was a practical goal. To this end, we aimed to perform the WT and DJ-1 brain lipid extraction procedures in at least triplicates. ^{1}H NMR analysis performed on zebrafish brains by van Amerongen *et al.* suggested a weight of 70 mg (10 adult brains) proved sufficient, so a pilot zebrafish brain lipid extraction experiment was performed to determine the mass needed for ^{31}P NMR analysis [157]. Extracting the lipids from 60 mg of zebrafish brain matter provided decent signal-to-noise ratios (notable peaks above the baseline "noise floor") for ^{31}P and ^{1}H NMR spectra, and this was therefore set as the minimum requirement of brain matter for successful NMR analysis, using the methodology and equipment available for this project. The ^{31}P spectra can be seen in Figure 5.2.1a.

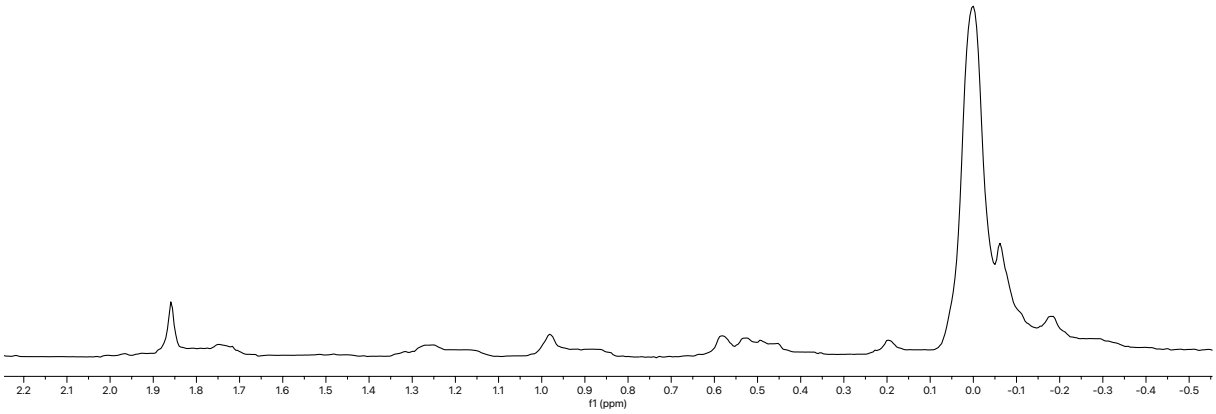

Figure 5.2.1a ^{31}P NMR spectrum of zebrafish brain lipids extracted using 60 mg brain matter. Brain lipids from WT zebrafish were extracted using a modified Bligh & Dyer approach, using a ternary solvent system consisting of DCM, methanol, and water [115, 135]. Extracted lipids were resuspended in CUBO (Culeddo-Bosco) solvent prior to ^{31}P NMR analysis. The data was acquired at 600 MHz, using a cryogenically cooled probe and 4k scans. The recycling delay and dwell time summed to 6.5 sec, and the total experimental time was approximately 7.5 hrs. MestreNova was used to present this figure.

5.2.2 Brain Lipid Extraction from WT and DJ-1 KO Zebrafish

In order to reach the goal of 60 mg brain matter per experiment, we were forced to use all available fish raised for this project. For many experiments on zebrafish, it is desirable to use male fish only, as hormonal cycles may affect signalling events and therefore biological results in female fish. However, due to material shortages, mostly male zebrafish were used, but with an addition of a fixed number (2) of female brains to avoid introducing a large difference in male/female brain ratio. This allowed the triplicate experiments to be performed with an average of 55.5 mg (19 brains; 17M, 2 F) of brain matter from the DJ-1 KO zebrafish, and 68 mg (17 brains; 15M, 2F) for the WT zebrafish. One WT and one DJ-1 KO ^{31}P NMR experiment (the two other WT and DJ-1 KO experiments can be found in appendix Figure 9.1) is displayed in Figure 5.2.2a to highlight the differences seen in the WT and DJ-1 KO spectra.

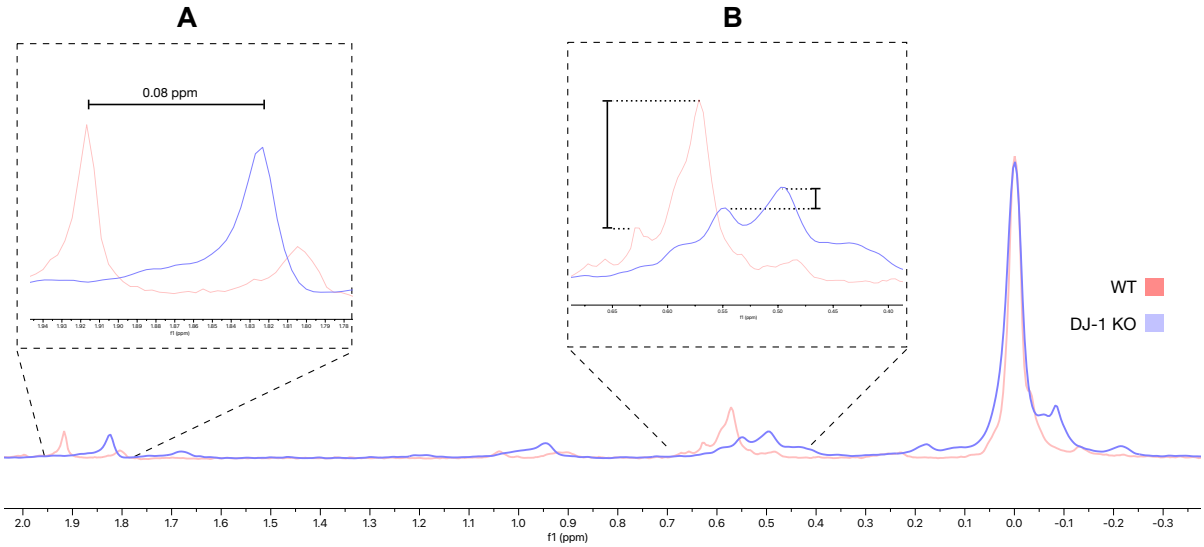

Figure 5.2.2a ^{31}P NMR spectra of brain lipids extracted from WT and DJ-1 KO zebrafish. The Figure displays two of six (3 WT, 3 DJ-1 KO) lipid extractions performed on brain matter originating from WT zebrafish, and a modified DJ-1 KO zebrafish line, functioning as a PD model. Brain lipids originating from 68 mg (17 brains; 15M, 2F) WT and 55.5 mg (19 brains; 17M, 2 F) DJ-1 KO zebrafish brain tissue were extracted and resuspended in CUBO solvent before ^{31}P NMR analysis was performed. PC, the highest peak, was set to 0 ppm. **A)** The chemical shifts of peaks in the WT spectra were noticeably shifted ~0.08 ppm to the left compared to the ppm values seen in the DJ-1 KO spectra. **B)** Differences could also be seen in the height of the peaks, with the WT spectra displaying a relatively tall peak at ~0.575 ppm, compared to the small respective peak (~0.5 ppm) in the DJ-1 KO sample. The figure was made using MestreNova.

As seen in Figure 5.2.2a, when setting the highest peak (PC) to 0 ppm, the chemical shift values for the peaks were different in the WT spectra when compared to the peaks seen in the DJ-1 KO spectra. With the two spectra superimposed, differences could be seen, such as a tall peak in the WT spectra

at ~0.575 ppm, which appeared to be smaller than the respective peak in the DJ-1 KO. However, trying to identify the phospholipid class by matching the spectral ppm value to known ppm values typically seen when dissolving phospholipids in CUBO, produced a challenge which proved to be consistent across all obtained zebrafish ^{31}P spectra. Phospholipid assignment was performed as shown in Figure 5.2.2b, in line with previously published work [135].

Faulty CUBO Solvent Sabotaged Zebrafish ^{31}P NMR Experiments

While all ^{31}P spectra appeared erroneous, all the ^{1}H spectra looked as expected – suggesting an error in only the samples analysed by ^{31}P NMR, and not with the lipids themselves. The only difference between the lipids analysed by ^{1}H and ^{31}P NMR was the solvent they were resuspended in, respectively d-Chloroform and CUBO. The CUBO recipe used in this thesis was matched to the original CUBO recipe, showing that the correct volumes of DMF and TEA had been used, but the amount of guanidium chloride was 1000x less concentrated than the original formulation from 1997 [156]. As the lipids from the zebrafish samples had already been extracted, these ^{31}P NMR results were the only ones to work with to identify their phospholipid profiles. An unsuccessful attempt was made to recover the ^{31}P zebrafish NMR samples with the addition of a concentrated guanidium chloride solution, but by then the lipids had already been significantly degraded. These spectra were therefore excluded from further analysis, but a representative example can be found in the appendix (Figure 9.3).

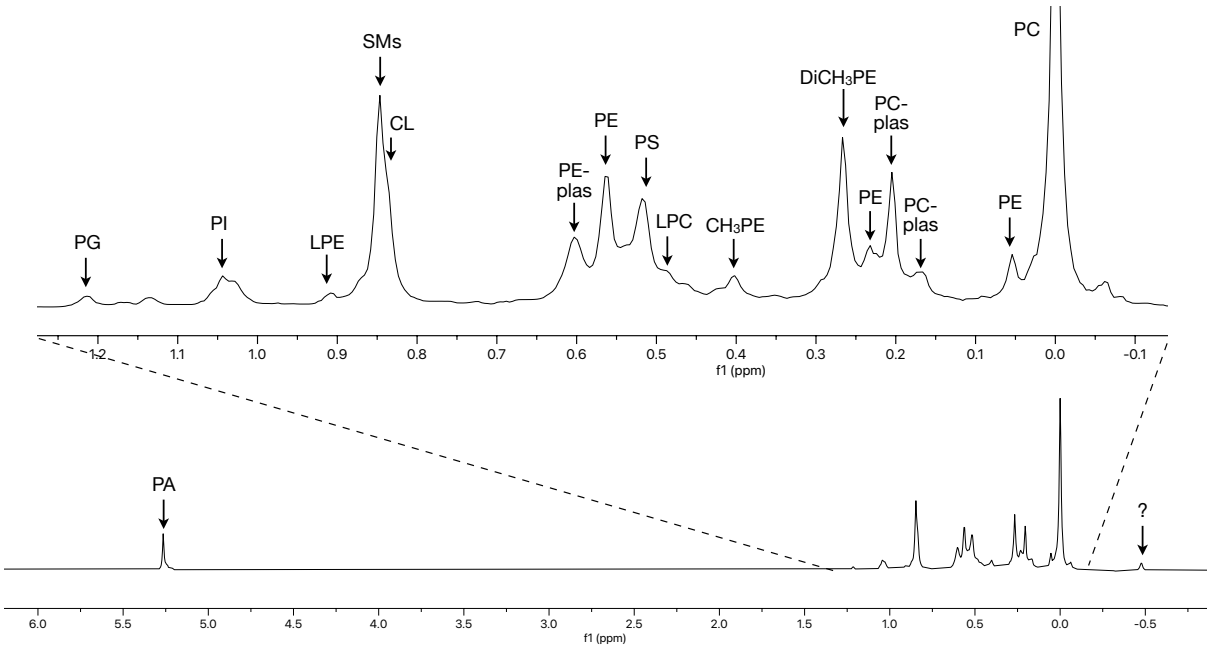

Figure 5.2.2b **^{31}P NMR phospholipid assignment with lipids dissolved in CUBO solvent**. A ^{31}P NMR spectrum obtained after lipid extraction on 73.8 mg human brain white matter of an individual with PD is used as the reference. The extracted lipids were dissolved in CUBO, using the original recipe by Bosco *et al.* [156], and the largest peak, PC, was set to 0 ppm. The figure was made using MestreNova. PG, phosphatidylglycerol; PI,

phosphatidylinositol; LPE, lyso-phosphatidylethanolamine; SMs, sphingomyelins; CL, cardiolipin; PE-plas, PE-plasmalogens; PE, phosphatidylethanolamine; PS, phosphatidylserine; LPC, lyso-PC; CH_3PE, methylated PE; DiCH_3PE, dimethylated PE; PC-plas, PC plasmalogens; PC, phosphatidylcholine; PA, phosphatidic acid.

Lipid extractions were performed on human brain samples to assess the suspicions related to the CUBO solvent, and they confirmed the lack of guanidium chloride in CUBO as the reason for phospholipids showing unreasonable ppm values in the zebrafish brain samples (Figure 5.2.2a). The result can be seen in Figure 5.2.2c, showing how the addition of sufficient amounts of guanidium chloride to the CUBO solvent is necessary for correct dispersion of the ^{31}P peaks.

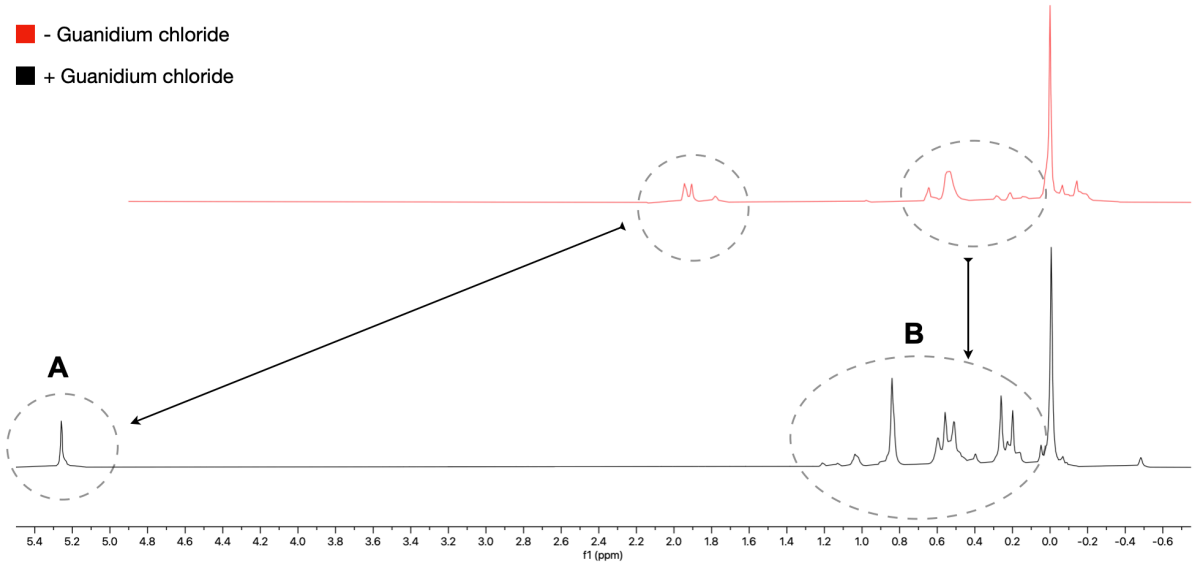

Figure 5.2.2c PD human brain ^{31}P NMR sample with incorrect and corrected CUBO solvent (-/+ guanidium chloride). Both samples originate from two lipid extractions performed on a PD human brain, with an initial 95 (red) or 73.8 mg (black) white matter from DL-PFC. **A)** Spectra are overlined across the same ppm axis, showing different chemical shifts for what is believed to be phosphatidic acid (PA). **B)** Phospholipid separation also differs across the ppm scale, with the ^{31}P spectra belonging to the sample with added guanidium chloride (black) showcasing greater dispersion of the peaks. PC was set to 0 ppm. The figure was made using MestreNova.

5.2.3 Brain Lipid Extraction from a Control and PD Human Brain

^{31}P NMR analysis was also performed on lipids extracted from the human brain tissue, including grey and white matter from Brodmann area 9 of the DL-PFC, from both a healthy female control and a male PD brain (Table 3.6.1). As white and grey matter are different types of brain tissue, their protein and lipid composition differ (go to section 4.2 for details). For this reason, the white matter lipid sample from the control brain was only compared to the other white matter sample from the PD brain, and similarly for the grey matter lipid samples.

The acquired ^{31}P NMR spectra of lipids extracted from DL-PFC grey matter from both a healthy control brain (n = 1) and the brain of an individual with sporadic PD (n = 1) can be seen in Figure 5.2.3a. A high degree of similarity in ^{31}P signal separation across the ppm axis can be seen when comparing the control and the PD sample, indicating similarities in the phospholipid composition in brain tissue from grey matter.

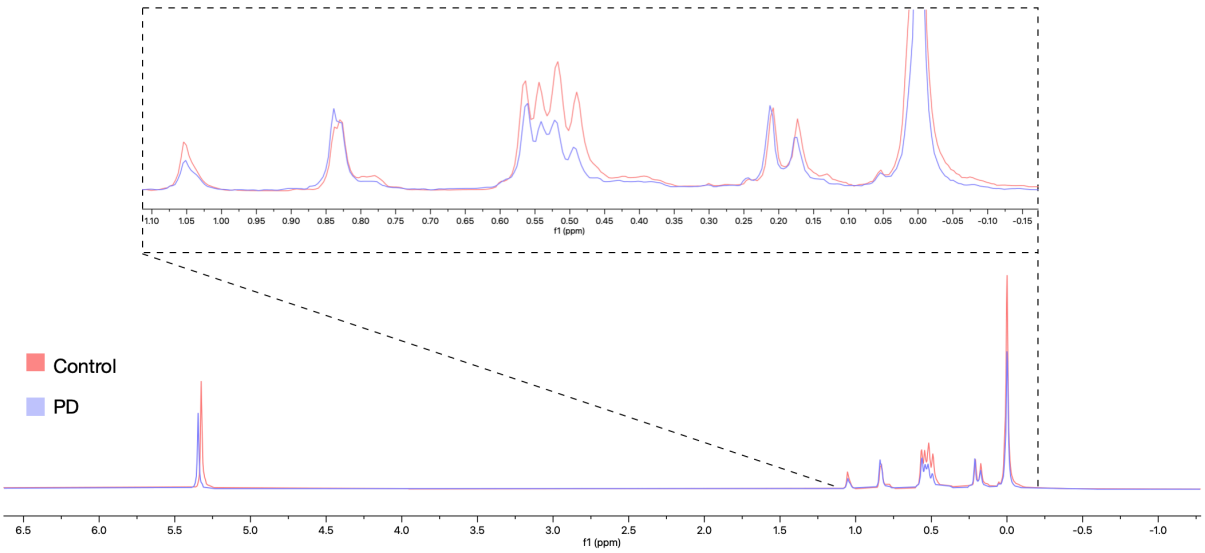

Figure 5.2.3a ^{31}P NMR spectra of lipids extracted from grey matter tissue from a control and PD human brain. Lipids were extracted from DL-PFC white matter of a control (84 mg, n = 1) and a sporadic PD individual (83 mg, n = 1) before they were resuspended in CUBO solvent. The largest peak, PC, was set to 0 ppm. The figure was made using MestreNova.

In order to quantify the ^{31}P signals seen in the control and PD spectra, the command "mldcon" was used in Bruker TopSpin 4.2.0 to deconvolute the spectra using machine-learning algorithms (see section 4.5.3 and its corresponding Figure for details). Identification and assignment of phospholipids was done according to previously published work, as shown in Figure 5.2.2b [135, 152]. A wide variety of phospholipids were identified, including PC, PE, PS, SM, PC-plas, LPC, PI, CL, DiCH$_3$PE, CH$_3$PE, and PG. PA, phosphatidic acid, was also identified, typically functioning as a measure of sample degradation in lipid analysis where high PA contents indicate a higher level of lipid degradation [158]. Figure 5.2.3b displays the total phospholipid composition identified in the grey matter samples of the human control and sporadic PD brain. The results show clear differences in the phospholipid composition, with altered levels of PC, PE, PA, PS, SM, PC-plas, LPC, PI and CL when comparing the control to PD brains. Furthermore, DiCH$_3$PE and PG were only present in the grey matter of the control brain, whilst CH$_3$PE was only found in the PD brain.

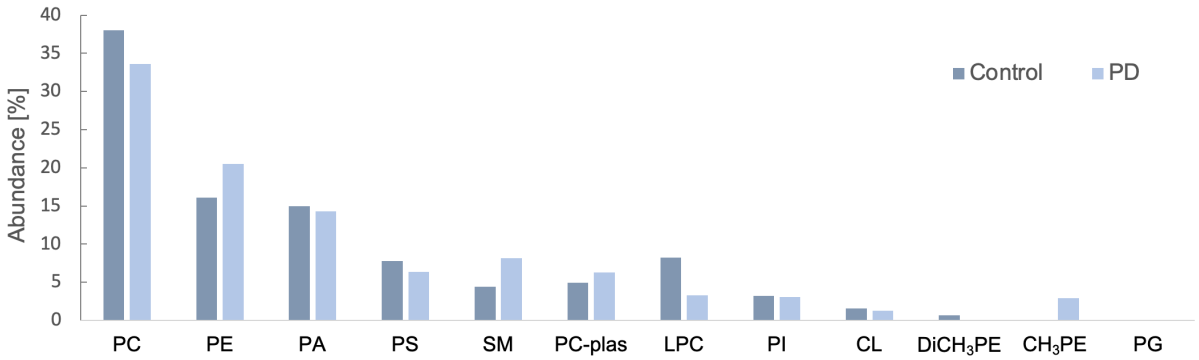

Figure 5.2.3b Phospholipid composition of human grey matter brain samples. Brain lipids were extracted from grey matter originating from human control (n = 1) and PD (n = 1) brains prior to ^{31}P NMR analysis. The ^{31}P spectra were subsequently deconvoluted using the command "mldcon" in Bruker TopSpin 4.2.0 to quantify and identify the phospholipid profile of the brain samples [141]. PC, phosphatidylcholine; PE, phosphatidylethanolamine; PA, phosphatidic acid; PS, phosphatidylserine; SM, sphingomyelin; PC-plas, PC plasmalogens; LPC, lyso-PC; PI, phosphatidylinositol; CL, cardiolipin; DiCH$_3$PE, dimethylated PE; CH$_3$PE, methylated PE; PG, phosphatidylglycerol; PE-plas, PE-plasmalogens; LPE, lyso-PE. PG is present but detected only in the control in very low amounts (<1%).

Phospholipid Composition of White Matter from Control and PD Human Brains

As for the grey matter samples, the lipids extracted from the DL-PFC white matter from the healthy control (n = 1) and sporadic PD (n = 1) human brains were analysed by ^{31}P NMR. Figure 5.2.3c displays their spectra, suggesting similarities and notable differences such as the presence of LPE, PE-plas, CH$_3$PE, DiCH$_3$PE, and a specific PE peak (slightly above 0.2 ppm), only in the PD brain sample.

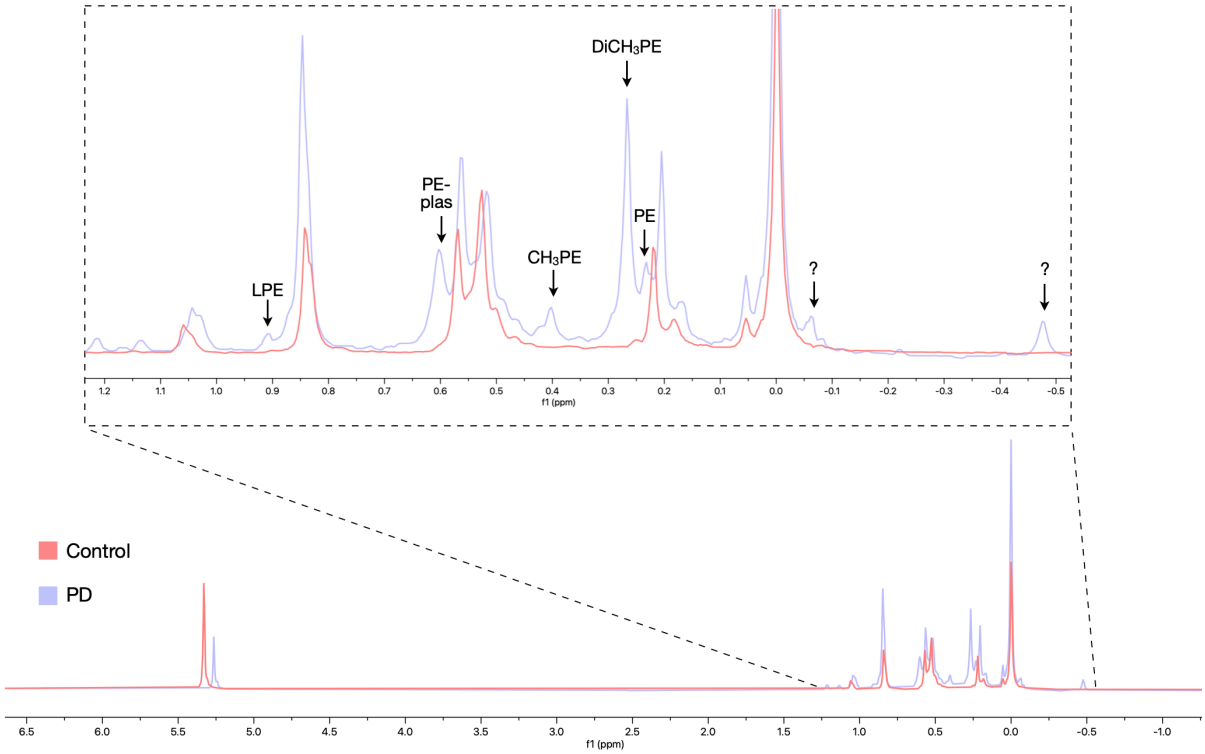

Figure 5.2.3c **^{31}P NMR spectra of lipids extracted from white matter tissue from a control and PD human brain.** Brain lipids were extracted from DL-PFC grey matter of a control (82 mg, *n* = 1) and a sporadic PD individual (73.8 mg, *n* = 1) before they were resuspended in CUBO. The largest peak, PC, was set to 0 ppm. Notable differences seen in the PD sample compared to the control are marked with black arrows, including the presence of unidentified compounds ("?") and the phospholipids LPE, PE-plas, CH_3PE, $DiCH_3PE$ and PE. The Figure was made using MestreNova. PE, phosphatidylethanolamine; LPE, lyso-PE; PE-plas, PE-plasmalogens; $DiCH_3PE$, dimethylated PE; CH_3PE, methylated PE.

Deconvolution of the ^{31}P spectra originating from the grey matter lipids of the control and PD brains (Figure 5.2.3c) confirmed the differences seen in their phospholipid composition, as can be seen in Figure 5.2.3d. Other differences were also identified, including the presence of CL only in the control brain, and PG only in the PD brain. Similarities were also observed, including the presence of identified PC, PE, PA, PS, SM, PC-plas, LPC, and PI in both the control and PD brains, although their abundance differs.

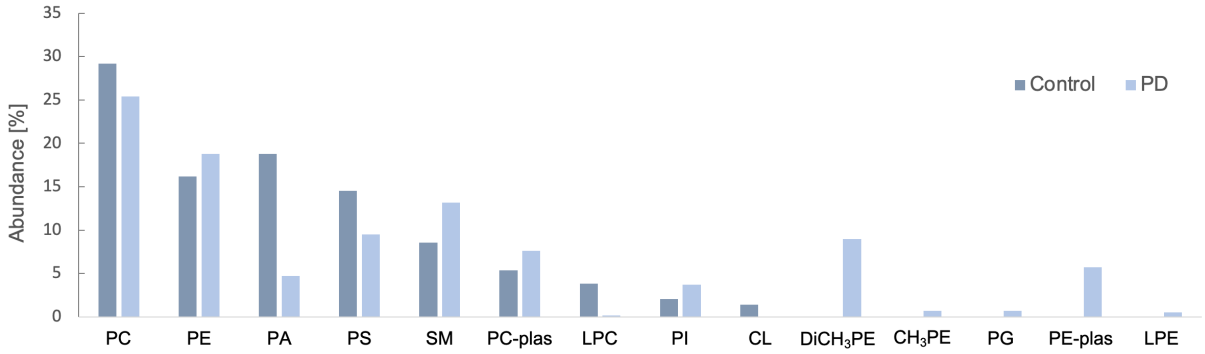

Figure 5.2.3d Phospholipid composition of human white matter brain samples. Brain lipids were extracted from white matter originating from human control (n = 1) and PD (n = 1) brains prior to ^{31}P NMR analysis. The ^{31}P spectra were subsequently deconvoluted using the command "mldcon" in Bruker TopSpin 4.2.0 to quantify and identify the phospholipid profile of the brain samples. PC, phosphatidylcholine; PE, phosphatidylethanolamine; PA, phosphatidic acid; PS, phosphatidylserine; SM, sphingomyelin; PC-plas, PC plasmalogens; LPC, lyso-PC; PI, phosphatidylinositol; CL, cardiolipin; DiCH$_3$PE, dimethylated PE; CH$_3$PE, methylated PE; PG, phosphatidylglycerol; PE-plas, PE-plasmalogens; LPE, lyso-PE.

Table 5.2.3 compares the phospholipid abundance of the phospholipids found in both the grey and white matter brain tissue samples of the control and PD brains. Altered phospholipid abundance is also quantified, showing whether the abundance of PC, PE, SM, LPC, CH$_3$PE, PC-plas and PS has increased or decreased in the grey/white matter when compared to its respective control tissue. To sum up, the quantitative ^{31}P NMR analysis suggests a decrease in PC, LPC and PS, and an increase in PE, SM, CH$_3$PE and PC-plas in the white and grey matter tissue of the PD brain when compared to the control brain.

Table 5.2.3 ^{31}P NMR quantification of total phospholipid abundance in grey and white matter of human PD brains compared to control brains. Only phospholipids found in both the grey and white matter tissue samples of the control and PD brains were included for comparison. Values are listed as percentage points (pp). PC, phosphatidylcholine; PE, phosphatidylethanolamine; SM, sphingomyelin; LPC, lyso-phosphatidylcholine; CH$_3$PE, methylated PE; PC-plas, PC plasmalogens; PS, phosphatidylserine; PA, phosphatidic acid. *Only detected in PD brain (not control).

Phospholipid	Grey Matter (pp)	White Matter (pp)
PC	- 4.40	- 3.78
PE	+ 4.41	+ 2.62
SM	+ 3.79	+ 4.64
LPC	- 4.97	- 3.66
CH$_3$PE	+ 2.90	+ 0.70*
PC-plas	+ 1.38	+ 2.20
PS	- 1.41	- 5.01
PA	- 0.64	- 14.1

5.3 Fatty Acid Identification and Semi-Quantification by UPLC-HRMS/MS

Of the lipids extracted from brain tissue of a healthy control and a PD individual human, as well as WT and DJ-1 KO brain tissue of zebrafish origin, a small fraction was set aside for qualitative and semi-quantitative analysis by UPLC-MS/MS. The extracted lipids were resuspended in a polar mixture of methanol and ethanol (experimental details stated in section 4.6) before accurate mass analysis was performed using a Dionex UltiMate 3000 LC system coupled to a QExactive mass spectrometer. In this way, FAs were separated during LC based on their physiochemical properties before they underwent ionization and fragmentation. Following accurate mass analysis, the data was analysed using Matlab scripts, LipMat, developed by Jakubec *et al.* [135]. This analysis allowed identification of phospholipid headgroups and their FA residues. The details on UPLC-HRMS/MS and subsequent data analysis are further described in section 1.5.2 and 4.6. Figure 5.3 describes how the LipMat scripts identifies lipids.

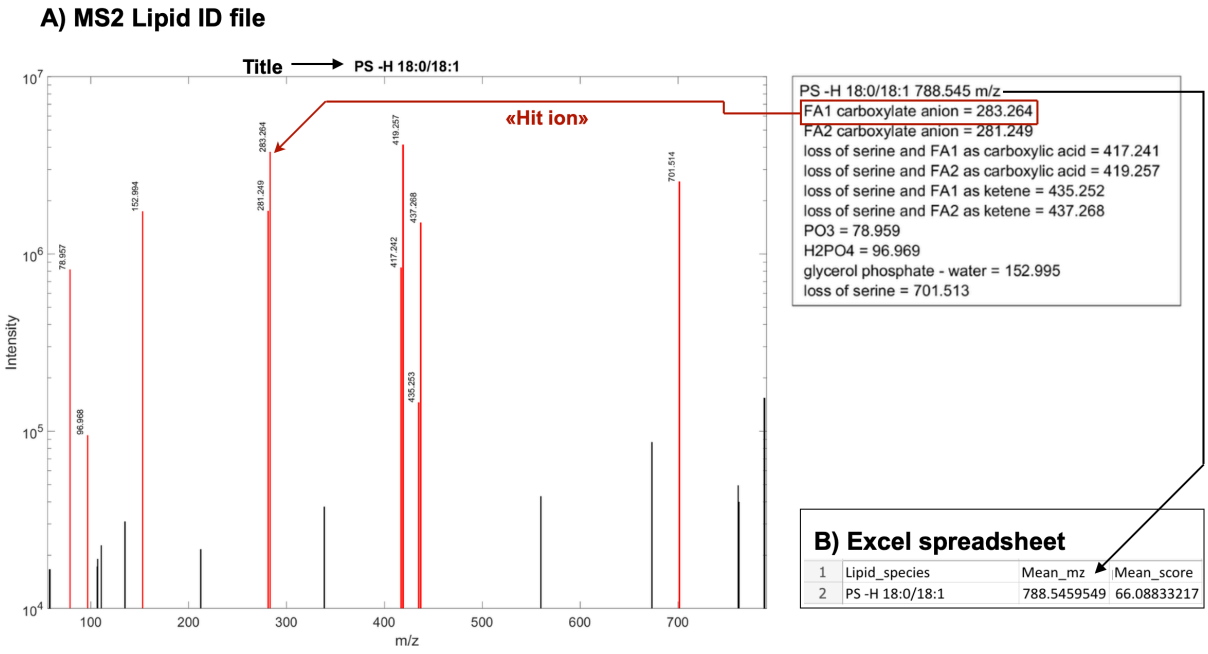

Figure 5.3 Lipid identification by UPLC-HRMS/MS analysis using LipMat scripts. A) The massive amount of data generated following accurate mass analysis of lipid samples by UPLC-HRMS/MS is analysed using LipMat scripts, generating possibly well over 200 MS2 Lipid ID files from a single sample. MS2 Lipid IDs are tandem MS files where the peaks along the m/z axis are ionized daughter fragments of a parent ion of interest that was chosen for fragmentation. Peaks marked in red are "hit ions"; their m/z ratio is as predicted. The higher the number of red hits, the higher the probability of the identification not being by chance. The table to the right of the spectrum first lists the m/z value of the parent ion, followed by the m/z values of the red hits, the daughter fragments. An example of a daughter ion is shown in red (marked "Hit ion"), with the m/z ratio predicted to belong to FA1 – one of the two FA residues of the phospholipid headgroup. Lipid ID files are prepared only if they score above a threshold limit of 20, a cut-off limit set to avoid hitting exact m/z by chance [135]. In other words, the lipids identified with a score above 20 are likely to be correctly predicted, and they are thereafter listed in a **B)**

Excel spreadsheet with their score ("mean_score"). In this case, it is very likely the lipid was correctly identified as the mean score is way above the threshold limit (66>>20). The title lists the identified phospholipid headgroup, in this case PS, followed by potential headgroup modifications (-H), and the identified side chain FAs (18:0/18:1). The scripts were developed by Jakubec *et al.* [135].

Semi-quantitative analysis was performed on the lipids identified using the LipMat script (Figure 5.3) by manually assessing the Lipid IDs found in an unfiltered list, a list including lipids that had been excluded during iterative exclusion processes (refer to section 4.6.5 for details). Filtered lists work well for qualitative analysis, but they exclude a lot of lipids that could otherwise be included in a semi-quantitative analysis. Instead, the unfiltered list was manually filtered. Two criteria had to be fulfilled for the lipids to be included in the semi-quantitative analysis; 1) multiple relevant ion fragment peaks ("hit ions") were present, and 2) FA1 and/or FA2 of the headgroup were detected (Figure 5.3).

5.3.1 Lipid Abundance in WT and DJ-1 KO Zebrafish Brain Tissue

Zebrafish brain lipids from the WT and DJ-1 KO lines were analysed by UPLC-MS/MS, and the data was thereafter run through the LipMat script and manually assessed to allow for semi-quantification of the FA residues within each phospholipid headgroup. Five classes of phospholipids were identified, including PC, PE, PI, PG and PS. Figure 5.3.1a presents the top five most abundant FAs identified within each of these groups as a result of triplicate lipid extractions from WT zebrafish brain tissue. Triplicate lipid extractions were also performed on the DJ-1 KO zebrafish brain tissue, so the same FAs are shown if they were also identified in the DJ-1 KO lipid samples.

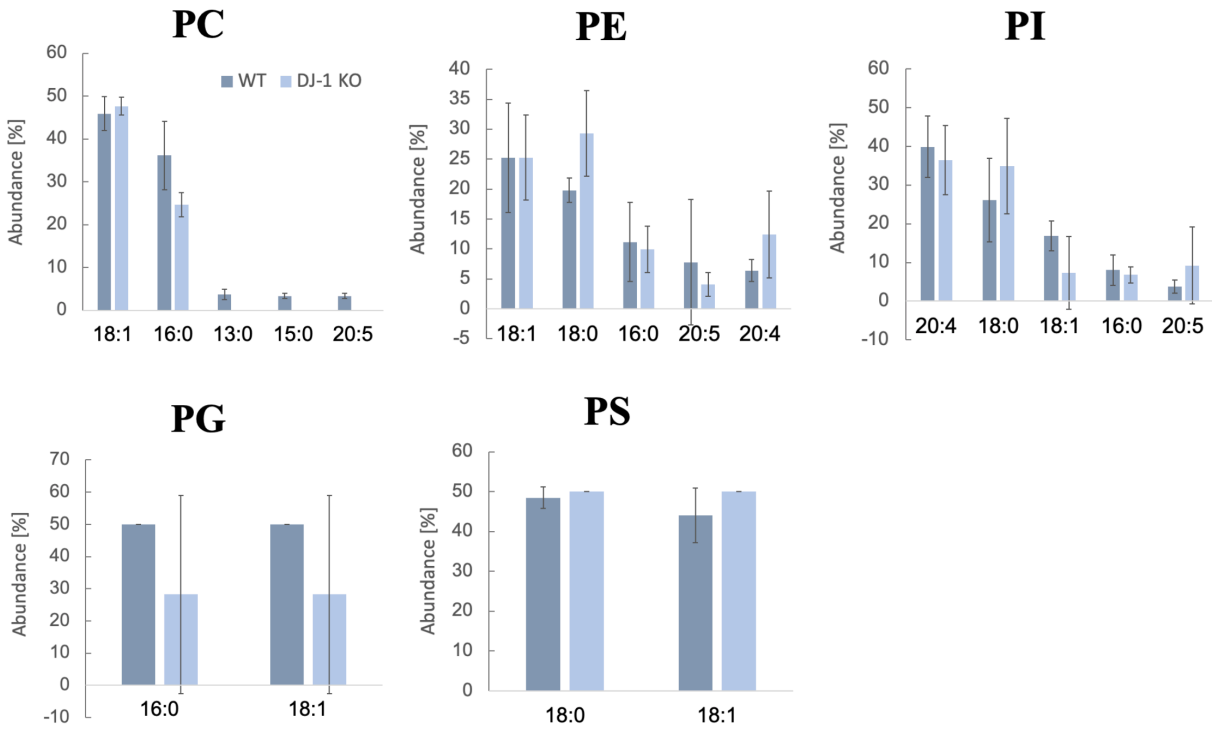

Figure 5.3.1a FA abundance in WT and DJ-1 KO zebrafish brain tissue. Extracted zebrafish brain lipids were analysed by UPLC-HRMS/MS and the lipids were subsequently identified using LipMat scripts developed by Jakubec *et al.* [135]. Data in each graph is displaying the top five most abundant (out of total 100%) FAs within the named phospholipid headgroup identified in from WT zebrafish brain tissue, displayed in the order of most to least abundant. Matched values seen from the analysis on the DJ-1 KO zebrafish are displayed next to the WT values, if present in these samples. The plots represent triplicate lipid extraction experiments performed on WT and DJ-1 KO zebrafish brain tissue. Standard deviation values are shown with grey error bars. PC, phosphatidylcholine; PE, phosphatidylethanolamine; PI, phosphatidylinositol; PG, phosphatidylglycerol; PS, phosphatidylserine.

As the top five most abundant FAs identified in the DJ-1 KO zebrafish samples were not the same as the top five most abundant in the WT samples, FAs that were notably altered in the DJ-1 KO dataset are presented separately in Figure 5.3.1b. A notable increase in PE 18:2 (8.19 ± 2.4 pp) and PC 18:0 (19.8 ± 4.3 pp) in the WT compared to the DJ-1 KO zebrafish tissue could be seen.

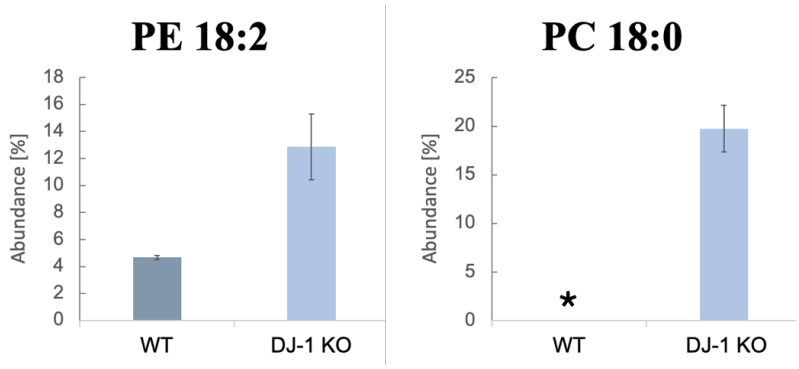

Figure 5.3.1b Notable FA abundance in DJ-1 KO zebrafish brain tissue. Triplicate lipid extractions were performed on WT and DJ-1 KO zebrafish brain tissue before the samples were analysed by UPLC-HRMS/MS. PE 18:2 and PC 18:0 are presented as their abundance was notably altered. Standard deviation values are marked with grey error bars. PC, phosphatidylcholine; PE, phosphatidylethanolamine. *Data not available as no lipids scored above the threshold cut-off limit of 20 for the LipMat script analysis [135].

5.3.2 Lipid Abundance in Grey Matter from Control and PD Human Brain Tissue

As for the zebrafish samples, human brain lipids from the grey matter of a healthy control and a sporadic PD brain were analysed by UPLC-MS/MS. The data was subsequently analysed using the LipMat script and manually assessed to allow for semi-quantification of the FA residues within each phospholipid headgroup. Five classes of phospholipids were identified, including PC, PE, PI, PG and PS. Figure 5.3.2a presents the top five most abundant FAs identified within each of these groups as a result lipid extractions the healthy control (n = 1) brain tissue. Lipid extraction was also performed on grey matter (n = 1) from the sporadic PD brain, so the same FAs are shown if they were also identified in the PD brain.

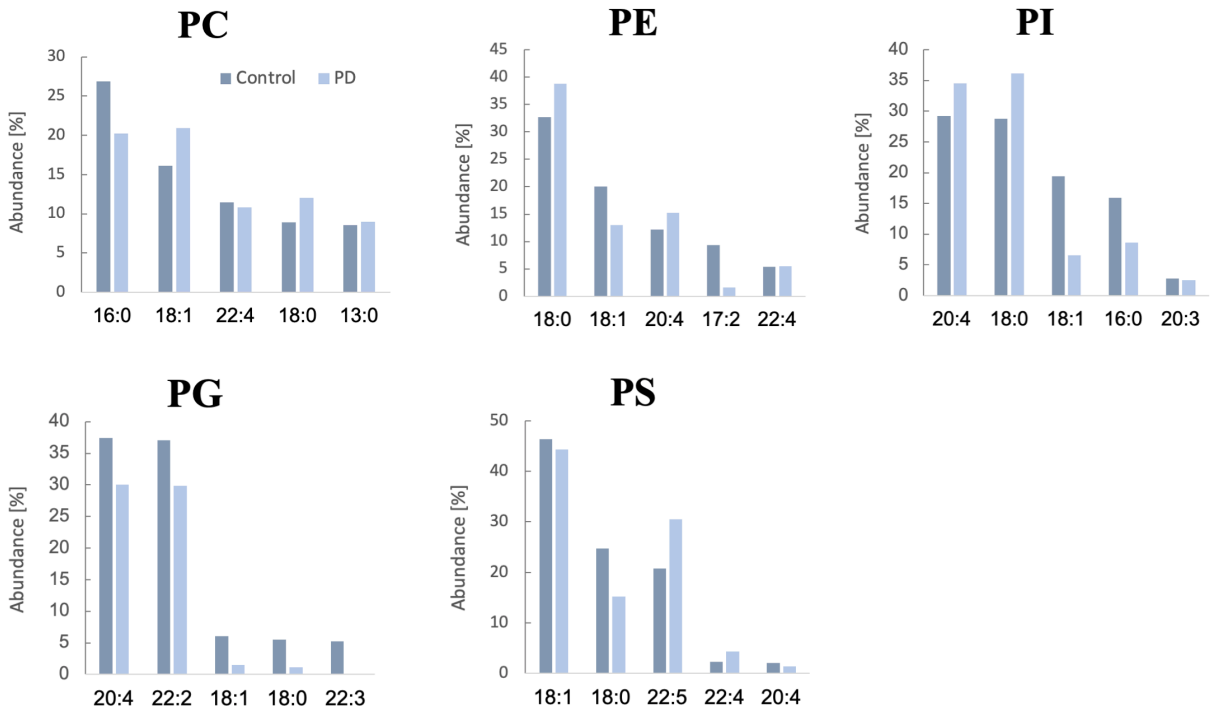

Figure 5.3.2a Lipid abundance in grey human brain matter of a control and an individual with sporadic PD. Lipid extraction was performed on grey matter from a control and sporadic PD human brain before the brain samples were analysed by UPLC-HRMS/MS. No error bars are presented as only one biological sample was analysed for the control (n = 1) and PD (n = 1) brain. PC, phosphatidylcholine; PE, phosphatidylethanolamine; PI, phosphatidylinositol; PG, phosphatidylglycerol; PS, phosphatidylserine.

FA abundance not represented in the grey matter of the PD brain in Figure 5.3.2a are instead presented in Figure 5.3.2b. A notable increase in PE 18:2 (3.8 pp), PI 10:3 (3.9 pp), and PI 30:3 (3.9 pp) could be seen in the grey matter brain tissue of the control compared to the PD brain.

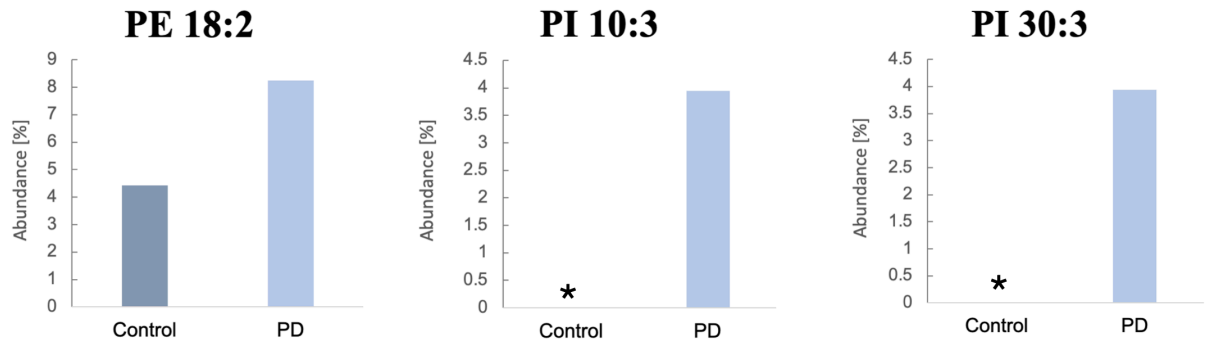

Figure 5.3.2b Notable FA abundance in healthy and PD human brain grey matter tissue. Lipid extraction was performed on grey matter from a control and sporadic PD human brain before the brain samples were analysed by UPLC-HRMS/MS. Bar plots presenting the abundance of PE 18:2, PI 10:3, and PI 30:3, are shown as their abundance was notably altered. PE, phosphatidylethanolamine; PI, phosphatidylinositol. *Data not available as no lipids scored above the threshold cut-off limit of 20 for the LipMat script analysis.

5.3.3 Lipid Abundance in White Matter from Control and PD Human Brain Tissue

Lastly, human brain lipids from the white matter of a healthy control and a sporadic PD brain was also analysed by UPLC-MS/MS. The same five classes of phospholipids were identified as for the grey matter brain samples, including PC, PE, PI, PG and PS. Figure 5.3.3a presents the top five most abundant FAs identified within each of these groups as a result lipid extractions the healthy control (n = 1) brain tissue. Lipid extraction was also performed on white matter (n = 1) from the sporadic PD brain, so the same FAs are shown if they were also identified in the PD brain.

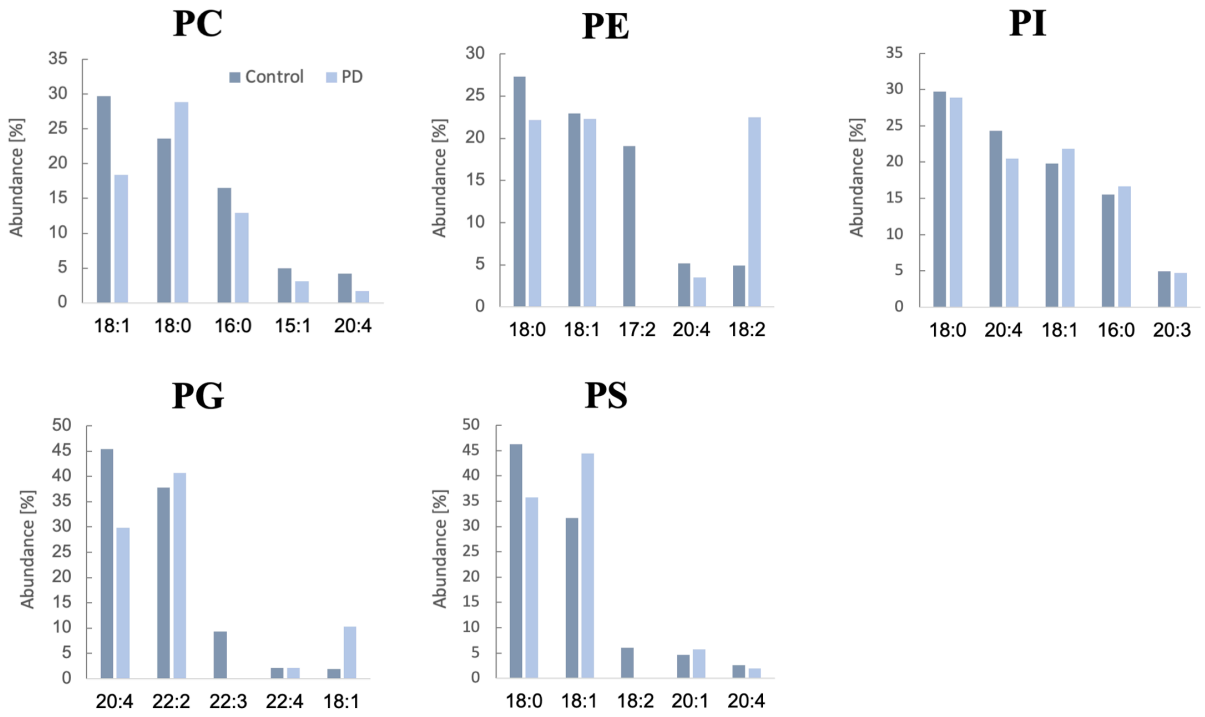

Figure 5.3.3a Lipid abundance in human brain white matter of a control and an individual with sporadic PD. Lipid extraction was performed on grey matter from a control and sporadic PD human brain before the brain samples were analysed by UPLC-HRMS/MS. No error bars are presented as only one biological sample was analysed for the control (n = 1) and PD (n = 1) brain. PC, phosphatidylcholine; PE, phosphatidylethanolamine; PI, phosphatidylinositol; PG, phosphatidylglycerol; PS, phosphatidylserine.

The abundance of certain FAs not displayed in Figure 5.3.3a was altered in the grey matter of the PD brain. These alterations are instead presented in Figure 5.3.3b. A notable increase in PC 15:0 (2.2 pp), PC 15:2 (18.8 pp), PE 18:2 (17.6 pp), and PS 22:5 (3.8 pp) could be seen in the grey matter brain tissue of the control compared to the PD brain.

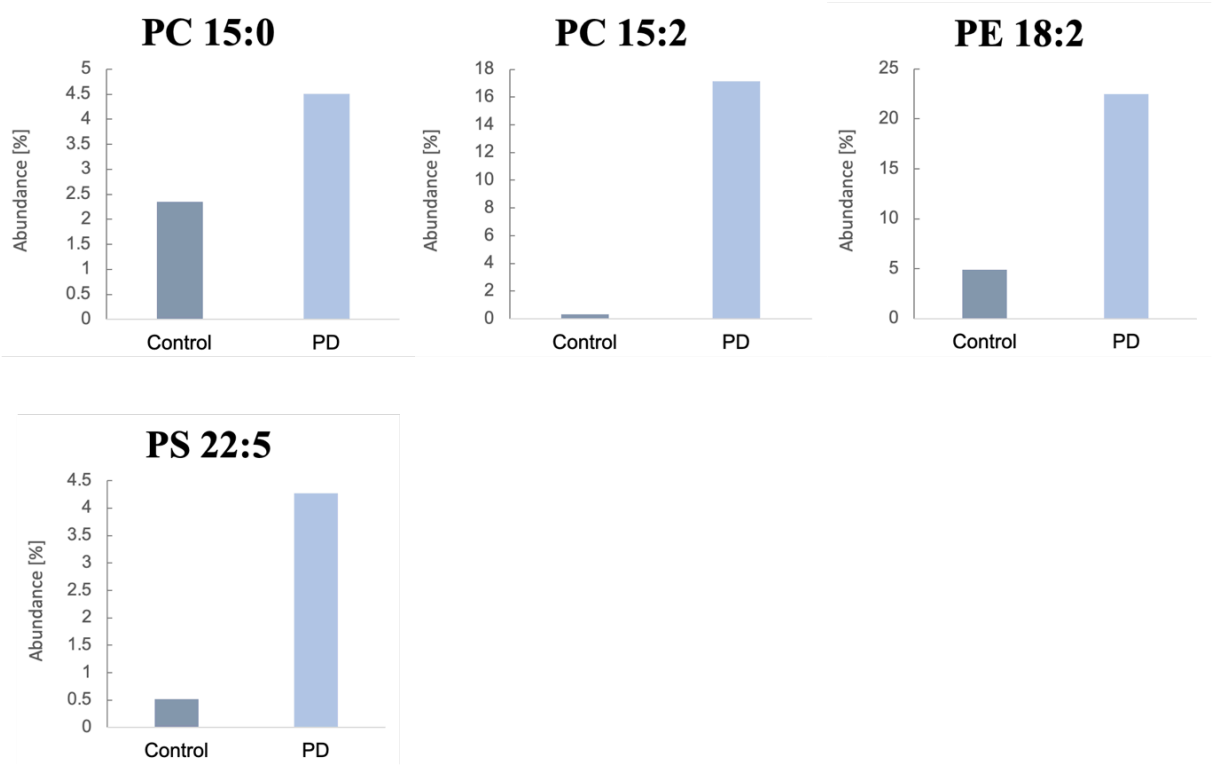

Figure 5.3.3b Notable FA abundance in healthy and PD human brain white matter tissue. Lipid extraction was performed on white matter from a control and sporadic PD human brain before the brain samples were analysed by UPLC-HRMS/MS. Bar plots presenting the abundance of PC 15:0, PC 15:2, PE 18:2, and PS 22:5 are shown as their abundance was notably altered. No error bars are presented as only one biological sample was analysed for the control (n = 1) and PD (n = 1) brain. PC, phosphatidylcholine; PE, phosphatidylethanolamine; PS, phosphatidylserine.

5.3.4 Semi-Quantitative Comparison of FA Abundance in DJ-1 KO & PD Brain Tissue

Considering the large amount of UPLC-HRMS/MS data to compare across brain tissue of both human and zebrafish origin, the analysis was focused on the data related to the aim of the thesis; to study PD-related alterations in PD-diseased relative to healthy brain tissue. Table 5.3.3 presents the FAs of which their abundance was notably increased or reduced in the grey and white matter of the human PD brain, as well as in zebrafish PD model (DJ-1 KO), when compared to the control or WT brains. An increase in the abundance of PC 18:0, PE 18:2, and PS 22:5, in addition to a decrease in the abundance of PC 16:0, PE 17:2 and PG 22:3 were the notable alterations in the PD/DJ-1 KO brain tissue observed from the datasets when comparing their abundance in the control brains. Among the FAs listed in Table 6.4, the reduction in abundance of PE palmitic acid (16:0) and increase in PE linoleic acid (18:2) are especially notable, as the FAs were represented in datasets from both the WT/control and DJ-1 KO/PD zebrafish and human samples, respectively.

Table 5.3.3 Alterations in FA abundance in human PD and DJ-1 KO zebrafish brains compared to control and WT brains, respectively. Both PG 22:3 and PS 22:5 were not detected in the zebrafish samples. Standard deviation values only apply to the zebrafish samples as triplicate (n = 3) biological samples were performed, compared to only one for the grey and white matter human samples. Values are listed as percentage points (pp). PC, phosphatidylcholine; PE, phosphatidylethanolamine; PG, phosphatidylglycerol; PS, phosphatidylserine. *Only detected in zebrafish DJ-1 KO sample. **Only detected in human control/zebrafish WT sample.

FA	Name	DJ-1 KO Zebrafish (pp)	Human PD Grey Matter (pp)	Human PD White Matter (pp)
PC 16:0	Palmitic acid	- 11.5 ± 2.3	- 6.6	- 3.5
PC 18:0	Stearic acid	+ 19.8 ± 4.3*	+ 3.1	+ 5.2
PE 17:2	Heptadecadienoic acid	- 5 ± 0.3**	- 7.7**	- 19.0
PE 18:2	Linoleic acid	+ 8.2 ± 2.4	+ 3.8	+ 17.6
PG 22:3	Docosatrienoic acid	-	- 5.2**	- 9.3**
PS 22:5	Docosapentaenoic acid (DPA)	-	+ 9.8	+ 3.8

6 Discussion

6.1 Expression Levels of DJ-1 and oxDJ-1 and Their Implications of PD

DJ-1 expression is closely linked to oxidative stress levels, due to its function as a neuroprotective antioxidant [99]. Quantification of DJ-1 and oxDJ-1 in both control and PD human brains revealed a notable alteration in their expression levels (Figure 5.1.2). In the PD brain, DJ-1 expression was reduced in both the grey (-30.9 pp) and white matter (-33.9 pp) compared to the control, while oxDJ-1 expression was only reduced in the white matter (-50.3 pp) with consistent levels in the grey matter. Abnormal DJ-1 expression has been reported in PD [159], showing variation of its expression across different brain regions [160]. For example, a study by Nural *et al.* demonstrated significantly decreased DJ-1 expression in the *substantia nigra* of sporadic PD patients, while no change was observed in the frontal cortex [161]. The decreased expression of DJ-1 suggests dysregulated DJ-1 expression, as has been reported in sporadic PD [161]. Furthermore, reduced levels of oxDJ-1 have also been reported in sporadic PD brains [154]. The decrease in DJ-1 expression in the PD brain could indicate a potential loss of its neuroprotective antioxidant function [99], thereby compromising the ability of the neurons to counteract the oxidative stress response associated with PD pathogenesis [162]. However, statistical limitations in making this assumption are recognized, as it is backed by a sample size of only $n = 1$.

Free radicals have been found to induce irreversible formation of a SDS-resistant DJ-1 dimer [160]. This finding may explain why oxDJ-1 was found with sizes around ~50 kDa (Figure 5.1.2), rather than at its monomeric size of 20 kDa [104]. In another study involving Western blot analysis of the human brain, Piston *et al.* also detected DJ-1 homodimers at approximately 50 kDa, suggesting that DJ-1 forms high molecular weight complexes [154]. This ROS-induced modification impairs the antioxidative function of DJ-1 as C106 of DJ-1 gets oxidized to an inactive sulfonic acid form (refer to Figure 1.4.2 for details) [160]. Oxidation of DJ-1 (C106) is deemed essential for DJ-1 to gain its neuroprotective properties, as this enables its participation in cytoprotective signalling pathways [106, 107]. However, the multimeric form of DJ-1 is unable to engage in this pathway, thus reducing the antioxidative capacity of cells and tissues [160].

Interestingly, in the Western blot analysis, anti-oxDJ-1 detected bands at 13 kDa in the grey matter of both control and PD brains (Figure 5.1.2 C)). A study by Bahmed *et al.* detected C106 oxDJ-1 at 15 kDa, described as “cleaved” oxDJ-1 [163], suggesting that the band observed at 13 kDa could potentially represent a cleaved form of oxDJ-1. Cleavage of oxDJ-1 is believed to occur in response to increased oxidative stress levels, and the C-terminal cleavage of a 15 amino acid peptide from

DJ-1 has been reported to enhance its cytoprotective properties against oxidative stress-induced apoptosis [164]. Although the quantification of this potentially cleaved form of oxDJ-1 is lacking, its presence in the grey matter of both the control and PD brain may indicate elevated levels of oxidative stress [164], a known characteristic of PD [5].

6.2 Establishment of a Good Lipid Extraction Protocol

Two of the goals of this thesis was to establish a good protocol for extraction of both brain material of human and zebrafish origin, as well an approach for extraction and analysis of their phospholipids. This raises the question; what does a good extraction protocol encompass?

First, factors affecting extraction efficiency and specificity were considered, such as the choice of solvent system. Simple biphasic solvent systems may or may not be able to extract all lipids effectively [113]. These can be modified with the addition of methanol or other solvents to improve extraction efficiency of certain lipids, such as anionic phospholipids like PS or PG (for further details, refer to «The Choice of Solvent System» in section 1.5.1) [113]. Second, other considerations of the procedure such as the time, as well as the choice of solvent and reagents, are important, and so is the impact of the approach on the environment and human health. Moreover, factors involving the harvesting and storage of the tissue prior to extraction are considered, with the goal being to limit the amount of lipid degradation. A good extraction protocol often represents a compromise, striking a balance between practicality and extraction efficiency, allowing for reproducible and reliable results that serve the purpose of the study. In the following sections, possible modifications and limitations of the current protocol are discussed.

6.2.1 Phosphatidic Acid as a Measure of Lipid Degradation

Lipids are readily degraded by oxygen, free radicals, lipases, heat and light [109]. Care must therefore be taken to avoid excessive lipid degradation from the moment the tissue of interest is isolated, until the lipids are extracted for analysis. Phosphatidic acid (PA) plays important roles in signalling and lipid biosynthesis, but it is not abundant in living organisms [165]. The enzyme phospholipase D hydrolyses phospholipids such as phosphatidylcholine (PC) to produce PA [166]. In this way, phospholipase D is involved in degradation of membrane phospholipids of post-harvest tissue [158]. High levels of its product, PA, therefore, indicates that other lipids have degraded [158]. This leads to a distorted representation of the true lipid profile present in cells and tissues. For this reason, large amounts of detected PA are considered a poor indicator in terms of lipid extraction, as it is typically a result of unplanned hydrolysis caused by inappropriate storage or

extraction conditions [158, 167]. The time it takes from tissue harvesting to when the lipids are extracted, including how they are stored, is therefore of the essence. For this reason, ways of limiting this timeframe is beneficial in terms of limiting the window of opportunity for lipid degradation.

The Challenge of PA Detection by UPLC-HRMS/MS Analysis

In ^{31}P NMR analysis of phospholipids dissolved in CUBO with the PC-signal set to 0 ppm, a signal representing PA is typically seen at ~5.37 ppm (Figure 5.2.2b) [152]. The PA abundance was not detected in the UPLC-HRMS/MS analysis (refer to section 5.3 for details). An explanation for this discrepancy could be that these lipids scored below the cut-off limit for the LipMat script (Figure 5.3) so their analysis was excluded [135], or that the PA presence was too low to be detected. As PA was detected by ^{31}P NMR analysis, and not by UPLC-HRMS/MS, it could be a result of the relatively low abundance of PA in biological samples [165]. The ion suppression effect (refer to section 1.5.2 for details), and thereby ion enhancement effects of more abundant phospholipids, is a challenge with ESI-based UPLC-HRMS/MS techniques. The lipid analytes were ionized using an H-ESI (experimental details in section 4.6), and the low abundant phospholipid PA may have been missed as a result of ion suppression, resulting in a lack of their detection during analysis [168]. Standard lipidomic platforms often fail to detect PA [169]. Nevertheless, the high-resolution mass spectrometry employed in this thesis should provide the resolution required for PA detection (refer to section 1.5.2 for details) [129]. In addition to the ion suppression effect, the rapid degradation caused by the inherent instability of PA makes it more challenging to detect [158]. This could explain why other low abundant lipids such as phosphatidylinositol (PI) [170], but not PA, were detected (figures 5.2.3 b, d).

6.2.2 The Effect of the "Freeze-Thaw Cycle"

Considering the qualitative analysis performed on the ^{31}P NMR spectra, three out of four human brain samples appeared to have a considerate abundance of PA (>14%), whilst the white matter sample originating from the sporadic PD male appeared to have PA-abundance of approximately 4.7% (figures 5.2.3b, d). This could indicate a lower level of lipid degradation of the latter sample in particular.

The white matter sample was the first one extracted, and the other samples were extracted several months later, after other failed ^{31}P NMR experiments (a result of erroneous CUBO – refer to section 5.2.2 for details) had been performed on lipids extracted from the same tissue. The other tissues had therefore been thawed at least twice, in addition to once for protein extraction for Western blot

analysis (Figure 5.1.2). An increase in PA could potentially be due to degradation during storage (-80°C), a characteristic of the white matter in PD brain tissue sample (Figure 5.2.3c), or a result of freeze-thaw cycles. A study by Ueland *et al.* on the effect of freezing on human decomposition, with respect to lipid degradation, pointed at significant differences observed between fresh and frozen lipids, where the freeze-thaw cycle impacted the FA abundance of human tissue to the extent of which fresh tissue was easily distinguishable from tissue that had been frozen prior to analysis [90]. Although performing lipid extractions directly after tissue harvesting could prove beneficial to avoid freezing and thawing the brain tissue, it is practically challenging. Rather, limiting the number of freeze-thawing cycles, and reducing the time the tissues spend stored, could avoid considerable lipid degradation.

6.2.3 Increasing the Amount of Solvent

Compared to the Folch extraction method, the Bligh & Dyer approach utilizes less solvent relative to the amount of tissue [117] (refer to section 1.5.1 for details). The amount of solvent is typically dependent on the amount of tissue, but another factor is the fat content of the sample. An increase in solvent/sample ratio has been recommended by Iverson *et al.* after lipid extractions performed on samples with a fat content ranging from 0.5 to 26.6% showed a correlation between increased fat content and a reduction in extraction efficiency [117]. Lipid extractions with the Bligh & Dyer approach performed on samples containing >2% lipids produced lower than actual estimates of the sample lipid content, and this effect significantly increased with an increase in lipid content [117]. This could be the result of reaching the limit of solubility of the organic solvent. In dry weight the brain consists of 50% lipids [171], and the lipid content of white and grey matter has been estimated to be 49-66 and 36-40%, respectively [87]. Considering the high abundance of lipids within the brain, increasing the extraction volume could therefore allow for better extraction efficiency. However, the increase in solvent volume will also require longer drying times as the lipid fraction will be larger. A compromise between time and extraction efficiency is therefore required.

6.2.4 Limiting the Number of Interexperimental Variables

Differences in Post-Mortem Interval Time

Time is also of the essence when brain tissue is extracted from the source organism. During zebrafish brain harvesting, the zebrafish were euthanized, and their brains were immediately extracted, sampled and snap-frozen in liquid nitrogen before they were stored at -80°C. On the other hand, the human brain tissue samples from the healthy control and the PD individual were harvested

with PMI times of 14 and 48h, respectively, before they were snap-frozen. PMI, post-mortem interval, is an estimate of the time elapsed since the death of an individual. When causes of death are investigated, the decomposition process of human remains can be used to estimate the PMI. Inversely, PMI can be a factor in the scale of decomposition [172]. A higher PMI, such as the 48h for the PD individual in this thesis, can therefore indicate a higher level of decomposition than what is seen in the control individual with a PMI of 14h. Although the stages of decomposition are initiated at different times from one individual to another [90], comparing brain tissue from two individuals with an approximately similar PMI is beneficial, and an a factor with room for improvement in future brain tissue extractions.

Differences in Age and Sex

The phospholipid composition of the human brain changes with ageing [173]. The age of the healthy control and sporadic PD individuals were not disclosed, but variety in their age provides a factor that has influenced their brain compositions. As for the zebrafish, the human brain samples to be compared should be of age-matched individuals, or at least similar age-brackets. Notable findings in altered lipid abundances could also be a result of sex-specific differences [174], and lipid extractions should therefore be performed with brain tissue from only female or male brains to limit the number of variables.

6.3 Alterations in Phospholipid Abundance with Implications of PD

The final aim of this thesis was to extract the phospholipids from healthy and PD-diseased brain tissue of zebrafish and human origin and analyse them by ^{31}P NMR and UPLC-HRMS/MS to critically assess PD-related differences. The relative phospholipid profiles of the brain samples were analysed by ^{31}P NMR. As representative ^{31}P NMR data is lacking for the zebrafish samples (refer to results section 5.2.2 for details), only the human brain samples were included for discussion on PD-related alterations in their relative phospholipid brain profiles. An overview of this data can be seen in Table 5.2.3, where notable alterations seen in both grey and white matter samples are listed. The discussion will be limited to notable alterations implicated in PD, including an increase in PE, SM and PC-plas abundance, and a decrease in PC and lyso-PC.

6.3.1 The PD Brain Phospholipid Profile

As ^{31}P NMR data for the zebrafish brains are missing (details in section 5.2.2), the data only represents the phospholipid composition seen in the human brain samples. Taking the sample assumed to be the least degraded into account, the white matter PD brain sample (Figure 5.2.3d),

its composition appears to align with the typical lipid profile of the human brain [87]. Ethanolamine phospholipids are typically the most abundant (35.6%) with PE plasmalogens making up most of the abundance. This can also be seen in the white matter PD sample (Figure 5.2.3d), as combining the amounts of PE, PE-plas, $DiCH_3PE$ and CH_3PE results in a total abundance of 34.2%. Furthermore, phosphatidylcholine (PC) abundance is typically around 32.8%, which aligns with the numbers from the ^{31}P NMR analysis, with a slightly reduced PC abundance of 25.4%. The amounts of phosphatidylserine (PS) are lower than reported amounts (16.6%), as the relative PS abundance was found to be 9.5% [43]. Excluding the exceptions noted above, the phospholipid profile appeared to be consistent with published data. Overall, the ^{31}P NMR analysis showed an increased abundance of PE, SM, CH_3PE and PC-plas, and a decrease in PC, LPC and PS abundance in the phospholipid profile of the white and grey matter in the human PD brain compared to the control brain (Table 5.3.3).

Differences in Grey and White Matter Samples

Some differences were seen when comparing the grey and white matter of the human brain, which is expected as their lipid composition is different [87]. For instance, an increase could be seen in the abundance of $DiCH_3PE$ and PI in the matter of the PD brain compared to the grey matter samples, and the overall relative lipid abundance in the control brain also differed when comparing gray to white matter (Figure 5.2.3b, Figure 5.2.3d). Information regarding the difference between grey and white matter of normal human brain can be found in sections 1.3.5 and 4.2.

6.3.2 Decrease in PC and Lyso-PC, and increase in SM

Phosphatidylcholine is one of the most common lipids in animal cells [175]. The enzyme phospholipase A_2 uses phosphatidylcholine (PC) as a substrate to produce lyso phosphatidylcholine (lyso-PC) [176]. A decrease in the abundance of PC has been reported in the frontal cortex of individuals with PD [177]. An overall decrease in PC and LPC species was also detected in early-stage PD model animals [176]. PC has shown to modulate anti-inflammatory signalling [178], so its low abundance could indicate decreased cell survival in relation to an increase in inflammatory processes.

PC can be used as a donor to synthesize sphingomyelin (SM) [179], which could describe the relationship between the decrease in PC and simultaneous increase in SM of the PD brain (Table 5.2.3). SM is one of the major components of the plasma membrane [179], and a recognized constituent of lipid rafts [50]. The abundance of sphingomyelin was increased in both grey and

white matter of the PD brain samples by 3.79 pp and 4.64 pp, respectively (Table 5.2.3). Alterations in sphingomyelins in neurodegenerative diseases, including PD, have been reported [177]. In the brain, SM supports myelination of neurons, which is a process that is associated with optimal neuronal cell function [180]. Moreover, SM is essential for both brain development and cognitive abilities [180]. The notable increase in SM could therefore be a neuroprotective response to the neurodegenerative changes induced by PD, in an effort to maintain optimal neuronal function.

Lacking UPLC-HRMS/MS data on Lyso-Phospholipids

Phospholipase A_2 is activated in response to elevated ROS, cleaving the sn-2 lipid bond between phospholipids and their unsaturated FA [181]. For this reason, hydrolysed phospholipids, lyso-phospholipids, function as markers of oxidative stress [182]. Unfortunately, lyso-phospholipids were not detected in the UPLC-HRMS/MS analysis, but they were detected by ^{31}P NMR analysis. The decrease in PC seen in the PD brains could have been explained by an increase in lyso-PC, but that was not the case for the white or grey brain matter samples as both PC and lyso-PC was decreased in both compared to the control brain (Figures 5.2.3b, Figure 5.2.3d).

6.3.3 Increase in PE

Phosphatidylethanolamine (PE) serves various cellular functions, including involvement in oxidative phosphorylation, maintenance of mitochondrial stability, and serving as a precursor for other lipids such as PC, as well as a substrate for GPI anchor formation [183]. In the sporadic PD brain, a notable increase in PE was found in the white (2.62 pp) and grey (4.41 pp) matter compared to the control brain (Table 5.2.3). However, it is typically observed that PD brains exhibit a significant reduction in PE abundance, which is also reported in the ageing brain [184]. In spite of this, there are also reports of local enrichment of PE abundance. Notably, PE abundance has shown to be significantly increased by 12% in PD lipid rafts [185]. Aberrant post-translational protein modifications such as glycation or glycosylation have been linked to mitochondrial dysfunction and inflammation in PD [186]. GPI-anchoring, a type of glycosylation typically added to the C-terminus of eukaryotic proteins, is associated with lipid rafts [183]. PE, as previously mentioned, is a substrate for GPI anchor formation [183]. The elevated levels of PE in the PD brain may indicate a stress-induced upregulation in the synthesis of GPI-anchored proteins that play a role in oxidative stress and inflammation [186], which are characteristics of PD pathogenesis [5].

6.3.4 Increase in PC-plasmalogens

Plasmalogens are a unique class of phospholipids with an alkenyl bond, and the head group is typically choline or ethanolamine in mammalian tissues [187]. The abundance of both PC- and PE-plasmalogens have been reported to be increased in the frontal cortex of PD brains [177]. Plasmalogen phospholipids have been proposed to function as antioxidants, protecting myelin from damage caused by ROS (refer to section 1.3.3 for details on ROS) [188]. The elevated level of PC-plas observed in the grey (1.38 pp) and white matter (2.2 pp) of the individual with PD compared to the control samples (Table 5.2.3), could indicate an elevated level of oxidative stress in the PD brain, where PC-plas plays a neuroprotective, defensive role against oxidative damage [188]. Alternatively, synthesis pathways of PC-plasmalogens may be altered as a result of PD. Lastly, as dysregulated lipid metabolism has been observed in PD [55], the increased levels of plasmalogens may not serve a functional purpose but rather represent a passive consequence of the progression of the disease.

6.4 Alterations in Fatty Acid Abundance with Implications of PD

The abundance of various FAs in the human and zebrafish brain samples was analysed by UPLC-HRMS/MS. A large amount of data was generated as triplicate brain samples were analysed from WT (n = 3) and DJ-1 KO (n = 3) zebrafish, in addition to human brain tissue samples from both grey and white matter of a healthy control (n = 2; 1 grey matter, 1 white matter) and PD (n = 2; 1 grey matter, 1 white matter) brain. Due to a limited number of replicated experiments, as well as the unknown data distribution, statistical tests have not been run on the data sets. Therefore, the analysis has been restricted to the observations of the investigator of FA that are deemed to be notably altered, compared to the control, in either all PD/DJ-1 KO brain samples (human and zebrafish samples), or all PD human brain samples (if data was lacking for the zebrafish samples). For instance, if an increase in PC 18:0 is seen only in the zebrafish samples, but not in the human samples, it has not been included in the analysis. An overview of alterations seen in the FA abundance of PD/DJ-1 KO brains compared to their respective healthy control brains can be seen in Table 5.3.3. The discussion will be limited to notable alterations implicated in PD, including an increase in stearic acid (PC 18:0), DPA (PS 22:5), and linoleic acid (PE 18:2).

6.4.1 Increase in PC 18:0

Palmitic acid (16:0) and stearic acid (18:0) are typically amongst the main lipid species of PC [43], and changes in their abundance were observed in the human PD and DJ-1 KO zebrafish brains, including a reduction in PC 16:0 and an increase in PC 18:0 abundance (Table 5.3.3). The amounts

of saturated fatty acids, specifically 16:0 and 18:0, have been shown to be significantly higher in lipid rafts of the frontal cortex of PD human brain tissue when compared to control brains [185]. A study by Shah *et al.* reported an increase in palmitate and stearate in the plasma of PD models, where a correlation between the increased abundance and motor dysfunction, a symptom of PD (refer to section 1.1 for details), were observed [189]. The increase observed for stearic acid in this study could be connected to the motor dysfunction symptoms seen in PD [5].

6.4.2 Increase in PS 22:5, Docosapentaenoic Acid (DPA)

DPA is a long chain polyunsaturated FA with limited studies to its name, and its biological function is therefore not certain. It has been reported to induce beneficial biological effects, including neuroprotective and neurorestorative effects as it reduces age-related oxidative changes, for instance through downregulation of microglial activation (refer to section 1.3.2 for more information on proinflammatory microglia activation) [190]. Aged rats fed DPA have showed improved cognitive functioning, including spatial learning and memory storage of the hippocampus [191]. The abundance of PS 22:5, docosapentaenoic acid (DPA), was notably increased in the grey (9.8 pp) and white (3.8 pp) matter brain tissue of the individual with sporadic PD when compared to the control brain (Table 5.3.3, figures 5.3.1a & 5.3.3b). DPA has shown to be predominantly esterified to phosphatidylserine (PS) [192], as was detected in the UPLC-HRMS/MS analysis (Table 5.3.3).

DPA as a Precursor for Docosahexaenoic acid (DHA)

Although the presence of DHA was not detected with the UPLC-HRMS/MS analysis in this thesis, the abundance of PS 22:5, DPA, was notably increased in the white and grey matter of the DL-prefrontal cortex (Brodmann area 9) of the PD brain (Table 5.3.3). DPA can be elongated to form tetracosapentaenoic acid (24:5n-3) which is desaturated to produce tetracosahexaenoic acid (24:6n-3), which can subsequently be used to synthesize DHA (22:6n-3) by a single round of beta-oxidation [192]. The content of docosahexaenoic acid (DHA), 22:6, has shown to be increased in PD in both the amygdala and Brodmann area 8 of the frontal cortex of the human brain [193]. DHA is a main component of the membrane phospholipids found in the brain, and has shown to be profoundly susceptible to oxidative stress [194]. Oxidation of DHA creates toxic, unstable oxidation products. It has been hypothesized that high levels of n-3 FAs such as DHA in membranes could lead to an increased probability of tissue disruption as it could enhance the susceptibility of said membrane to lipid peroxidation [194]. In relation to PD, an alteration in the phospholipid composition of membranes to a more DHA-rich profile could thereby increase the amount of peroxidative tissue

damage. In the normal human brain, DHA and AA usually account for approximately 25% of the total fatty acid abundance [195]. Therefore, its absence in the datasets of both the control and the PD brains may indicate a limitation of the method in DHA detection. The limitation in DHA detection aligns with a previous study by Bariås *et al.*, where a comparable LC-MS/MS method was utilized to determine the relative FA abundance in cells and DHA was not detected [196].

6.4.3 Increase in PE 18:2, Linoleic Acid

Linoleic acid (LA), 18:2(*n*-6), is a precursor in arachidonic acid (AA), 20:4(n-6), synthesis [197]. The UPLC-HRMS/MS analysis found the abundance of PE 18:2 to be notably increased in the zebrafish PD model (8.2 ± 2.4 pp), and the grey (3.8 pp) and white (17.6 pp) matter of the individual with sporadic PD when compared to the control samples (Figure 6.4.3). Both AA and LA have shown protective properties where they reduce the amount of oxidative stress, in response to MPP^+ toxicity, known to induce textbook PD symptoms [198]. A further explanation of the neurotoxic implications of MPP^+ in development of PD can be found in section 1.2.2 of the introduction. Both PD cell lines and PD mouse models treated with LA have shown LA to have neuroprotective and anti-inflammatory properties [199], suggesting a potential treatment of PD with the use of omega 6 FAs such as AA and LA [198]. Upregulation of PE 18:2 could therefore suggest a neuroprotective defensive mechanism in response to elevated oxidative stress levels that are typically associated with PD [108].

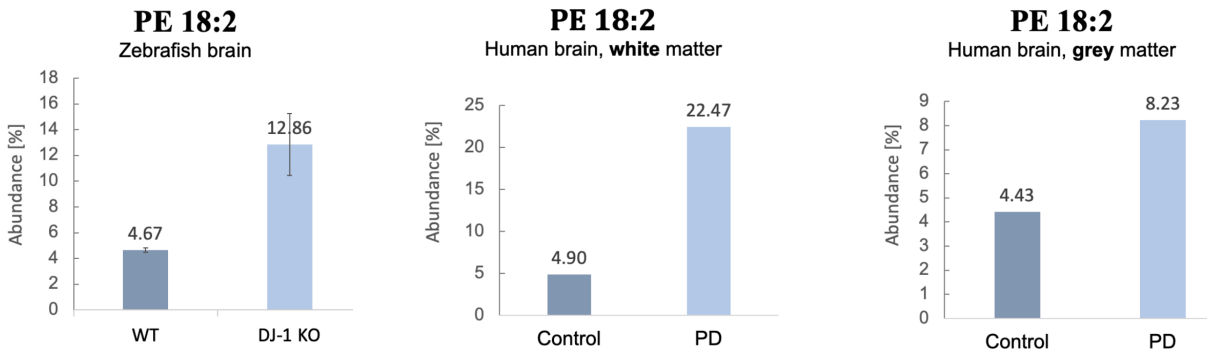

Figure 6.4.3 Increase in PE 18:2 observed in tissue from DJ-1 KO zebrafish and human PD brains. Compared to the control brains, the abundance of PE 18:2, linoleic acid, a precursor in arachidonic acid synthesis [197], was notably increased in the sporadic PD brain. PE 18:2 abundance is shown in the three plots, representing its abundance in the brains of WT and DJ-1 KO zebrafish (left), as well as human brain tissue from both white (middle) and grey (right) matter. While the human brain data represented is a result of singular biological experiments, the zebrafish data is a result of triplicate experiments (n = 3). Error bars are therefore shown for the zebrafish datasets. PE, phosphatidylethanolamine.

7 Conclusion and Future Prospects

Overall, the findings in this thesis suggest an elevated level of oxidative stress and a potential loss of neuroprotective antioxidant functions due to reduced levels of the antioxidant DJ-1. However, an increase in the abundance of PC plasmalogens, sphingomyelin, PE 18:2 (linoleic acid), and PS 22:5 (DPA) (Table 5.2.3, Table 5.3.3), suggests a potential counteracting homeostatic response against oxidative stress and inflammation, owing to their neuroprotective and anti-inflammatory properties [180, 199]. This could suggest an effort to maintain neuronal function, preventing the progression from mitochondrial dysfunction and oxidative stress to neuronal cell death [200].

Slight deviations found in the phospholipid profile of the sporadic PD brain compared to the ones reported in literature, along with the observed up-and downregulations of phospholipid and fatty acids, highlight the dysregulated lipid metabolism reported in PD [55]. At the same time, it points at the limitations of the study, including the lacking detection of lipid species such as DHA and AA, and possibly degraded phospholipids as shown by the elevated levels of PA abundance in both the control and PD brains (Figure 5.2.3b, Figure 5.2.3d). Altogether, the findings indicate that the protocols for tissue harvesting and phospholipid extraction serve their purpose, but with room for improvement. Future experiments could address shortcomings by age-matching human samples, minimizing variations in PMI times, and minimizing the levels of lipid degradation by adding lipase inhibitors, and by avoiding freeze-thaw cycles, and long-term storage of lipid samples. Additionally, as PD is an age-related disorder, repeating the study in older DJ-1 KO zebrafish would allow the assessment of the phospholipid profile of late-stage PD, combined with the changes in phospholipid and fatty acid abundance as the disease progresses with age.

The lack of detection of lyso-phospholipid species by MS/MS poses a missing piece in the puzzle, as they could provide some insight into phospholipid degradation and related signalling pathways implicated in PD [176]. The absence of DHA could also be attributed to its conversion into toxic oxidative products as a result of oxidative stress conditions. Future experiments could focus on developing methods for detection of lyso-phospholipids and oxidized lipids, potentially by tailoring the scripts and lipid libraries used in targeted UPLC-HRMS/MS metabolomics [169]. This approach may also result in detection of the absent DHA and AA. Assessing cholesterol levels is another missing piece. Considering its abundance in the brain [201], including its peroxidated species, cholesterol should be included in the analysis to obtain a more comprehensive understanding of its role in the complex lipid metabolism in PD [55]. The obtained ^{1}H NMR data, coupled with the

neural network deconvolution method applied in this thesis, could be utilized to compare the abundance of cholesterol with known amounts of a standard.

It is important to acknowledge the statistical limitations of this study, particularly in the case of human brain tissue samples where the sample size was only $n = 1$. Replicated experiments with larger sample sizes are necessary to obtain more reliable data and draw reasonable conclusions. Despite these limitations, the notable upregulation of PE 18:2 abundance, observed in both the zebrafish model and the white and grey matter of the sporadic PD brain, presents interesting data that could be further investigated.

8 References

1. Geldmacher, D.S. and P.J. Whitehouse, *Evaluation of dementia.* N Engl J Med, 1996. **335**(5): p. 330-6.
2. *Global, regional, and national burden of Alzheimer's disease and other dementias, 1990-2016: a systematic analysis for the Global Burden of Disease Study 2016.* Lancet Neurol, 2019. **18**(1): p. 88-106.
3. Iwagami, M., et al., *Blood cholesterol and risk of dementia in more than 1·8 million people over two decades: a retrospective cohort study.* The Lancet Healthy Longevity, 2021. **2**(8): p. e498-e506.
4. Shon, C. and H. Yoon, *Health-economic burden of dementia in South Korea.* BMC Geriatr, 2021. **21**(1): p. 549.
5. Antony, P.M.A., et al., *The hallmarks of Parkinson's disease.* The FEBS Journal, 2013. **280**(23): p. 5981-5993.
6. Goetz, C.G., *The history of Parkinson's disease: early clinical descriptions and neurological therapies.* Cold Spring Harb Perspect Med, 2011. **1**(1): p. a008862.
7. James Parkinson, Member of the Royal College of Surgeons, *An Essay on the Shaking Palsy.* The Journal of Neuropsychiatry and Clinical Neurosciences, 2002. **14**(2): p. 223-236.
8. Bloem, B.R., *Postural instability in Parkinson's disease.* Clinical Neurology and Neurosurgery, 1992. **94**: p. 41-45.
9. Sheridan, M.R. and K.A. Flowers, *Movement variability and bradykinesia in Parkinson's disease.* Brain, 1990. **113 (Pt 4)**: p. 1149-61.
10. Berardelli, A., et al., *Pathophysiology of bradykinesia in Parkinson's disease.* Brain, 2001. **124**(11): p. 2131-2146.
11. Park, A. and M. Stacy, *Non-motor symptoms in Parkinson's disease.* Journal of Neurology, 2009. **256**(3): p. 293-298.
12. Iversen, S.D. and L.L. Iversen, *Dopamine: 50 years in perspective.* Trends in Neurosciences, 2007. **30**(5): p. 188-193.
13. Ehringer, H. and O. Hornykiewicz, *[Distribution of noradrenaline and dopamine (3-hydroxytyramine) in the human brain and their behavior in diseases of the extrapyramidal system].* Klin Wochenschr, 1960. **38**: p. 1236-9.
14. Freund, T.F., J.F. Powell, and A.D. Smith, *Tyrosine hydroxylase-immunoreactive boutons in synaptic contact with identified striatonigral neurons, with particular reference to dendritic spines.* Neuroscience, 1984. **13**(4): p. 1189-215.
15. Hodge, G.K. and L.L. Butcher, *Pars compacta of the substantia nigra modulates motor activity but is not involved importantly in regulating food and water intake.* Naunyn Schmiedebergs Arch Pharmacol, 1980. **313**(1): p. 51-67.
16. Johns, P., *Chapter 13 - Parkinson's disease*, in *Clinical Neuroscience*, P. Johns, Editor. 2014, Churchill Livingstone. p. 163-179.
17. Yuan, A. and R.A. Nixon, *Neurofilament Proteins as Biomarkers to Monitor Neurological Diseases and the Efficacy of Therapies.* Front Neurosci, 2021. **15**: p. 689938.
18. Mezey, E., et al., *Alpha synuclein is present in Lewy bodies in sporadic Parkinson's disease.* Molecular Psychiatry, 1998. **3**(6): p. 493-499.
19. Spillantini, M.G., et al., *α-Synuclein in Lewy bodies.* Nature, 1997. **388**(6645): p. 839-840.
20. Plotegher, N., et al., *The chaperone-like protein 14-3-3η interacts with human α-synuclein aggregation intermediates rerouting the amyloidogenic pathway and*

reducing α-synuclein cellular toxicity. Human Molecular Genetics, 2014. **23**(21): p. 5615-5629.
21. Shahmoradian, S.H., et al., *Lewy pathology in Parkinson's disease consists of crowded organelles and lipid membranes.* Nature Neuroscience, 2019. **22**(7): p. 1099-1109.
22. Ball, N., et al., *Parkinson's Disease and the Environment.* Front Neurol, 2019. **10**: p. 218.
23. Verstraeten, A., J. Theuns, and C. Van Broeckhoven, *Progress in unraveling the genetic etiology of Parkinson disease in a genomic era.* Trends in Genetics, 2015. **31**(3): p. 140-149.
24. Hindle, J.V., *Ageing, neurodegeneration and Parkinson's disease.* Age and Ageing, 2010. **39**(2): p. 156-161.
25. Nussbaum, R.L. and C.E. Ellis, *Alzheimer's Disease and Parkinson's Disease.* New England Journal of Medicine, 2003. **348**(14): p. 1356-1364.
26. Tysnes, O.-B. and A. Storstein, *Epidemiology of Parkinson's disease.* Journal of Neural Transmission, 2017. **124**(8): p. 901-905.
27. de Lau, L.M.L. and M.M.B. Breteler, *Epidemiology of Parkinson's disease.* The Lancet Neurology, 2006. **5**(6): p. 525-535.
28. Zárate, S., T. Stevnsner, and R. Gredilla, *Role of Estrogen and Other Sex Hormones in Brain Aging. Neuroprotection and DNA Repair.* Frontiers in Aging Neuroscience, 2017. **9**.
29. Van Den Eeden, S.K., et al., *Incidence of Parkinson's Disease: Variation by Age, Gender, and Race/Ethnicity.* American Journal of Epidemiology, 2003. **157**(11): p. 1015-1022.
30. Yang, F., et al., *Socioeconomic status in relation to Parkinson's disease risk and mortality: A population-based prospective study.* Medicine (Baltimore), 2016. **95**(30): p. e4337.
31. Wirdefeldt, K., et al., *Epidemiology and etiology of Parkinson's disease: a review of the evidence.* European Journal of Epidemiology, 2011. **26**(1): p. 1.
32. Gorell, J.M., et al., *Occupational exposures to metals as risk factors for Parkinson's disease.* Neurology, 1997. **48**(3): p. 650-8.
33. Quik, M., et al., *Multiple roles for nicotine in Parkinson's disease.* Biochemical Pharmacology, 2009. **78**(7): p. 677-685.
34. Popat, R.A., et al., *Coffee, ADORA2A, and CYP1A2: the caffeine connection in Parkinson's disease.* European Journal of Neurology, 2011. **18**(5): p. 756-765.
35. Brown, T.P., et al., *Pesticides and Parkinson's disease--is there a link?* Environ Health Perspect, 2006. **114**(2): p. 156-64.
36. Langston, J.W., et al., *Chronic Parkinsonism in Humans Due to a Product of Meperidine-Analog Synthesis.* Science, 1983. **219**(4587): p. 979-980.
37. Sofroniew, M.V. and H.V. Vinters, *Astrocytes: biology and pathology.* Acta Neuropathol, 2010. **119**(1): p. 7-35.
38. Pajares, M., et al., *Inflammation in Parkinson's Disease: Mechanisms and Therapeutic Implications.* Cells, 2020. **9**(7).
39. Thomas, B. and M.F. Beal, *Parkinson's disease.* Human Molecular Genetics, 2007. **16**(R2): p. R183-R194.
40. Klein, C. and A. Westenberger, *Genetics of Parkinson's Disease.* Cold Spring Harbor Perspectives in Medicine, 2012. **2**(1).
41. Lesage, S. and J. Trinh, *Special Issue "Parkinson's Disease: Genetics and Pathogenesis".* Genes, 2023. **14**(3): p. 737.
42. Chang, D., et al., *A meta-analysis of genome-wide association studies identifies 17 new Parkinson's disease risk loci.* Nat Genet, 2017. **49**(10): p. 1511-1516.

43. Jové, M., et al., *Lipids and lipoxidation in human brain aging. Mitochondrial ATP-synthase as a key lipoxidation target.* Redox Biology, 2019. **23**: p. 101082.
44. Piomelli, D., G. Astarita, and R. Rapaka, *A neuroscientist's guide to lipidomics.* Nature Reviews Neuroscience, 2007. **8**(10): p. 743-754.
45. Qin, Z., et al., *Effect of 4-Hydroxy-2-nonenal Modification on α-Synuclein Aggregation *.* Journal of Biological Chemistry, 2007. **282**(8): p. 5862-5870.
46. Choi, M.L., et al., *Pathological structural conversion of α-synuclein at the mitochondria induces neuronal toxicity.* Nat Neurosci, 2022. **25**(9): p. 1134-1148.
47. Zhang, L., et al., *Role of DJ-1 in Immune and Inflammatory Diseases.* Frontiers in Immunology, 2020. **11**.
48. Muro, E., G.E. Atilla-Gokcumen, and U.S. Eggert, *Lipids in cell biology: how can we understand them better?* Molecular Biology of the Cell, 2014. **25**(12): p. 1819-1823.
49. Fahy, E., et al., *Lipid classification, structures and tools.* Biochim Biophys Acta, 2011. **1811**(11): p. 637-47.
50. Kubo, S., T. Hatano, and N. Hattori, *Lipid rafts involvement in the pathogenesis of Parkinson's disease.* Front Biosci (Landmark Ed), 2015. **20**(2): p. 263-79.
51. Fortin, D.L., et al., *Lipid Rafts Mediate the Synaptic Localization of α-Synuclein.* The Journal of Neuroscience, 2004. **24**(30): p. 6715-6723.
52. Kim, K.S., et al., *DJ-1 associates with lipid rafts by palmitoylation and regulates lipid rafts-dependent endocytosis in astrocytes.* Hum Mol Genet, 2013. **22**(23): p. 4805-17.
53. Fantini, J., D. Carlus, and N. Yahi, *The fusogenic tilted peptide (67–78) of α-synuclein is a cholesterol binding domain.* Biochimica et Biophysica Acta (BBA) - Biomembranes, 2011. **1808**(10): p. 2343-2351.
54. Varshney, P., V. Yadav, and N. Saini, *Lipid rafts in immune signalling: current progress and future perspective.* Immunology, 2016. **149**(1): p. 13-24.
55. Alecu, I. and S.A.L. Bennett, *Dysregulated Lipid Metabolism and Its Role in α-Synucleinopathy in Parkinson's Disease.* Front Neurosci, 2019. **13**: p. 328.
56. Xicoy, H., B. Wieringa, and G.J.M. Martens, *The Role of Lipids in Parkinson's Disease.* Cells, 2019. **8**(1): p. 27.
57. Falkenburger, B.H., et al., *Phosphoinositides: lipid regulators of membrane proteins.* J Physiol, 2010. **588**(Pt 17): p. 3179-85.
58. Chakraborty, M. and X.C. Jiang, *Sphingomyelin and its role in cellular signaling.* Adv Exp Med Biol, 2013. **991**: p. 1-14.
59. Kim, D., *Fatty acid-sensitive two-pore domain K+ channels.* Trends in Pharmacological Sciences, 2003. **24**(12): p. 648-654.
60. Duchen, M.R., *Mitochondria and calcium: from cell signalling to cell death.* The Journal of Physiology, 2000. **529**(1): p. 57-68.
61. Rodriguez de Turco, E.B., et al., *Diacylglycerol kinase ε regulates seizure susceptibility and long-term potentiation through arachidonoyl– inositol lipid signaling.* Proceedings of the National Academy of Sciences, 2001. **98**(8): p. 4740-4745.
62. Halliwell, B., *Reactive oxygen species in living systems: Source, biochemistry, and role in human disease.* The American Journal of Medicine, 1991. **91**(3, Supplement 3): p. S14-S22.
63. Moldovan, L. and N.I. Moldovan, *Oxygen free radicals and redox biology of organelles.* Histochemistry and Cell Biology, 2004. **122**(4): p. 395-412.
64. Venero, J.L., et al., *Evidence for dopamine-derived hydroxyl radical formation in the nigrostriatal system in response to axotomy.* Free Radic Biol Med, 2003. **34**(1): p. 111-23.

65. Ayala, A., M.F. Muñoz, and S. Argüelles, *Lipid peroxidation: production, metabolism, and signaling mechanisms of malondialdehyde and 4-hydroxy-2-nonenal.* Oxid Med Cell Longev, 2014. **2014**: p. 360438.
66. Volinsky, R. and P.K.J. Kinnunen, *Oxidized phosphatidylcholines in membrane-level cellular signaling: from biophysics to physiology and molecular pathology.* The FEBS Journal, 2013. **280**(12): p. 2806-2816.
67. Delic, V., et al., *Biological links between traumatic brain injury and Parkinson's disease.* Acta Neuropathologica Communications, 2020. **8**(1): p. 45.
68. Esterbauer, H., P. Eckl, and A. Ortner, *Possible mutagens derived from lipids and lipid precursors.* Mutation Research/Reviews in Genetic Toxicology, 1990. **238**(3): p. 223-233.
69. Zarkovic, K., *4-Hydroxynonenal and neurodegenerative diseases.* Molecular Aspects of Medicine, 2003. **24**(4): p. 293-303.
70. Bernardi, S., et al., *The Complex Interplay between Lipids, Immune System and Interleukins in Cardio-Metabolic Diseases.* Int J Mol Sci, 2018. **19**(12).
71. Wang, S., et al., *α-Synuclein, a chemoattractant, directs microglial migration via H2O2-dependent Lyn phosphorylation.* Proceedings of the National Academy of Sciences, 2015. **112**(15): p. E1926-E1935.
72. Chen, S.-H., E.A. Oyarzabal, and J.-S. Hong, *Critical role of the Mac1/NOX2 pathway in mediating reactive microgliosis-generated chronic neuroinflammation and progressive neurodegeneration.* Current Opinion in Pharmacology, 2016. **26**: p. 54-60.
73. Smith, A.N., et al., *Therapeutic targeting of microglia mediated oxidative stress after neurotrauma.* Frontiers in Medicine, 2022. **9**.
74. Tang, Y., *Editorial: Microglial Polarization in the Pathogenesis and Therapeutics of Neurodegenerative Diseases.* Frontiers in Aging Neuroscience, 2018. **10**.
75. Wang, W.Y., et al., *Role of pro-inflammatory cytokines released from microglia in Alzheimer's disease.* Ann Transl Med, 2015. **3**(10): p. 136.
76. Gardner, R.C., et al., *Mild TBI and risk of Parkinson disease.* A Chronic Effects of Neurotrauma Consortium Study, 2018. **90**(20): p. e1771-e1779.
77. Woodcock, T. and C. Morganti-Kossmann, *The Role of Markers of Inflammation in Traumatic Brain Injury.* Frontiers in Neurology, 2013. **4**.
78. Walkon, L.L., J.O. Strubbe-Rivera, and J.N. Bazil, *Calcium Overload and Mitochondrial Metabolism.* Biomolecules, 2022. **12**(12).
79. Dudek, J., *Role of Cardiolipin in Mitochondrial Signaling Pathways.* Frontiers in Cell and Developmental Biology, 2017. **5**.
80. Khalifat, N., et al., *Lipid packing variations induced by pH in cardiolipin-containing bilayers: the driving force for the cristae-like shape instability.* Biochim Biophys Acta, 2011. **1808**(11): p. 2724-33.
81. Davidson, W.S., et al., *Stabilization of alpha-synuclein secondary structure upon binding to synthetic membranes.* J Biol Chem, 1998. **273**(16): p. 9443-9.
82. Ferreon, A.C.M., et al., *Interplay of α-synuclein binding and conformational switching probed by single-molecule fluorescence.* Proceedings of the National Academy of Sciences, 2009. **106**(14): p. 5645-5650.
83. Angelova, P.R., et al., *Ca2+ is a key factor in α-synuclein-induced neurotoxicity.* Journal of Cell Science, 2016. **129**(9): p. 1792-1801.
84. Sharon, R., et al., *The Formation of Highly Soluble Oligomers of α-Synuclein Is Regulated by Fatty Acids and Enhanced in Parkinson's Disease.* Neuron, 2003. **37**(4): p. 583-595.

85. Ludtmann, M.H.R., et al., *α-synuclein oligomers interact with ATP synthase and open the permeability transition pore in Parkinson's disease.* Nature Communications, 2018. **9**(1): p. 2293.
86. Lane, N., *A unifying view of ageing and disease: the double-agent theory.* Journal of Theoretical Biology, 2003. **225**(4): p. 531-540.
87. O'Brien, J.S. and E.L. Sampson, *Lipid composition of the normal human brain: gray matter, white matter, and myelin.* J Lipid Res, 1965. **6**(4): p. 537-44.
88. Skinner, E.R., et al., *Differences in the fatty acid composition of the grey and white matter of different regions of the brains of patients with Alzheimer's disease and control subjects.* Brain, 1993. **116**(3): p. 717-725.
89. Sinclair, E., et al., *Metabolomics of sebum reveals lipid dysregulation in Parkinson's disease.* Nature Communications, 2021. **12**(1): p. 1592.
90. Ueland, M., et al., *Fresh vs. frozen human decomposition – A preliminary investigation of lipid degradation products as biomarkers of post-mortem interval.* Forensic Chemistry, 2021. **24**: p. 100335.
91. Razali, K., et al., *The Promise of the Zebrafish Model for Parkinson's Disease: Today's Science and Tomorrow's Treatment.* Frontiers in Genetics, 2021. **12**.
92. Kishi, S., et al., *Zebrafish as a genetic model in biological and behavioral gerontology: where development meets aging in vertebrates--a mini-review.* Gerontology, 2009. **55**(4): p. 430-41.
93. Best, J.D. and W.K. Alderton, *Zebrafish: An in vivo model for the study of neurological diseases.* Neuropsychiatric Disease and Treatment, 2008. **4**(3): p. 567-576.
94. Anderson, J.L., J.D. Carten, and S.A. Farber, *Zebrafish lipid metabolism: from mediating early patterning to the metabolism of dietary fat and cholesterol.* Methods Cell Biol, 2011. **101**: p. 111-41.
95. Grosser, T., et al., *Developmental expression of functional cyclooxygenases in zebrafish.* Proceedings of the National Academy of Sciences, 2002. **99**(12): p. 8418-8423.
96. Marza, E., et al., *Developmental expression and nutritional regulation of a zebrafish gene homologous to mammalian microsomal triglyceride transfer protein large subunit.* Developmental Dynamics, 2005. **232**(2): p. 506-518.
97. Clifton, J.D., et al., *Identification of novel inhibitors of dietary lipid absorption using zebrafish.* PLoS One, 2010. **5**(8): p. e12386.
98. Pankratz, N., et al., *Mutations in DJ-1 are rare in familial Parkinson disease.* Neuroscience Letters, 2006. **408**(3): p. 209-213.
99. Repici, M. and F. Giorgini, *DJ-1 in Parkinson's Disease: Clinical Insights and Therapeutic Perspectives.* J Clin Med, 2019. **8**(9).
100. Gao, H.-M. and J.-S. Hong, *Gene–environment interactions: Key to unraveling the mystery of Parkinson's disease.* Progress in Neurobiology, 2011. **94**(1): p. 1-19.
101. Edson, A.J., et al., *Dysregulation in the Brain Protein Profile of Zebrafish Lacking the Parkinson's Disease-Related Protein DJ-1.* Mol Neurobiol, 2019. **56**(12): p. 8306-8322.
102. Chavali, L.N.M., et al., *Progressive Motor and Non-Motor Symptoms in Park7 Knockout Zebrafish.* International Journal of Molecular Sciences, 2023. **24**(7): p. 6456.
103. Canet-Avilés, R.M., et al., *The Parkinson's disease protein DJ-1 is neuroprotective due to cysteine-sulfinic acid-driven mitochondrial localization.* Proceedings of the National Academy of Sciences, 2004. **101**(24): p. 9103-9108.
104. Liu, C., et al., *DJ-1 in Ocular Diseases: A Review.* Int J Med Sci, 2018. **15**(5): p. 430-435.
105. Ahmad, S., et al., *Protein oxidation: an overview of metabolism of sulphur containing amino acid, cysteine.* Front Biosci (Schol Ed), 2017. **9**(1): p. 71-87.

106. Wilson, M.A., *The Role of Cysteine Oxidation in DJ-1 Function and Dysfunction.* Antioxidants & Redox Signaling, 2011. **15**(1): p. 111-122.
107. Kiss, R., et al., *Structural features of human DJ-1 in distinct Cys106 oxidative states and their relevance to its loss of function in disease.* Biochimica et Biophysica Acta (BBA) - General Subjects, 2017. **1861**(11, Part A): p. 2619-2629.
108. Saito, Y., *DJ-1 as a Biomarker of Parkinson's Disease.* Adv Exp Med Biol, 2017. **1037**: p. 149-171.
109. Martínez-Yusta, A., E. Goicoechea, and M.D. Guillén, *A Review of Thermo-Oxidative Degradation of Food Lipids Studied by 1H NMR Spectroscopy: Influence of Degradative Conditions and Food Lipid Nature.* Comprehensive Reviews in Food Science and Food Safety, 2014. **13**(5): p. 838-859.
110. Li, Y., et al., *A comparative study: the impact of different lipid extraction methods on current microalgal lipid research.* Microbial Cell Factories, 2014. **13**(1): p. 14.
111. Halim, R., et al., *Mechanical cell disruption for lipid extraction from microalgal biomass.* Bioresource Technology, 2013. **140**: p. 53-63.
112. Furse, S., M.R. Egmond, and J.A. Killian, *Isolation of lipids from biological samples.* Mol Membr Biol, 2015. **32**(3): p. 55-64.
113. Kolarovic, L. and N.C. Fournier, *A comparison of extraction methods for the isolation of phospholipids from biological sources.* Analytical Biochemistry, 1986. **156**(1): p. 244-250.
114. Folch, J., M. Lees, and G.H.S. Stanley, *A SIMPLE METHOD FOR THE ISOLATION AND PURIFICATION OF TOTAL LIPIDES FROM ANIMAL TISSUES.* Journal of Biological Chemistry, 1957. **226**(1): p. 497-509.
115. Bligh, E.G. and W.J. Dyer, *A rapid method of total lipid extraction and purification.* Can J Biochem Physiol, 1959. **37**(8): p. 911-7.
116. Breil, C., et al., *"Bligh and Dyer" and Folch Methods for Solid-Liquid-Liquid Extraction of Lipids from Microorganisms. Comprehension of Solvatation Mechanisms and towards Substitution with Alternative Solvents.* Int J Mol Sci, 2017. **18**(4).
117. Iverson, S.J., S.L. Lang, and M.H. Cooper, *Comparison of the Bligh and Dyer and Folch methods for total lipid determination in a broad range of marine tissue.* Lipids, 2001. **36**(11): p. 1283-7.
118. Breil, C., et al., *Bio-Based Solvents for Green Extraction of Lipids from Oleaginous Yeast Biomass for Sustainable Aviation Biofuel.* Molecules, 2016. **21**(2): p. 196.
119. Cequier-Sánchez, E., et al., *Dichloromethane as a Solvent for Lipid Extraction and Assessment of Lipid Classes and Fatty Acids from Samples of Different Natures.* Journal of Agricultural and Food Chemistry, 2008. **56**(12): p. 4297-4303.
120. Stefanov, I., B. Vlaeminck, and V. Fievez, *A novel procedure for routine milk fat extraction based on dichloromethane.* Journal of Food Composition and Analysis, 2010. **23**(8): p. 852-855.
121. Furse, S., et al., *Evidence that Listeria innocua modulates its membrane's stored curvature elastic stress, but not fluidity, through the cell cycle.* Scientific Reports, 2017. **7**(1): p. 8012.
122. Jurowski, K., et al., *Analytical Techniques in Lipidomics: State of the Art.* Critical Reviews in Analytical Chemistry, 2017. **47**(5): p. 418-437.
123. van den Ouweland, J.M.W. and I.P. Kema, *The role of liquid chromatography–tandem mass spectrometry in the clinical laboratory.* Journal of Chromatography B, 2012. **883-884**: p. 18-32.
124. Zehethofer, N. and D.M. Pinto, *Recent developments in tandem mass spectrometry for lipidomic analysis.* Analytica Chimica Acta, 2008. **627**(1): p. 62-70.

125. Pitt, J.J., *Principles and applications of liquid chromatography-mass spectrometry in clinical biochemistry.* Clin Biochem Rev, 2009. **30**(1): p. 19-34.
126. Kebarle, P., *A brief overview of the present status of the mechanisms involved in electrospray mass spectrometry.* Journal of Mass Spectrometry, 2000. **35**(7): p. 804-817.
127. Eliuk, S. and A. Makarov, *Evolution of Orbitrap Mass Spectrometry Instrumentation.* Annu Rev Anal Chem (Palo Alto Calif), 2015. **8**: p. 61-80.
128. McLafferty, F.W., *Tandem Mass Spectrometry.* Science, 1981. **214**(4518): p. 280-287.
129. Vogeser, M. and C. Seger, *Pitfalls Associated with the Use of Liquid Chromatography–Tandem Mass Spectrometry in the Clinical Laboratory.* Clinical Chemistry, 2010. **56**(8): p. 1234-1244.
130. Koelmel, J.P., et al., *Expanding Lipidome Coverage Using LC-MS/MS Data-Dependent Acquisition with Automated Exclusion List Generation.* Journal of the American Society for Mass Spectrometry, 2017. **28**(5): p. 908-917.
131. Todd, J.F.J., *Recommendations for nomenclature and symbolism for mass spectroscopy (including an appendix of terms used in vacuum technology). (Recommendations 1991).* Pure and Applied Chemistry, 1991. **63**(10): p. 1541-1566.
132. Malm, L., et al., *Guide to Semi-Quantitative Non-Targeted Screening Using LC/ESI/HRMS.* Molecules, 2021. **26**(12).
133. Bothwell, J.H.F. and J.L. Griffin, *An introduction to biological nuclear magnetic resonance spectroscopy.* Biological Reviews, 2011. **86**(2): p. 493-510.
134. Chatham, J.C. and S.J. Blackband, *Nuclear magnetic resonance spectroscopy and imaging in animal research.* Ilar j, 2001. **42**(3): p. 189-208.
135. Jakubec, M., et al., *Fast and Quantitative Phospholipidomic Analysis of SH-SY5Y Neuroblastoma Cell Cultures Using Liquid Chromatography-Tandem Mass Spectrometry and (31)P Nuclear Magnetic Resonance.* ACS Omega, 2019. **4**(25): p. 21596-21603.
136. Sotirhos, N., B. Herslöf, and L. Kenne, *Quantitative analysis of phospholipids by 31P-NMR.* Journal of Lipid Research, 1988. **27**(4): p. 386-392.
137. Mardor, Y. and J.S. Cohen, *Magnetic Resonance Spectroscopy and Magnetic Resonance Imaging, Introduction*, in *Encyclopedia of Cancer (Second Edition)*, J.R. Bertino, Editor. 2002, Academic Press: New York. p. 89-103.
138. Koga, Y. and H. Goldfine, *Biosynthesis of phospholipids in Clostridium butyricum: kinetics of synthesis of plasmalogens and the glycerol acetal of ethanolamine plasmalogen.* Journal of Bacteriology, 1984. **159**(2): p. 597-604.
139. Emwas, A.-H., et al., *NMR Spectroscopy for Metabolomics Research.* Metabolites, 2019. **9**(7): p. 123.
140. Aue, W.P., J. Karhan, and R.R. Ernst, *Homonuclear broad band decoupling and two-dimensional J-resolved NMR spectroscopy.* The Journal of Chemical Physics, 2008. **64**(10): p. 4226-4227.
141. Schmid, N., et al., *Deconvolution of 1D NMR spectra: A deep learning-based approach.* Journal of Magnetic Resonance, 2023. **347**: p. 107357.
142. Edson, A.J., et al., *Dysregulation in the Brain Protein Profile of Zebrafish Lacking the Parkinson's Disease-Related Protein DJ-1.* Molecular Neurobiology, 2019. **56**(12): p. 8306-8322.
143. Mercadante, A.A. and P. Tadi, *Neuroanatomy, Gray Matter*, in *StatPearls*. 2023, StatPearls Publishing
Copyright © 2023, StatPearls Publishing LLC.: Treasure Island (FL).
144. Goldberg, M.P. and B.R. Ransom, *New Light on White Matter.* Stroke, 2003. **34**(2): p. 330-332.

145. Javed, K., V. Reddy, and F. Lui, *Neuroanatomy, Cerebral Cortex*. 2022: StatPearls Publishing, Treasure Island (FL).
146. Strotzer, M., *One Century of Brain Mapping Using Brodmann Areas*.* Klinische Neuroradiologie, 2009. **19**(3): p. 179-186.
147. Mónico, A., et al., *Drawbacks of Dialysis Procedures for Removal of EDTA.* PLoS One, 2017. **12**(1): p. e0169843.
148. Stadtman, E.R., *Metal ion-catalyzed oxidation of proteins: Biochemical mechanism and biological consequences.* Free Radical Biology and Medicine, 1990. **9**(4): p. 315-325.
149. Smith, P.K., et al., *Measurement of protein using bicinchoninic acid.* Analytical Biochemistry, 1985. **150**(1): p. 76-85.
150. Furse, S., et al., *Evidence that Listeria innocua modulates its membrane's stored curvature elastic stress, but not fluidity, through the cell cycle.* Sci Rep, 2017. **7**(1): p. 8012.
151. Pettitt, T.R., et al., *Analysis of intact phosphoinositides in biological samples.* J Lipid Res, 2006. **47**(7): p. 1588-96.
152. Murgia, S., S. Mele, and M. Monduzzi, *Quantitative characterization of phospholipids in milk fat via 31P NMR using a monophasic solvent mixture.* Lipids, 2003. **38**(5): p. 585-91.
153. Ni, Z., et al., *Guiding the choice of informatics software and tools for lipidomics research applications.* Nature Methods, 2023. **20**(2): p. 193-204.
154. Piston, D., et al., *DJ-1 is a redox sensitive adapter protein for high molecular weight complexes involved in regulation of catecholamine homeostasis.* Hum Mol Genet, 2017. **26**(20): p. 4028-4041.
155. Choi, J., et al., *Separation of native and C106-oxidized DJ-1 proteins by using column chromatography.* Protein Expression and Purification, 2022. **195-196**: p. 106092.
156. Bosco, M., et al., *Organic Solvent Systems for31P Nuclear Magnetic Resonance Analysis of Lecithin Phospholipids: Applications to Two-Dimensional Gradient-Enhanced1H-Detected Heteronuclear Multiple Quantum Coherence Experiments.* Analytical Biochemistry, 1997. **245**(1): p. 38-47.
157. van Amerongen, Y.F., et al., *Zebrafish brain lipid characterization and quantification by ^{1}H nuclear magnetic resonance spectroscopy and MALDI-TOF mass spectrometry.* Zebrafish, 2014. **11**(3): p. 240-7.
158. Sun, J., et al., *Effects of a phospholipase D inhibitor on postharvest enzymatic browning and oxidative stress of litchi fruit.* Postharvest Biology and Technology, 2011. **62**(3): p. 288-294.
159. Huang, M. and S. Chen, *DJ-1 in neurodegenerative diseases: Pathogenesis and clinical application.* Progress in Neurobiology, 2021. **204**: p. 102114.
160. Yasuda, T., et al., *Free radicals impair the anti-oxidative stress activity of DJ-1 through the formation of SDS-resistant dimer.* Free Radical Research, 2017. **51**(4): p. 397-412.
161. Nural, H., et al., *Dissembled DJ-1 high molecular weight complex in cortex mitochondria from Parkinson's disease patients.* Molecular Neurodegeneration, 2009. **4**(1): p. 23.
162. Krebiehl, G., et al., *Reduced Basal Autophagy and Impaired Mitochondrial Dynamics Due to Loss of Parkinson's Disease-Associated Protein DJ-1.* PLOS ONE, 2010. **5**(2): p. e9367.
163. Bahmed, K., et al., *The effect of cysteine oxidation on DJ-1 cytoprotective function in human alveolar type II cells.* Cell Death & Disease, 2019. **10**: p. 638.
164. Chen, J., L. Li, and L.-S. Chin, *Parkinson disease protein DJ-1 converts from a zymogen to a protease by carboxyl-terminal cleavage.* Human Molecular Genetics, 2010. **19**(12): p. 2395-2408.

165. Knittelfelder, O.L., et al., *A versatile ultra-high performance LC-MS method for lipid profiling.* J Chromatogr B Analyt Technol Biomed Life Sci, 2014. **951-952**: p. 119-28.
166. Exton, J.H., *Phospholipase D-structure, regulation and function.* Rev Physiol Biochem Pharmacol, 2002. **144**: p. 1-94.
167. Li, M., Y. Hong, and X. Wang, *Phospholipase D- and phosphatidic acid-mediated signaling in plants.* Biochimica et Biophysica Acta (BBA) - Molecular and Cell Biology of Lipids, 2009. **1791**(9): p. 927-935.
168. Yang, K. and X. Han, *Accurate Quantification of Lipid Species by Electrospray Ionization Mass Spectrometry — Meets a Key Challenge in Lipidomics.* Metabolites, 2011. **1**(1): p. 21-40.
169. Triebl, A., et al., *Quantitation of phosphatidic acid and lysophosphatidic acid molecular species using hydrophilic interaction liquid chromatography coupled to electrospray ionization high resolution mass spectrometry.* J Chromatogr A, 2014. **1347**: p. 104-10.
170. Balla, T., *Phosphoinositides: Tiny Lipids With Giant Impact on Cell Regulation.* Physiological Reviews, 2013. **93**(3): p. 1019-1137.
171. Sastry, P.S., *Lipids of nervous tissue: composition and metabolism.* Prog Lipid Res, 1985. **24**(2): p. 69-176.
172. Gelderman, H.T., et al., *The development of a post-mortem interval estimation for human remains found on land in the Netherlands.* Int J Legal Med, 2018. **132**(3): p. 863-873.
173. Söderberg, M., et al., *Lipid Compositions of Different Regions of the Human Brain During Aging.* Journal of Neurochemistry, 1990. **54**(2): p. 415-423.
174. Svennerholm, L., K. Boström, and B. Jungbjer, *Changes in weight and compositions of major membrane components of human brain during the span of adult human life of Swedes.* Acta Neuropathologica, 1997. **94**(4): p. 345-352.
175. van der Veen, J.N., et al., *The critical role of phosphatidylcholine and phosphatidylethanolamine metabolism in health and disease.* Biochim Biophys Acta Biomembr, 2017. **1859**(9 Pt B): p. 1558-1572.
176. Farmer, K., et al., *Major Alterations of Phosphatidylcholine and Lysophosphotidylcholine Lipids in the Substantia Nigra Using an Early Stage Model of Parkinson's Disease.* International Journal of Molecular Sciences, 2015. **16**(8): p. 18865-18877.
177. Wood, P.L., et al., *Augmented frontal cortex diacylglycerol levels in Parkinson's disease and Lewy Body Disease.* PLOS ONE, 2018. **13**(3): p. e0191815.
178. Treede, I., et al., *Anti-inflammatory Effects of Phosphatidylcholine* *. Journal of Biological Chemistry, 2007. **282**(37): p. 27155-27164.
179. Huitema, K., et al., *Identification of a family of animal sphingomyelin synthases.* The EMBO Journal, 2004. **23**(1): p. 33-44.
180. Signorelli, P., C. Conte, and E. Albi, *The Multiple Roles of Sphingomyelin in Parkinson's Disease.* Biomolecules, 2021. **11**(9).
181. Adibhatla, R.M. and J.F. Hatcher, *Phospholipase A(2), reactive oxygen species, and lipid peroxidation in CNS pathologies.* BMB Rep, 2008. **41**(8): p. 560-7.
182. Beaulieu, E., et al., *Oxidative-stress induced increase in circulating fatty acids does not contribute to phospholipase A2-dependent appetitive long-term memory failure in the pond snail Lymnaea stagnalis.* BMC Neuroscience, 2014. **15**(1): p. 56.
183. Calzada, E., O. Onguka, and S.M. Claypool, *Phosphatidylethanolamine Metabolism in Health and Disease.* Int Rev Cell Mol Biol, 2016. **321**: p. 29-88.
184. Patel, D. and S.N. Witt, *Ethanolamine and Phosphatidylethanolamine: Partners in Health and Disease.* Oxidative Medicine and Cellular Longevity, 2017. **2017**: p. 4829180.

185. Fabelo, N., et al., *Severe Alterations in Lipid Composition of Frontal Cortex Lipid Rafts from Parkinson's Disease and Incidental Parkinson's Disease.* Molecular Medicine, 2011. **17**(9): p. 1107-1118.
186. Videira, P.A.Q. and M. Castro-Caldas, *Linking Glycation and Glycosylation With Inflammation and Mitochondrial Dysfunction in Parkinson's Disease.* Front Neurosci, 2018. **12**: p. 381.
187. Braverman, N.E. and A.B. Moser, *Functions of plasmalogen lipids in health and disease.* Biochimica et Biophysica Acta (BBA) - Molecular Basis of Disease, 2012. **1822**(9): p. 1442-1452.
188. Luoma, A.M., et al., *Plasmalogen phospholipids protect internodal myelin from oxidative damage.* Free Radical Biology and Medicine, 2015. **84**: p. 296-310.
189. Shah, A., et al., *Palmitate and Stearate are Increased in the Plasma in a 6-OHDA Model of Parkinson's Disease.* Metabolites, 2019. **9**(2): p. 31.
190. Kaur, G., et al., *Docosapentaenoic acid (22:5n-3): A review of its biological effects.* Progress in Lipid Research, 2011. **50**(1): p. 28-34.
191. Kelly, L., et al., *The polyunsaturated fatty acids, EPA and DPA exert a protective effect in the hippocampus of the aged rat.* Neurobiology of Aging, 2011. **32**(12): p. 2318.e1-2318.e15.
192. Dyall, S.C., *Long-chain omega-3 fatty acids and the brain: a review of the independent and shared effects of EPA, DPA and DHA.* Frontiers in Aging Neuroscience, 2015. **7**.
193. Dalfó, E., et al., *Evidence of Oxidative Stress in the Neocortex in Incidental Lewy Body Disease.* Journal of Neuropathology & Experimental Neurology, 2005. **64**(9): p. 816-830.
194. Song, J.H., K. Fujimoto, and T. Miyazawa, *Polyunsaturated (n-3) Fatty Acids Susceptible to Peroxidation Are Increased in Plasma and Tissue Lipids of Rats Fed Docosahexaenoic Acid–Containing Oils.* The Journal of Nutrition, 2000. **130**(12): p. 3028-3033.
195. Sambra, V., et al., *Docosahexaenoic and Arachidonic Acids as Neuroprotective Nutrients throughout the Life Cycle.* Nutrients, 2021. **13**(3).
196. Bariås, E., et al., *Contrasting the phospholipid profiles of two neoplastic cell lines reveal a high PC:PE ratio for SH-SY5Y cells relative to A431 cells.* Biochemical and Biophysical Research Communications, 2023. **656**: p. 23-29.
197. Singh, M., *Essential fatty acids, DHA and human brain.* The Indian Journal of Pediatrics, 2005. **72**(3): p. 239-242.
198. Tang, K.S., *Protective effect of arachidonic acid and linoleic acid on 1-methyl-4-phenylpyridinium-induced toxicity in PC12 cells.* Lipids in Health and Disease, 2014. **13**(1): p. 197.
199. Alarcon-Gil, J., et al., *Neuroprotective and Anti-Inflammatory Effects of Linoleic Acid in Models of Parkinson's Disease: The Implication of Lipid Droplets and Lipophagy.* Cells, 2022. **11**(15).
200. Hattingen, E., et al., *Phosphorus and proton magnetic resonance spectroscopy demonstrates mitochondrial dysfunction in early and advanced Parkinson's disease.* Brain, 2009. **132**(12): p. 3285-3297.
201. Jin, U., S.J. Park, and S.M. Park, *Cholesterol Metabolism in the Brain and Its Association with Parkinson's Disease.* Exp Neurobiol, 2019. **28**(5): p. 554-567.

9 Appendix

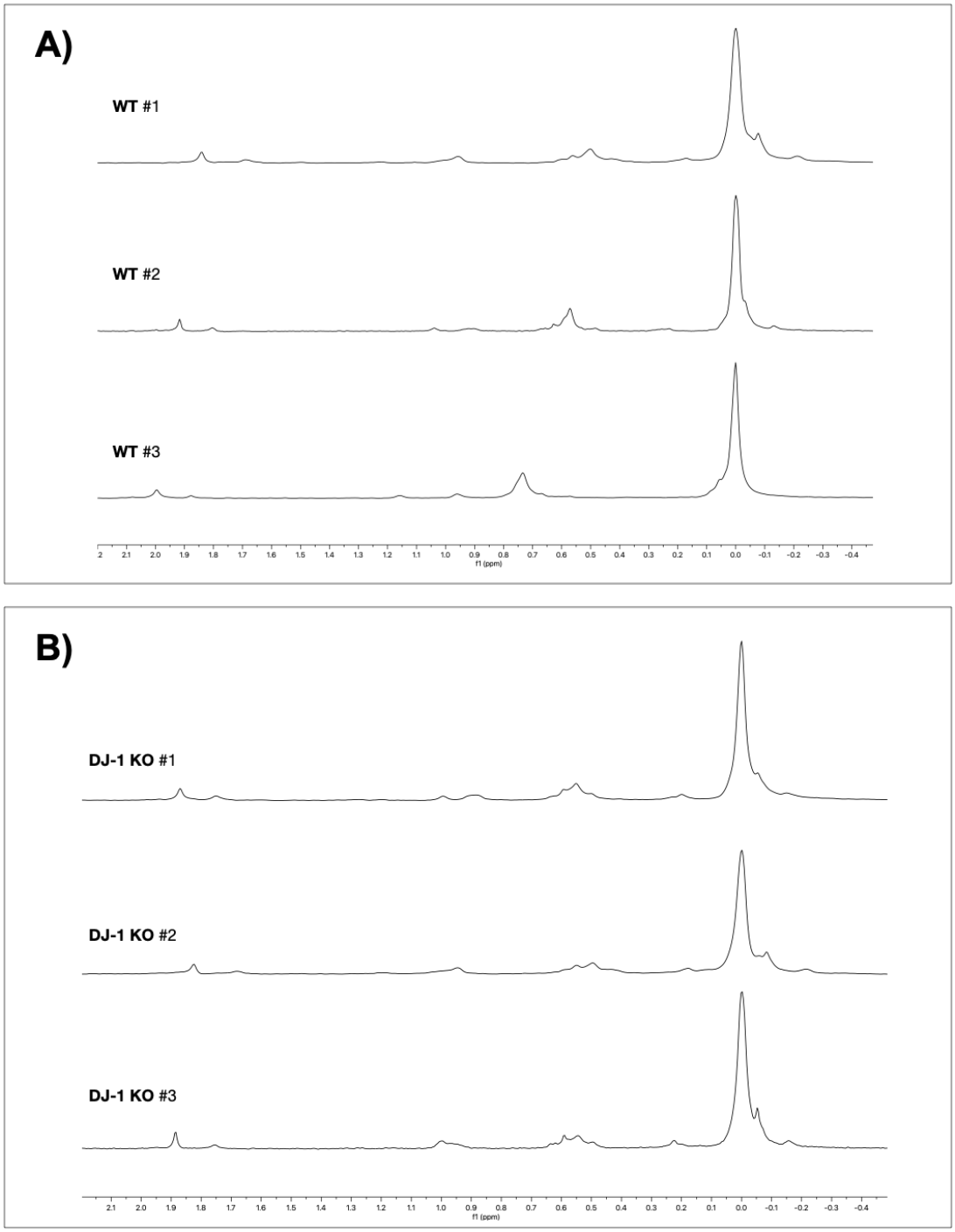

Figure 9.1 **^{31}P NMR spectra of brain lipids extracted from WT and DJ-1 KO Zebrafish.** Brain lipids originating from zebrafish brain tissue were extracted and resuspended in CUBO solvent before ^{31}P NMR analysis was performed according to the parameters listed in Table 4.5. Triplicate experiments (n = 3) were performed on brain matter originating from a WT and DJ-1 KO zebrafish line (Table 3.5.1). The triplicate spectra showed a similar outlook, with a notable sharp peak around 0.55 ppm. The figure was made using MestreNova.

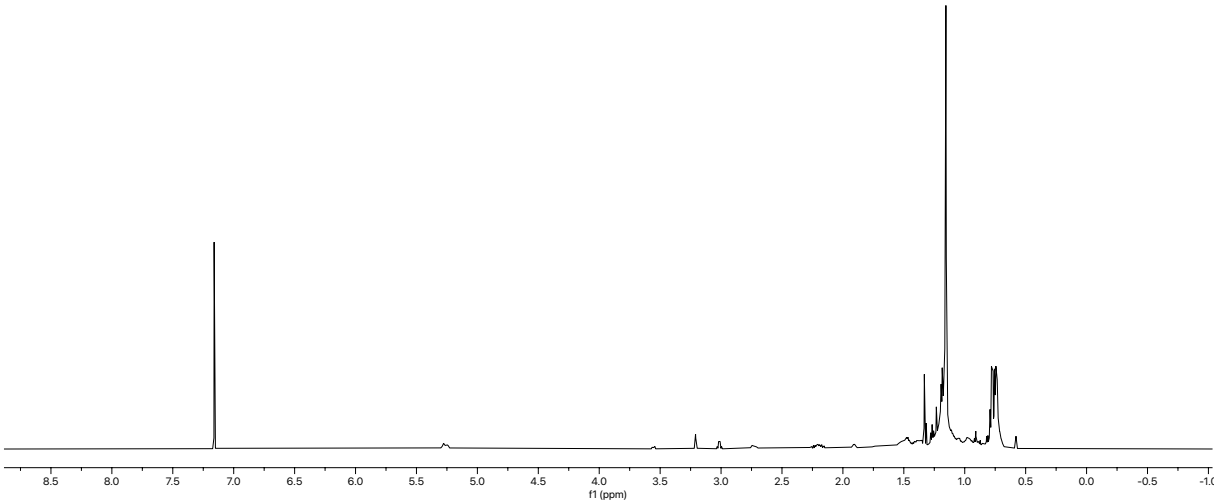

Figure 9.2 Example of ^{1}H NMR spectra of DJ-1 KO zebrafish brain. Brain lipids originating from DJ-1 KO zebrafish brain tissue were extracted and resuspended in d-Chloroform before ^{1}H NMR analysis was performed according to the parameters listed in Table 4.5. The figure was made using MestreNova.

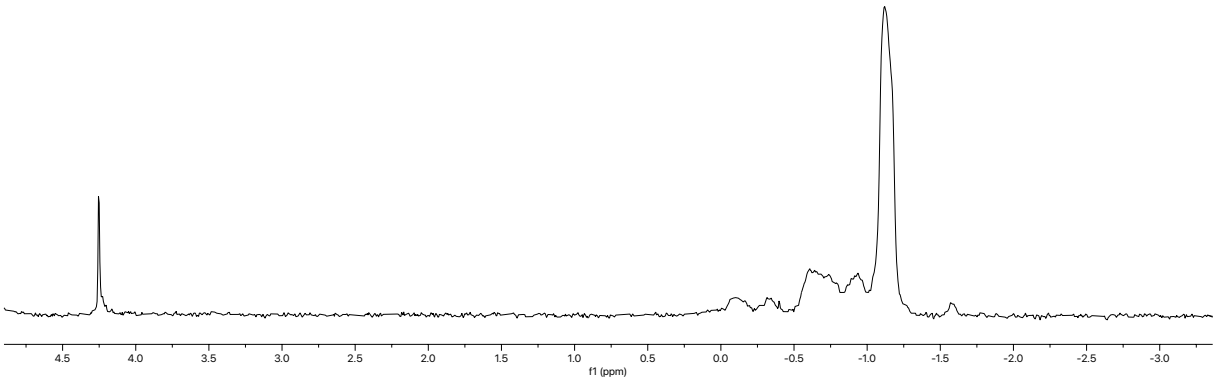

Figure 9.3 ^{31}P NMR spectra of DJ-1 KO zebrafish brain after the addition of guanidium chloride. Brain lipids originating from DJ-1 KO zebrafish brain tissue were extracted and resuspended in CUBO solvent before ^{31}P NMR analysis was performed according to the parameters listed in Table 4.5. A concentrated solution of guanidium chloride was added to try to "salvage" the sample. The figure was made using MestreNova.